# MATHEMATICAL

# PROBLEMS

# OF COMPUTER

# SCIENCE

**LXII**

**Yerevan**

**2024**

# Կոմպյուտերային գիտության մաթեմատիկական խնդիրներ

# Математические проблемы компьютерных наук

# Mathematical Problems of Computer Science

# LXII

ԵՐԵՎԱՆ 2024 **YEREVAN**

# Կոմպյուտերային գիտության մաթեմատիկական խնդիրներ, LXII

Журнал **Математические проблемы компьютерных наук** издается два раза в год Институтом проблем информатики и автоматизации НАН РА. Он охватывает современные направления теоретической и прикладной математики, информатики и вычислительной техники.

Он включен в список допустимых журналов Высшей квалификационной комиссии.

Печатается на основании решения N 28-11/1 заседания
Редакционного совета от 28 ноября 2024г.

# Mathematical Problems of Computer Science, LXII

The periodical **Mathematical Problems of Computer Science** is published twice per year by the Institute for Informatics and Automation Problems of NAS RA. It covers modern directions of theoretical and applied mathematics, informatics and computer science.

It is included in the list of acceptable journals of the Higher Qualification Committee.

*Պարբերականի սույն պրակը նվիրվում է ֆիզիկա-մաթեմատիկական գիտությունների դոկտոր, պրոֆեսոր, ՀՀ ԳԱԱ թղթակից-անդամ, Ռուսաստանի բնական գիտությունների ակադեմիայի ակադեմիկոս Հրանտ Բաբկենի Մարանջյանի 85 ամյակին:*

*Данный выпуск журнала посвящается 85-летию Гранта Бабкеновича Маранджяна, доктора физико-математических наук, профессора, члена-корреспондента НАН РА, академиака Российской академии естественных наук.*

*This issue of the Periodical is dedicated to the 85-th anniversary of Hrant B. Marandjian, Doctor of Physical and Mathematical Sciences, Professor, Corresponding Member of NAS RA, Academician of the Russian Academy of Natural Sciences.*

## Hrant Babken Marandjyan

Professor,  Doctor of Physical and Mathematical Sciences,
Corresponding Member of NAS RA
(1939-2020)

This issue of the Periodical is dedicated to the 85th anniversary of Hrant Babken Marandjyan, a famous scientist in the field of mathematical cybernetics and information technology. He would have turned 85 years old if his earthly life had not been interrupted on March 14, 2020. A wide range of scientific interests: mathematical logic, recursion theory, complexity theory of the degree of algorithmic unsolvability, the theory of probabilistic automata, automatic analysis and synthesis of algorithms and programs, automatic synthesis and optimization of computer programs, was formed in the schools of prominent scientists who made a quite tangible contribution to the development of mathematical logic, theory of algorithms and control theory.

Among the numerous works of Hrant Marandjyan, those highly appreciated by specialists in the field of mathematical logic and theory of algorithms (both in the former Soviet Union and in Western and Eastern Europe, as well as in the USA), are particularly distinguished by their focus on the study of Kolmogorov complexity properties. These works are considered some of the most significant contributions to the mentioned area.

Investigations concerning the properties of sets of minimal indices in complete and precomplete numberings, are also crucial. It is sufficient to note the solution of generalizing the well-known A. Mayer problem on m-degrees of sets of minimal numbers in the main

numberings. The existence of main numberings is proved, the sets of minimal numbers of which are complete with respect to a number of reducibilities.

The issues of representing partially recursive functions using recursive equations of a general form were thoroughly considered, which is a new direction in this sphere, since earlier only recursive equations with separable variables were considered in the literature, and equations of a more general form were considered only in special areas. A necessary and sufficient condition for the existence of solutions to extensional recursive equations of a general form was found. A similar result was obtained in the study of intensional recursive equations of a general form.

For more than fifty years, Marandjyan's scientific and organizational activities have closely been connected with the establishment of the Computing Center of the Armenian Academy of Sciences (now the Institute for Informatics and Automation Problems of the National Academy of Sciences of the Republic of Armenia), where he headed the Laboratory of the Theory of Algorithms and was also the Deputy Director for Science.

The developments in the field of automatic synthesis and optimization of computer programs, fulfilled under the leadership of Marandjyan, are of great applied value.

Being engaged in fruitful pedagogical activity, Hrant Marandjyan prepared a large number of highly qualified specialists who work effectively in various institutes.

Since the 1990s, his involvement in projects with the Armenian branches of prominent foreign companies in the field of information technology has determined the high scientific level of these companies.

Hrant Marandjyan's integrity, professionalism and devotion to science, along with his attentiveness to colleagues, have earned him respect from the scientific community in Armenia and gratitude from everyone with whom he has collaborated.

# CONTENTS

UDC  510.64

# On Quantified Splitting Proof System for Propositional Calculi

Anahit A. Chubaryan

Yerevan State University, Yerevan, Armenia
e-mail: achubaryan@ysu.am

### Abstract

In this paper, some new quantified propositional proof system is introduced and compared by proof complexities with other quantified and not quantified propositional proof systems. It is proved that the introduced system 1) is polynomially equivalent to its quantifier-free variant and 2) has exponential speed-up by sizes over some variants of the quantified resolution system. As the introduced system has a very simple proof construction strategy, it can be very useful not only in Logic, and therefore in Artificial Intelligence, but also in areas such as Computational Biology and Medical Diagnosis.
**Keywords:** Quantified propositional proof systems, Generalized Splitting system, Proof steps, Proof size, Exponential speed-up.
**Article info:** Received 29 September 2024; sent for review 15  October 2024; accepted 7 November 2024.

## 1. Introduction

It is well known that Mathematical Logic, in particular propositional calculi, is the base of Artificial Intelligence and therefore, has very *interesting applications*  in fields such as Computational Biology and Medical Diagnosis.

Propositional proof complexity originates from the seminal paper by Cook and Reckhow. [1]. It provides a path for approaching the P vs. NP problem: proving super-polynomial lower bounds to all propositional proof systems is equivalent to showing that NP is different from coNP and

therefore P is different from NP. It is well known that the exponential lower bounds for proof sizes of some sets of tautologies are obtained in many systems, but for some of the most natural calculi, in particular, for Frege systems, the question about polynomially bounded sizes is still open. While traditionally the complexity of proofs for propositional tautologies has been at the centre of research, the past two decades have witnessed a surge in proof complexity of quantified boolean formulas (QBFs), which give not only a new class of tautologies, but some quantifier-free tautologies can be proved simpler in any quantified systems. Some interesting survey of proof complexity for QBFs is given in [2], where the complexities for some QBF families are compared in different quantified propositional proof systems: variants of QBF resolution, QBF Frege systems, quantified versions of cutting planes, QBF sequent calculi and some others.

Based on the propositional system GS (Generalized Splitting), described in [3], a new quantified propositional proof system is introduced here. The place of the system GS in the hierarchy of propositional proof systems [1] remains unknown and moreover: by the comparison of the two main proof complexity characteristics (*step*s and *size*) for two classes of formulas in the system GS and Frege systems it is shown that for one class of considered formulas the bounds in the system GS are much better than those in the Frege systems, while for the second class the situation is quite the opposite [4].

From all the above mentioned it follows that the investigations of proof complexities in some quantified variants of the system GS can be important. Consequently, the possible practical applications of these systems in different non-mathematical areas may also be important.

## 2. Preliminaries

We will use the current concepts of a propositional formula, a proof system for propositional logic, proof complexity, and well-known notions of polynomial equivalence and exponential speed-up. The language of considered systems contains the propositional variables, logical connectives $\neg, \&, \vee, \supset, \leftrightarrow$ and parentheses (,). Following the usual terminology, we call the variables and negated variables *literals*. In [3], the following notions were introduced. Each of the following trivial identities for a propositional formula $\psi$ we call a replacement rule.

$$
\begin{array}{llll}
0 \,\&\, \psi = 0, & \psi \,\&\, 0 = 0, & 1 \,\&\, \psi = \psi, & \psi \,\&\, 1 = \psi, \\
0 \vee \psi = \psi, & \psi \vee 0 = \psi, & 1 \vee \psi = 1, & \psi \vee 1 = 1, \\
0 \supset \psi = 1, & \psi \supset 0 = \bar{\psi}, & 1 \supset \psi = \psi, & \psi \supset 1 = 1, \\
\bar{0} = 1, & \bar{1} = 0, & \bar{\bar{\psi}} = \psi, \\
0 \leftrightarrow \psi = \bar{\psi}, & \psi \leftrightarrow 0 = \bar{\psi}, & 1 \leftrightarrow \psi = \psi, & \psi \leftrightarrow 1 = \psi.
\end{array}
$$

The application of a replacement rule to some words consists in replacing some of its sub-words, having the form of the left-hand side of one of the above identities, by the corresponding right-hand side.

**The proof system GS.** Let φ be some formula and p be some of its variables. The results of the splitting method of formula φ by variable p (split variable) are the formulas φ[p$^\delta$] for every **δ** from the set {0,1}, which are obtained from φ by assigning **δ** to each occurrence of p and successively using replacement rules. The generalization of the splitting method allows associating every formula φ with some tree with root, the nodes of which are labeled by formulas and edges, labeled by literals. The root is labeled by itself formula φ. If some node is labeled by formula v and α is its some variable, then both edges, which go out from this node, are labeled by one of literals α$^\delta$ for every **δ** from the set {0,1}, and each of the 2 "sons" of this node is labeled by the corresponding formula v[α$^\delta$]. Each leaf of the tree is labeled with some constant from the set {0,1}. The tree, which is constructed for formula φ by the described method, will be called a ***splitting tree*** (s.t.) of φ. It is obvious that by changing the order of split variables in the given formula φ, we can obtain different splitting trees of φ. We can note that the strategy of splitting tree construction is quite simple.

The *GS* proof system can be defined as follows: for every formula φ, some s.t. must be constructed and if all the leaves of the tree are labeled with the value 1, then the formula φ is a tautology and therefore we can consider the pointed constant 1 as an axiom, and for every formula $v$, which is the label of some s.t. node, and p is its split variable, then the following figure $v\,[p^0]$, $v\,[p^1] \vdash v$ can be considered as some inference rule, hence every above-described s.t. can be considered as some proof of φ in the system *GS*. Note that if we consider the splitting method for formulas given in disjunctive normal form, then the *GS* system is the well-known Analytic Tableaux system.

By | $\varphi$| we denote the size of a formula $\varphi$, defined as the number of all logical signs in it. It is obvious that the full size of a formula, which is understood to be the number of all symbols, is bounded by some linear function in |$\varphi$ |.

The T-complexity (L-complexity) of s.t. is the *number (the sum of sizes) of different formulas*, with which its nodes are labeled. The **T-complexity (L-complexity) of GS-proof for tautology φ** is the value of minimal T-complexity (L-complexity) of its splitting trees.

## 3. Main Results

**Quantified Splitting system (QS).** A QBF is a propositional formula augmented with Boolean quantifiers ∀, ∃ that range over the Boolean values 0, 1. Every propositional formula is already a QBF. Let ϕ be a QBF. The semantics of the quantifiers are: ∀xϕ(x) ≡ ϕ[x$^0$] & ϕ[x$^1$] and ∃xϕ(x) ≡ ϕ[x$^0$] ∨ ϕ[x$^1$]. In standardized QBF investigated in computer science , all quantifiers appear outermost in a (quantifier) prefix and are followed by a propositional formula, called a *matrix*. The variables following the quantifier ∀ are called *universal* variables, and the variables following the quantifier ∃ are called *existential variables*. The system **QS** works as follows: for any QBF formula φ, we use the system *GS* to the matrix of φ. S.t. for every GBF tautology φ must be the following: if for any step the splinted variable α is a universal variable of φ, then both subtrees, stuffed from the α$^0$ and α$^1$ labeled edges must have some branch, ended with value 1 labeled leaves; if for any step the splinted variable α is an existential variable of φ, then at least one of the subtrees, stuffed from the α$^0$ or α$^1$ labeled edges must have some branch, ended with value 1 labeled leaves.

**QU-Resolution system**. *Propositional resolution* [2] is a refutational system operating with clauses, i.e., it demonstrates the unsatisfiability of a given CNF. It has only a well-known *resolution rule. QBF resolution systems* work with fully quantified prenex QCNFs. As in propositional resolution, these QBF systems are refutational calculi, i.e., they refute false QBFs to be obtained by augmenting the propositional resolution system using the resolution rule by just one new rule, the *universal reduction rule*, $\frac{c}{\sigma(c)}$ , where $\sigma$ is partial substitution that allows a universal variable from a clause $C$ to be replaced by either 0 or 1, provided that $u$ appears right of all variables in $C$ in the prefix $Q$. Intuitively, this means that a universal variable $u$ can be deleted from a clause $C$ if $u$ is rightmost in $C$ with respect to $Q$, i.e., no variable in $C$ depends on $u$.

**Theorem. 1)** The systems GS and QS are polynomially equivalent by steps and sizes;

        **2)** The system QS has an exponential speed-up by size over the QU-Resolution

        system.

Proof of 1) is obvious because every quantifier-free tautology $A(x_1, \ldots, x_n)$ can be presented as a QFB formula $\forall x_1 \ldots x_n A(x_1, \ldots, x_n)$, the matrix of which is $A(x_1, \ldots, x_n)$. Proof of 2) is based on the investigation of proof steps and sizes of equality families of QBFs

$$SC_n = \exists x_1 \ldots x_n \forall u_1 \ldots u_n \exists t_1 \ldots t_n \left( \bigwedge_{1 \le i \le n} (x_i \leftrightarrow u_i) \supset \bar{t_i} \right) \wedge \left( \bigvee_{1 \le i \le n} t_i \right).$$

For every s.t., we use its scheme, which is the same tree without node labels. It is not difficult to see that the s.t. of $SC_1$-matrix and the s.t. of $SC_2$ –matrix have the following schemes:
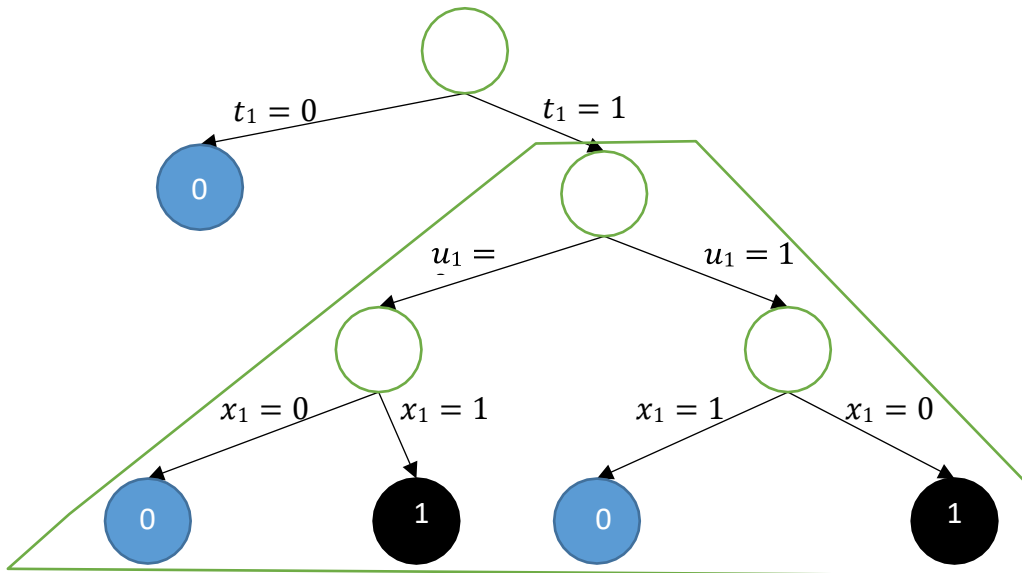


Fig. 1. $SG_1$
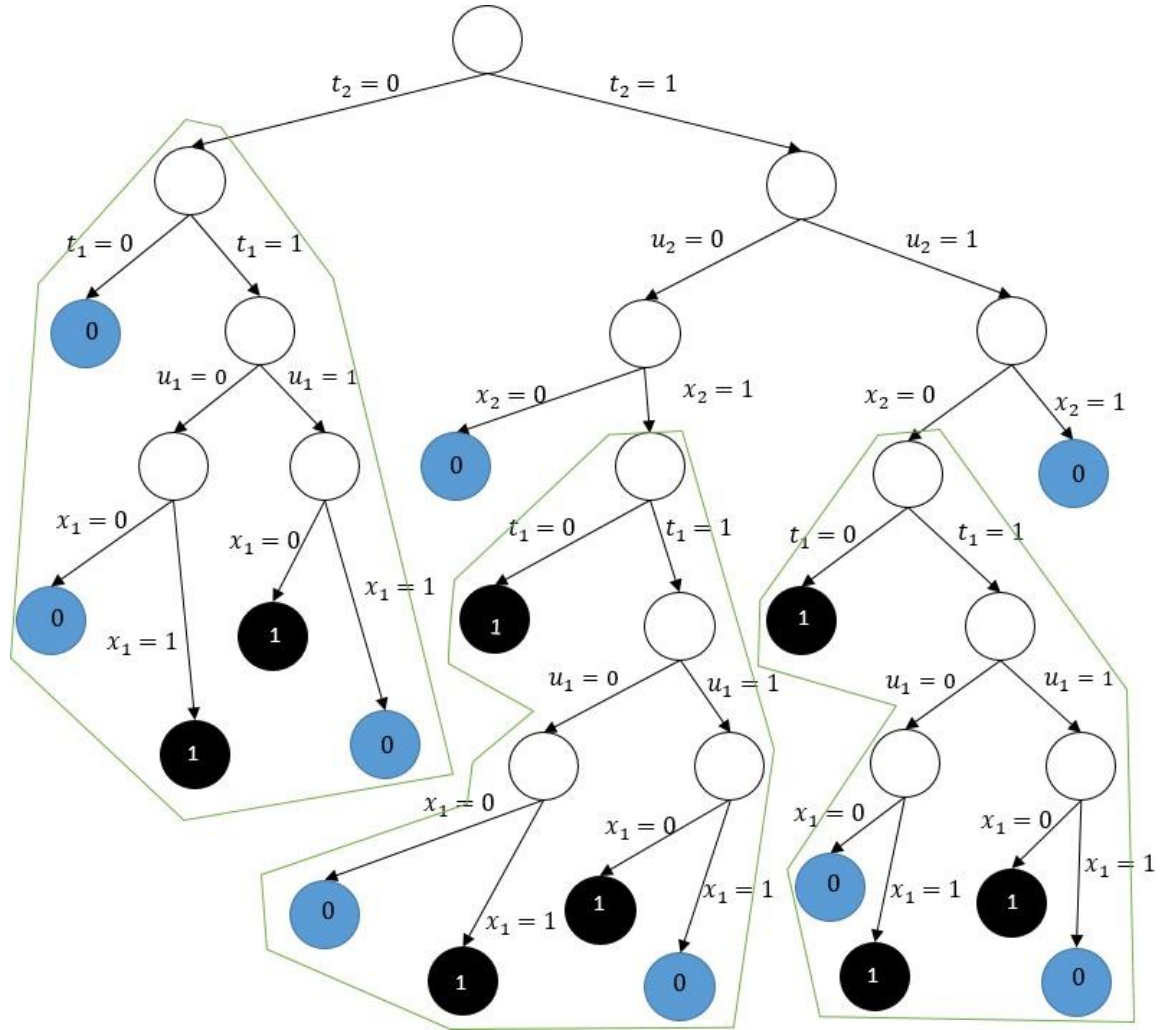
Fig 2. $SG_2$

It is not difficult to note that in the s.t. for $SG_2$-matrix the same subtree is repeated three times after splitting by $t_2 = 0$, by $t_2 = 1, u_2 = 0, x_2 = 1$ successively and by $t_2 = 1, u_2 = 1, x_2 = 0$ successively, and this subtree is the s.t. of SC$_1$-matrix.

It is not difficult to prove by analogy that in s.t. for SC$_n$-matrix the same subtree - s.t. for SC$_{n-1}$ is repeated three times after splitting by $t_n = 0$, by $t_n = 1, u_n = 0, x_n = 1$ successively and by $t_n = 1, u_n = 1, x_n = 0$ successively.

If we denote the number of different formulas in the constructed s.t. of $SG_n$ − matrix by $(n)$, then we have $(1) = 6$ and $(n) = (n-1) + 4$, therefore $(n) = 4n + 2$. Note, that the longest branch in any s.t. of $SG_n$ −matrix must have $3n + 1$ nodes and size of $SG_n$ −matrix $4n − 3$, therefore $T$-complexity of $QS$-proof for $SG_n$ is $\theta(n)$ and $L$- complexity of $QS$-proof for $SG_n$ is no more than $(4n + 2)(4n − 3) = \theta(n^2)$.

As it is mentioned in [2], the equality formulas $SG_n$ are exponentially hard for QU-Resolution (i.e., they require proofs of exponential size), the point 2) of the theorem will be proved, if it is shown that the system QS p-simulates the system QU-Resolution. The last statement is obvious

because a) the system GS p-simulates Resolution system and b) the *universal reduction rule*, $\frac{C}{\sigma(C)}$, where $\sigma$ is a partial substitution that allows substituting a universal variable from a clause $C$ by either 0 or 1, while in the system QS it is allowed to substitute every variable by either 0 or 1.

Note that analogies of the GS and QS systems can be constructed for Many-valued logic [5], which is more applicable in such fields as Formal Verification, Artificial Intelligence, Operations Research, Computational Biology and Medical Diagnosis.

## 4. Conclusion and Future Work

All the above results, besides their mathematical significance, have practical applications in many areas, therefore the following investigations can be useful:

a) as it is proved that the GS and QS systems are polynomially equivalent and as mentioned in the Introduction, the GS system and Frege systems are incomparable, then Frege systems and the QS system are also incomparable, therefore it is interesting to compare the QS system with the other quantifier-free and quantified systems, in particular, with quantified Frege;

b) as the introduced system has a very simple strategy for constructing proofs it is interesting to investigate how to use the many-valued analogies of the GS and QS systems in medical diagnosis.

## References

[1]    S.A. Cook and A. R. Reckhow, "The relative efficiency of propositional proof systems", *Journal of Symbolic Logic*, vol. 44, pp. 36-50, 1979.

[2]    O. Beyersdorff, *Proof Complexity of Quantified Boolean Logic — A Survey*, World Scientific Publishing Company, Chapter 15, 2023.

[3]    A. Chubaryan and Arm.Chubaryan, "Bounds of some proof complexity characteristics in the system of splitting generalization", (in Russian), *Otechestv. Nauka w epokhu izmenenij*, vol.10, no. 2(7), pp. 11-14, 2015.

[4]    A. Chubaryan, S. Hovhanisyan and G. Gasparyan, "On some properties of the generalized splitting system", (in Russian), *Vestnik RAU*, vol. 2, pp. 34-42, 2019.

[5]    A. Chubaryan, "Universal system for many-valued logic, based on splitting method, and some of its properties", *IJISSET*, vol. 5, no. 5, pp. 52-55, 2019. www.ijisset.org/articles/2019-2/volume-5-issue-5/

# Ասույթային հաշվի ծավալիչներով տրոհման արտածման համակարգի վերաբերյալ

Անահիտ Ա. Չուբարյան

Երևանի պետական համալսարան, Երևան, Հայաստան

e-mail: achubaryan@ysu.am

## Ամփոփում

Այս հոդվածում ներմուծվել է ասույթային հաշվի արտածման նոր ծավալիչներով համակարգ և ըստ արտածումների բարդությունների, այն համեմատվել է ասույթային հաշվի ծավալիչներով և առանց ծավալիչների արտածումների այլ համակարգերի հետ: Ապացուցվել է, որ ներմուծված համակարգը՝ 1) բազմանդամորեն համարժեք է իր իսկ առանց ծավալիչների տարբերակին, 2) ըստ արտածումների երկարությունների ունի ցուցչային արագացում ծավալիչներով ռեզոլուցիոն համակարգի մի տարբերակի նկատմամբ: Քանի որ ներմուծված համակարգն ունի արտածումների որոնման շատ պարզ ընթացակարգ, այն կարող է օգտակար լինել ոչ միայն տրամաբանությունում, հետևաբար՝ արհեստական բանականության մշակումներում, այլ նաև այնպիսի ոլորտներում, ինչպիսիք են համակարգչային կենսաբանությունը և բժշկական ախտորոշումը:

**Բանալի բառեր`** Ասույթային հաշվի արտածումների ծավալիչներով համակարգ, ընդհանրացված տրոհման համակարգ, արտածման քայլեր, արտածման երկարություն, ցուցչային արագացում:

# О квантифицированной системе расщеплений исчисления высказываний

Анаит А. Чубарян

Ереванский государственный университет, Ереван, Армения

e-mail: achubaryan@ysu.am

## Аннотация

В данной статье введена новая квантифицированная система выводов исчисления высказываний и она сравнена по сложностям выводов с иными квантифицированными и неквантифицированными системами выводов исчисления высказываний. Доказано, что введённая система: 1) полиномиально эквивалентна своему неквантифицированному варианту, 2) имеет экспоненциальное ускорение по длинам выводов относительно некоторого варианта квантифицированной системы резолюций. Так как стратегия поиска выводов в введённой системе очень проста, то она может быть полезна не только в логике,

а следовательно, при разработках искусственного интеллекта, но также в таких сферах, каковы компъютерная биология и медицинская диагностика.

# On the Proof of the Existence of Nontotal Partial Degree and on the Turing Degree of Representative of This Partial Degree

Arsen H. Mokatsian

Institute for Informatics and Automation Problems of NAS RA, Yerevan, Armenia
e-mail: arsenmokatsian@gmail.com

## Abstract

The ordering of *e*-degrees (of total functions) is known to be isomorphic to the ordering of *T*-degrees. It is possible to form equivalence classes with respect to $=_e$ and in the set of all functions (not necessarily total). The resulting *e*-degrees are called *partial degrees*.

In H. Rogers' *Theory of Recursive Functions and Effective Computability* [1], a proof of the existence of a non-total partial degree is given along with a corollary to this theorem.

The article contains a modification of the proof of the theorem given above, which allows us to significantly strengthen the results of the corollary, namely to prove that $(\exists \psi)[\psi$ is not partial computable $\& \ \psi \leq_T \mathbf{0}' \ \& \ (\forall f)[f \leq_e \psi \Rightarrow f$ is computable]] (in the above-mentioned corollary, it is noted that the constructed function is only computably enumerable in $\mathbf{0}'$).

**Keywords:** *e*-reducibility, partial degree, partial computable function, Turing degree.

**Article info:** Received 30 September 2024; sent for review 15 October 2024; accepted 14 November 2024.

## 1. Introduction

Formal definitions of many concepts mentioned in the Introduction will be given in the Preliminary section.

The concept of enumeration reducibility was introduced in the works of Friedberg and Rogers [2], Myhill [3] and Selman [4]. Informally, $A \subseteq \omega$ (where $\omega$ is the set of the nonnegative integers), is enumeration reducible to $B \subseteq \omega$ if there is a uniform way to compute an enumeration of $A$ from an enumeration of $B$.

If a partial degree contains at least one total function, it is called total. The total degrees therefore constitute a subordering of the partial degrees.

The structure of enumeration degrees $\mathcal{D}_e$ is an upper semi-lattice with the least upper bound induced by effective join operation $A \oplus B$ and the least element $\mathbb{0}_e$, the degree of all computably enumerable sets. The relationship between the following three reducibilities: $e$-reducibility, $T$-reducibility and relative computable enumerability (c.e. in) is expressed using a proposition

$$A \leq_T B \iff A \oplus \bar{A} \text{ is } B\text{-c.e.} \iff A \oplus \bar{A} \leq_e B \oplus \bar{B} .$$

Myhill [3] used this relationship to define a natural embedding of Turing degrees into enumeration degrees. He proved that the embedding $\iota \colon \mathcal{D}_T \to \mathcal{D}_e$, defined by $\iota(d_T(A)) = d_e(A \oplus \bar{A})$, preserves the order and the least upper bound.

Research in the field of e-degrees has continued over the past decades. Among the latest works, we can note [5], [6], and [7].

In [1], the existence of a nontotal partial degree is proved, along with a corollary of this theorem. In the Results section of this article, a modified proof of the aforementioned theorem is presented, which substantially strengthens the results of its corollary.

## 2. Preliminaries

**Notations**. In this section, we shall give the necessary definitions. We shall use the notions and terminology introduced in Rogers [1], and Soare [8].

We deal with sets and functions over the nonnegative integers $\omega = \{0,1,2,\cdots\}$.

Let $\varphi_e$ be the $e^{th}$ partial computable function in the standard listing (see [8], p.15, p.25).

If $A \subseteq \omega$ and $e \in \omega$, let $\Phi_e^A(x) = \Phi_e(A\colon x) = \{e\}^A(x)$ (see [8], pp. 48-50).

$\chi_A$ denotes the characteristic function of $A$, which is often identified with $A$ and written simply as $A(x)$.

We write $\varphi_{e,s}(x) = y$ if $x, y, e < s$ and $y$ is the output of $\varphi_e(x)$ in $< e$-steps of the Turing program $P_e$. If such a $y$ exists, we say $\varphi_{e,s}(x)$ *converges*, which we write as $\varphi_{e,s}(x) \downarrow$, and *diverges* ($\varphi_{e,s}(x) \uparrow$), otherwise.

Similarly, we write $\varphi_e(x) \downarrow$ if $\varphi_{e,s}(x) \downarrow$ for some $s$, and we write $\varphi_e(x) \downarrow = y$ if $\varphi_e(x) \downarrow$ and $\varphi_e(x) = y$, and similarly for $\varphi_{e,s}(x) \downarrow = y$ (see [8], pp.16-17).

$W_e = dom \; \varphi_e = \{x \colon \varphi_e(x) \downarrow\}$.

max $(A)$ denotes the maximum element of a finite set $A$, if $A$ is not $\emptyset$, and 0, otherwise.

$f \upharpoonright x$ denotes the restriction of $f$ to arguments $y < x$, and $A \upharpoonright x$ denotes $\chi_A \upharpoonright x$.

**Definition 1.** $\tau(x,y) = \frac{1}{2}(x^2 + 2xy + y^2 + 3x + y)$.

It is known that $\tau$ is a computable one-one mapping of $\omega \times \omega$ onto $\omega$.

We shall use $\langle x, y \rangle$ as an abbreviation for $\tau(x,y)$.

**Definition 2.** Given $x, y$, $<x, y>$ is the *ordered pair* consisting of $x$ and $y$ in that order.

Let $R$ be any 2-ary relation. We say that $R$ *is a single-valued* relation if for every $x$ there exists at most one $z$ such that $<x, z> \in R$.

A set $A$ is *single-valued* if $\{<x, y> | \langle x, y \rangle \in A\}$ is a single-valued relation.

**Definition 3.** Let $K^A = \{x | \Phi_x^A(x) \downarrow\} = \{x | x \in W_x^A \downarrow\}$. $K^A$ is called the *jump of* $A$ and is denoted by $A'$ (read as "$A$ prime") (see [8], p. 53).

**Definition 4.** $\mathbf{0} = \deg(\emptyset) = \{B | B \text{ is computable}\}$,

$$\mathbf{0}' = \deg(\emptyset'), \text{ where } \emptyset' =_{dfn} K^{\emptyset} \text{ (see [8], p. 54).}$$

**Definition 5.** a) Let $A \text{ join } B$, written $A \oplus B$ be $\{2x \mid x \in A\} \cup \{2x + 1 \mid x \in B\}$.

b) Let $\{A_y\}_{y \in \omega}$ be any countable sequence of sets. Define the *infinite join*

$$\oplus \{A_y\}_{y \in \omega} =_{dfn} \{\langle x, y \rangle | x \in A_y \ \& \ y \in \omega\} \text{ (see [8], p. 54).}$$

**Definition 6.** *(i)* A sequence of (total) functions $\{f_s(x)\}$ *converges* (*pointwise*) to $f(x)$, written $f = \lim_s, f_s$, if for all $x$, $f_s(x) = f(x)$ for a.e. $s$ (all but finitely many $s$).

*(ii)* A *modulus* (*of convergence*) for $\{f_s\}_{s \in \omega}$ is a function $m(x)$ such that for all $s$, if $s \geq m(x)$, then $f_s(x) = f(x)$ (Hence, $f_m(x) = f(x)$.) The *least modulus* is the function $m(x) = (\mu s)(\forall t \geq s)[f_s(x) = f(x)]$.

*(iii)* The sequence $\{f_s(x)\}_{s \in \omega}$ is *computable* if there exists a computable function $\hat{f}(x, s)$ such that $f_s(x) = \hat{f}(x, s)$ for all $x, s$.

Let $\{f_s(x)\}_{s \in \omega}$ be a computable sequence. Note that the least modulus is computable in any modulus. If $f = \lim_s, f_s$ and $m$ is any modulus, then

$$f \leq_T m$$

because $f_{m(x)}(x) = f(x)$. However, $m \leq_T f$ usually fails even for the least modulus. Remarkably, if $f$ has c.e. degree, then $m \leq_T f$ holds for some modulus $m$ of a particular computable sequence, as we prove in the following lemma.

**Modulus Lemma.** *If $A$ is c.e. set and $f \leq_T A$, then there exists a computable sequence $\{f_s\}_{s \in \omega}$ such that $\lim_s f_s = f$, and a modulus $m$ of $\{f_s\}_{s \in \omega}$, which is computable in $A$.* (see [8], p.56)

Let us present the Limit Lemma along with its proof, since it will be used in proving our theorem.

**Limit Lemma.** *For any function $f$, $f \leq_T A'$ iff there exists an $A$-computable sequence $\{f_s\}_{s \in \omega}$ (i.e., an $A$-computable function $\hat{f}(x, s) = f_s(x)$) such that $f = \lim_s f_s$.*

**Proof.** $(\Rightarrow)$. Let $f \leq_T A'$. Now $A'$ is c.e. in $A$. Hence, the $A$-computable sequence $\{f_s\}_{s \in \omega}$ exists by the Modulus Lemma relativized to $A$.

$(\Leftarrow)$. Let $f = \lim, f_s$. Define

$$A_x = \{s : (\exists t) [s \leq t \ \& \ f(x) \neq f_{t+1}(x)]\}.$$

Now $A_x$ is finite, and $B = \oplus_x A_x = \{(s, x) : s \in A_x\}$ is $\Sigma_1^A$ and hence $A$-c.e., so $B \leq_T A'$.

Thus, given $x$, we can $B$-computably (and therefore $A'$-computably) compute the least modulus $m(x) = (\mu s)[s \notin A_x]$. Hence, $f \leq_T m \text{ A} \leq_T B \oplus A \leq_T A'$.

In particular, $f \leq_T \mathbf{0}'$ if and only if $f = \lim_s f_s$ for some computable sequence $\{f_s\}_{s \in \omega}$. This will be the most useful characterization of degrees below $\mathbf{0}'$. Since not all degrees below $\mathbf{0}'$ are c.e., the following corollary selects those that are.

**Corollary of the Limit Lemma.** *A function $f$ has c.e. degree iff $f$ is the limit of a computable sequence $\{f_s\}_{s \in \omega}$, which has a modulus $m \leq_T f$* (see [8], p.57).

**Definition 7.** Given a finite set $A = \{x_1, x_2, \cdots, x_k\}$, where $x_1 < x_2 < \cdots < x_k$, the number $y = 2^{x_1} + 2^{x_2} + \cdots + 2^{x_k}$ is the *canonical index* of $A$. Let $D_y$ denote a finite set with canonical index $y$, and $D_0$ denote $\emptyset$.

**Definition 8.** $A \subseteq \omega$ is an *enumeration reducible* to a set $B \subseteq \omega$ ($A \leq_e B$) if there is c.e. set $W_z$ such that $A = \{n \mid (\exists e)[\langle n, e \rangle \in W_z \ \& \ D_e \subseteq B]\}$, where $D_e$ is the $e$-th finite set in canonical enumeration.

Thus, any $z$ and any $B$ determine a unique corresponding $A$ such that $A \leq_e B$ via $z$, namely $\{x \mid (\exists u)[\langle x, u \rangle \in W_z \ \& \ D_u \subseteq B]\}$. Hence, each $z$ determines a total mapping from $2^\omega$ to $2^\omega$. We call such mappings *enumeration operations* and denote the operator corresponding to $z$ as $\Phi_z$ (see [1], pp.146-147).
Every $T$-degree (of total functions) is a subcollection of some partial degree. If a partial degree contains a $T$-degree (of total functions), we call it a *total degree* (see [1], p. 280).

## 3. Results

In [1], Theorem13.XVIII is proved (announced by Medvedev [9]): $(\exists\psi)$ [$\psi$ *is not partial computable* & $(\forall f)[f \leq_e \psi \Rightarrow f$ *is computable*]] and the Corollary is presented: $(\exists\psi)$ [$\psi$ is not partial computable and $\psi$ is computably enumerable in $\mathbf{0}'$ and $(\forall f)[f \leq_e \psi \Rightarrow f$ is computable]] (see [1], pp. 280-281).

Let us prove the following Theorem.

**Theorem 1.** $(\exists\psi)$ [$\psi$ *is not partial computable* & $\psi \leq_T \mathbf{0}'$ & $(\forall f)[f \leq_e \psi \Rightarrow f$ *is computable*]].

**Proof.** Note that we identify functions with their graphs and define $f \leq_e g$ if $\tau(f) \leq_e \tau(g)$.
Recall that $\Phi_n(\tau(\psi))$ is the enumeration operator of index $n$. We use the following notation in the proof.
$\Phi_n(\psi)$ abbreviates $\Phi_n(\tau(\psi))$. (Thus $\Phi_n(\psi)$ is a set that may not be single-valued.) If $\Phi_n(\psi)$ is single-valued, we also abbreviate $\tau^{-1}(\Phi_n(\psi))$ as $\Phi_n(\psi)$. (Thus, for example, we can write $f \leq_e \psi \Leftrightarrow (\exists n)[f = \Phi_n(\psi)]$.)
At each stage $s$, we construct finite segments $\psi_{m,s}$ such that $\max(dom\ \psi_{m,s}) < s \ \& \ m < s$. The function $\psi$ will be called a *finite segment* if the domain of $\psi$ is finite. A finite segment will be called a *monotone extension* of $\psi$ if
$$\psi \subset \tilde{\psi} \text{ and } (\forall x)(\forall y)[[x \in dom\ \psi \text{ and } y \in dom(\tilde{\psi} - \psi)] \Rightarrow x < y].$$

The construction will be such that for any $s$ $(\forall m < s)(\forall n < s)[m < n \Rightarrow \psi_{n,s}$ is a monotone extension of $\psi_{m,s}$] and for any $m$ $(\exists s_0)(\forall s \geq s_0)(\psi_{m,s} = \psi_{m,s_0} =_{dfn} \psi_m)$ (since the construction uses the finite injury priority method).
We prove the theorem by obtaining the desired $\psi$ as the union of a sequence of finite segments $\psi_0, \psi_1, \cdots$, where $m < n \Rightarrow \psi_n$ is a monotone extension of $\psi_m$.
Note that the construction is such that the set $\{\langle m, s, x, \psi_{m,s}(x)\rangle \mid \psi_{m,s}(x) \downarrow\}$ is computable.
As a result, we will have $(\forall x)(\exists m_0)(\exists s_0)(\forall m > m_0)(\forall s > s_0) \psi \upharpoonright x = \psi_{m,s} \upharpoonright x$.
In the process of constructing $\psi$, stages are implemented to ensure that for any $n$, the function $\Phi_n(\psi)$ will ultimately be either computable or nontotal (if $\Phi_n(\psi)$ is single-valued).
Let us denote the number $n$ by $Q(k)$, if $k = 2n + 1 \ \vee \ k = 2n + 2$.
For any $n$, the finite segment $\psi_n$ is intended to work with the operator $\Phi_{Q(n)}$ or the function $\varphi_{Q(n)}$.

Let $v_1(n) = \max\{k \mid k \leq n$ & the actions taken (at stage $n$) concerning the function $\varphi_k$ are not canceled} (i.e., remains *valid* at stage $n$).

Let $v_2(n) = \max\{k \mid k \leq n$ & the actions taken (at stage $n$) concerning the operator $\Phi_k$ are not canceled} (i.e., remains *valid* at stage $n$).

If the actions taken (at stage $n$) concerning the operator $\Phi_k$ (the function $\varphi_k$) are canceled, we will briefly say, $\Phi_k$ ($\varphi_k$) is canceled (at stage $n$).

Stage 0. Let $\psi_0 = \emptyset$.

Stage $2n + 1$. *See* whether there exists $k \leq Q(v_1(2n))$ such that
$$\varphi_{k,2n}(\max(dom\,\psi_{2k,2n}) + 1) \uparrow \,\&\, \varphi_{2k,2n+1}(\max(dom\,\psi_{2k,2n}) + 1) \downarrow.$$
*If so,* then let $k_0$ be the least of such numbers and $p_0 = \max(dom\,\psi_{2k_0,2n})$.

We set $\psi_{2k_0+1,2n+1} = \psi_{2k_0,2n} \cup \{<p_0, \varphi_{k_0,2n+1}(p_0)+1>\}$.

Then we cancel $\varphi_k$ for all $k > k_0$ and $\Phi_k$ for all $k \geq k_0$.

*If not,* then let $\tilde{q} = \max(\{q \mid \varphi_q$ is not canceled at stage $2n\})$ and $p_1 = \max(dom\,\psi_{2\tilde{q}+1,2n}) + 1$.

We set $\psi_{2\tilde{q}+1,2n+1} = \psi_{2\tilde{q}+1,2n} \cup \{<p_1, 0>\}$.

(Stage $2n + 1$ ensures that $\psi \neq \varphi_n$; therefore, $\psi$ cannot be partial computable.)

Stage $2n + 2$. Substage (a). *See* whether there exists $k \leq Q(v_2(2n + 1))$ such that there exists a monotone extension $\tilde{\psi}$ of the segment $\psi_{k,n+1}$ such that $\Phi_k(\tilde{\psi})$ is not single-valued and $\max(dom\,\tilde{\psi}) < 2n + 2$.

*If so*, then let $k_0$ be the least of such members. Then we set $\psi_{k_0,2n+2} = \tilde{\psi}$ and go to stage $2n + 3$. (In this case, the actions taken (at stage $2n + 2$, substage (a)) concerning the operators and functions with numbers greater than $k_0$ are canceled.) *If not*, we go to substage (b).

Substage (b). **Notation**. $\mathrm{Div}(m, s)$ means that there exist a number $y$ and monotone extensions $\tilde{\psi}^1$ and $\tilde{\psi}^2$ of the segment $\psi_{m,s}$ such that the values of the functions $\Phi_{2m}(\tilde{\psi}^1)$ and $\Phi_{2m}(\tilde{\psi}^2)$ as partial functions, are defined and unequal for the argument $y$ & $\max(dom\,\tilde{\psi}^1) < s + 1$ & $\max(dom\,\tilde{\psi}^2) < s + 1$.

*See* whether there exists a number $k \leq Q(v_2(2n + 1))$ such that $\mathrm{Div}(k, 2n + 1)$.

*If so*, then let $k_1$ be the least of such numbers. Then set $\psi_{k_1,2n+2} = \psi_{k_1,2n+1} \cup \{<z, 0>\}$, where $z$ is the least of the numbers greater than all the elements of the domains of both the segment $\tilde{\psi}^1$ and the segment $\tilde{\psi}^2$. (In this case, the function $\Phi_{2k_1}(\psi)$ must be undefined at $y$, for, otherwise, $\psi$ could be used together with $\tilde{\psi}^1$ or else $\tilde{\psi}^2$ to provide a monotone extension $\tilde{\psi}$ of the segment $\psi_{k_1,2n+1}$, for which $\Phi_{2k_1}(\tilde{\psi})$ is not single-valued, contrary to the result of substage (a)). In this case, the actions taken (at stage $2n + 2$, substage (b)) concerning the operators and functions with numbers greater than $k_1$, are canceled.

*If not*, then let $\psi_{k_1,2n+2} = \psi_{k_1,2n+1}$. (In this case, $\Phi_{2k_1}(\psi)$ must be computable, if total, for it can be effectively computed by enumerating all monotone extensions of $\psi_{k_1,2n+1}$ and putting them through $\Phi_{2k_1}$.)

Note that according to the construction, at any stage $n$, the transition from the finite segment constructed at stage $n$ to the finite segment that will be constructed at stage $n+1$ occurs effectively (uniformly over $n$).

As already noted, we have defined $\psi =_{dfn} \bigcup_{i\in\omega} \psi_i$ (the definition of $\psi_i$ is given above).

Set $S_x = \{s \mid (\exists m)(s \leq m\, \&\, \psi_m \upharpoonright x \neq \psi_{m+1} \upharpoonright x)\}$.

Then $S_x$ is finite, just like $A_x$ in the proof of the Limit Lemma.

$\tilde{B} =_{dfn} \oplus S_x = \{\langle s, x\rangle \mid s \in S_x\}$.

$\tilde{B}$ is a computably enumerable set (similarly, the set $B$ in the proof of Limit Lemma is $A$- computably enumerable).

Then, given $x$, we can $\tilde{B}$ -computably (and therefore $\mathbf{0}'$- computably ) compute the function $\tilde{m}(x) =_{dfn} \{\mu x | s \notin S_x\}$. Hence, $\psi \leq_T \tilde{m} \leq_T \tilde{B} \leq_T \mathbf{0}'.$ ∎

## 4. Conclusion

In the above theorem from [1], when constructing the function $\psi$, to achieve nontotality of $\deg_e(\psi)$, actions were performed on the e-operators $\Phi_e$ (for any e), only one stage was sufficient to complete the necessary actions on each specific $e$-operator. In the proof given in this article, a much larger (but finite) number of stages may be required to complete the necessary actions on each specific $e$-operator.

This modification of the proof allows us to substantially strengthen the results of the corollary of the mentioned theorem. The results are presented in more detail in Section 3.

## References

[1]    H. Rogers Jr., *Theory of Recursive Functions and Effective Computability*, McGraw-Hill, 1967.

[2]    R. M. Friedberg and H. Rogers Jr., *Reducibility and completeness for sets of integers*, Zeitschrift für mathematische Logik und Grundlagen der Mathematik 5, pp. 117–125, 1959.

[3]    J. Myhill, "Note on degrees of partial functions", *Proceedings of the American Mathematical Society* 12, pp. 519–521, 1961.

[4]    A. L. Selman, "Arithmetical reducibilities"*, I, Zeitschrift für mathematische Logik und Grundlagen der Mathematik* 17, pp. 335–350, 1971.

[5]    M. I. Soskova, *The theory of the enumeration degrees, definability, and automorphisms*, Contemporary Logic and Computing. Adrian Rezus, editor. College publications, pp.706-730, 2020.

[6]    S. Lempp, Th. Slaman and M. I. Soskova, "Fragments of the theory of the enumeration degrees", *Advances of Mathematics*, vol. 383, no. 4, pp.107686, 2021.

[7]    H. Ganchev, I. Kalimullin, J. S. Miller, and M. I. Soskova, "A structural dichotomy in the enumeration degrees", *J. Symb. Log.*, vol. 87, no. 2, pp. 527-544, 2022.

[8]    R.I. Soare, *Recursively Enumerable Sets and Degree: A study of computable functions and computably generated sets*, Perspectives in Mathematical Logic, Springer-Verlag, 1987.

[9]    Yu. T. Medvedev, *Degrees of difficulty of the mass problem* (in Russian), Doklady Academii Nauk SSSR, vol. 104, pp. 501-504, 1955.

# Ո՞չ տոտալ մասնակի աստիճանի գոյության ապացույցի և այդ մասնակի աստիճանի ներկայացուցչի թյուրինգյան աստիճանի մասին

Արսեն Հ. Մոկացյան

ՀՀ ԳԱԱ Ինֆորմատիկայի և ավտոմատացման պրոբլեմների ինստիտուտ, Երևան, Հայաստան
e-mail: arsenmokatsian@gmail.com

## Ամփոփում

Հայտնի է, որ ամենուրեք որոշված ֆունկցիաների $e$-աստիճանների կարգավորումը իզոմորֆ է $T$-աստիճանների կարգավորմանը: Հնարավոր է ըստ $=_e$-ի համարժեքության դասեր ձևավորել նաև բոլոր ֆունկցիաների (պարտադիր չէ ամենուրեք որոշված) ամբողջության մեջ: Ստացված $e$-աստիճանները անվանվում են *մասնակի աստիճաններ*:

Հ. Ռոջերսի «Ռեկուրսիվ ֆունկցիաների տեսություն և էֆեկտիվ հաշվարկելիություն» գրքում [1] ներկայացված են ո՞չ տոտալ մասնակի աստիճանի գոյության ապացույցը և այդ պնդման հետևությունը:

Տվյալ հոդվածում ներկայացված է վերոհիշյալ թեորեմի ապացույցի մոդիֆիկացիան, ինչը թույլ է տալիս էականորեն ուժեղացնել թեորեմի հետևության արդյունքները, այսինքն՝ ապացուցել, որ (∃$\psi$)[$\psi$-ն մասնակի հաշվարկելի չէ & $\psi \leq_T \mathbf{0}'$ & ($\forall f$)[$f \leq_e \psi \Rightarrow f$ հաշվարկելի է]] (վերոնշյալ հետևության մեջ նշվում է, որ կառուցված ֆունկցիան ընդամենը հաշվարկելիորեն թվարկելի է ըստ $\mathbf{0}'$-ի):

**Բանալի բառեր՝** $e$-հանգեցում, մասնակի աստիճան, մասնակի հաշվարկելի ֆունկցիա, թյուրինգյան աստիճան:

# О доказательстве существования нетотальной частичной степени и о тьюринговой степени представителя этой частичной степени

Арсен А. Мокацян

Институт проблем информатики и автоматизации НАН РА, Ереван, Армения
e-mail: arsenmokatsian@gmail.com

## Аннотация

Известно, что упорядочение $e$-степеней всюду определенных функций изоморфно упорядочению $T$-степеней. Можно образовать классы эквивалентности относительно $=_e$ и

в совокупности всех функций (не обязательно всюду определенных). Полученные при этом *e*-степени называются *частичными степенями*.

В книге Х. Роджерса, *"Теория рекурсивных функций и эффективная вычислимость",* [1] дано доказательство существования нетотальной частичной степени и приведено следствие из этой теоремы.

Статья содержит модификацию доказательства теоремы, приведенной выше, которая позволяет существенно усилить результаты следствия, а именно доказать, что $(\exists\psi)$[функция $\psi$ не является частично рекурсивной & $\psi \leq_T \mathbf{0}'$ & $(\forall f)[f \leq_e \psi \Rightarrow$ функция $f$ рекурсивна]] (в приведенном выше следствии отмечено, что построенная функция всего лишь рекурсивно перечислима относительно $\mathbf{0}'$).

**Ключевые слова:** *e*-сводимость, частичная степень, частично рекурсивная функция, тьюрингова степень.

# Adequacy and Application of Models of Cognizing by Combinatorial Games

Sedrak V. Grigoryan and Zaven H. Naghashyan

Institute for Informatics and Automation Problems of NAS RA, Yerevan, Armenia
e-mail: sedrak.grigoryan@iiap.sci.am, znaghash@gmail.com

## Abstract

We aim to provide constructive adequate models of human cognizing of the Universe. Arguing that combinatorial games are adequate models for studying human-universe problem, we introduce a class of Reproducible Game Trees (RGT) combinatorial games, generally, not limited in the representation of competitive, defense and communication problems.

We develop expert knowledge-based RGT Solver for unified searching of plausible RGT strategies arguing that such strategies are transferable to the entire RGT class.

We estimate the adequacy of models of cognizing, particularly, by progressing in solving RGT problems, which simultaneously provide solutions for urgent applications.

In this work, we outline our RGT approach to arguing the adequacy of cognizing models to the human one and bring together successful applications induced by such arguing.

**Keywords:** Modeling cognizing, Combinatorial games, Intrusion protection, Defense strategies, Marketing, Learning, Meaning processing.

**Article info:** Received 6 October 2024; sent for review 15 October 2024; accepted 26 November 2024.

## 1. Introduction

Following the founders of computer science [1, 2], we interpret Artificial Intelligence as a branch of science aimed to provide adequate constructive models of cognizing, at least, comparable by effectiveness with those of humans.

Our model of cognizing roots in developmental psychology by Jean Piaget [3], follows researchers in modeling cognizing by solvers of combinatorial games [4, 5, 6], enriches object-oriented representatives of realities by input classifiers and relationships in English, while tends to be consistent with questioning the origination of cognizing in nature [7].

Letś outline our approach to arguing the adequacy of models of cognizing to human ones, followed by comprising our successful applications of the models induced by arguing this adequacy.

1.1. We examine the adequacy of our models following Churchś idea, that the hypothesis on the adequacy of models is examined empirically until they are refitted by some interpretations of models or other alternative models not equal to the original ones [8].

We overcome the barrier of studying the incredibly complex Human-Universe problem by approximating it with game models [6, 7]. We assume that

- Combinatorial games with known hierarchies of utilities and solutions in spaces of possible strategies in game trees can represent the Human-Universe (HU) problem with proper adequacy.

- HU is a contemplation of problems, where the unsolved ones appear to be identified as combinatorial ones.

- Human cognizers are positioned as universal means of solving new problems appearing, as a rule, in combinatorial modes.

Then, we narrow HU to the Solvers of problems represented as Reproducible Game Trees (RGT) with only a few requirements to belong to: - there are (a) interacting actors (players, competitors, etc.) performing (b) identified types of actions at (c) specified moments of time and (d) specified types of situations, - there are identified benefits for each of the actors, - situations, in which the actors act and in which are transformed after the actions, can be specified by certain rules, regularities.

We argued [7, 9] that RGT problems and RGT Solvers are constructively regularized, are models of HU and human cognizers, correspondingly, moreover, computer models of RGT Solvers can be developed to become their adequate models.

We also argue that

- RGT, first of all, embrace combinatorial problems, have no visible limits on their enrichment up to ones of HU.

- RGT Solvers demonstrate an ability to successfully involve models of any means of cognizing of human cognizers to resolve RGT.

- RGT problems are reducible to each other, particularly, to some standard kernel RGT problem K, thus, we get an opportunity to integrate the best-known achievements in solving particular RGT problems into the entire RGT class, i.e., letting us apply those achievements to any of RGT one, as well as experimenting with particular RGT problems [10, 11].

1.2. RGT studying in a variety of modes have successfully been started since 1957 at the Institute for Informatics and Automation Problems of the Academy of Sciences of the Republic of Armenia

In what follows we bring together the descriptions of some successful applications of our models of cognizing induced by arguing their adequacy by RGT games and mainly attained since 2003 [7].

The applications include urgent problems of combinatorial nature in network protection from various types of intrusions by hackers, problems of decision-making in battlefields, marketing (oligopoly competitions) and management (supply chain management), chess and chess-like problems, etc., that can be reduced to RGT ones [11, 12, 13, 14, 15, 16, 17, 18, 19, 20].

## 2. Problems of Computer Network Protection Against Various Attacks

The game tree model for Intrusion Protection, in brief, is presented as a game between two playing in turn sides with opposite interests - the attacker (A) and the defender (D) playing in turn. The game is described by a set of states and a collection of conversion procedures from one position to another. The main goals of the attackers and defenders are to bring the system in critical states and avoid them, correspondingly. The counteraction game model is represented by AND/OR game. At first, the attacker moves from the initial state s0 S then the defender replies in turn. Thus, the initial node s0 is an AND type. The terminal nodes correspond to the winning states of the defender [13, 21].

IGAF1 and IGAF2 algorithms were proposed, which, based on common knowledge planning and dynamic testing provided decision making for defender against attackers, while expert knowledge utilized in the decisions was acquired in the form of goals and rules.

The decision-making algorithms consisted of the following general steps:

1. Standard min-max technique with alpha-beta pruning was used, based on the range of critical/normal state values introduced as the goal 1. A current node is created and the value of its local state calculated. If the node is terminal, the local state value is compared with sibling nodes, and their max (or min) value is sent to the parent node.

2. Determines all suspicious resources.

3. Builds the game subtree for suspicious resources starting from the root state of the tree and using certain rules that determine the trajectories of attacks.

4. Calculates the values of the terminal states of the tree, finds the values of others by min-max procedure and determines the best min-max action from the root state.

5. Determines the trajectories of attacks induced by the best action from the root of the tree to its critical states and considers them as targets.

6. Builds the zones of counteractions for the target trajectories using the cetrain group of rules, then calculates the values of the states of the corresponding subtree using the minmax.

7. Chooses the defenders action from the root as the one leading to the state with min value, i.e., to the most stable state estimated by the minmax.

8. Ends the defense analysis and waits for the attackers actions.

The provided approach concluded with the following remarkable results:

The viability of the IGAF algorithm was successfully tested in the network intrusion protection problems against the representatives of four classes of attacks: SYN-Flood, Fraggle, Smurf and Login-bomb, allowing to formulate the following statements:

- Sampling means for Distance to Safety and Productivity of the IGAF and min-max algorithms are compatible.

- The number of nodes searched by the IGAF algorithm with all expert rules and sub-goals is decreasing compared with other algorithms and the minimax one.

- The number of nodes and the time searched by the IGAF algorithm with all expert rules and sub-goals is the smallest compared with the number of nodes generated by existing at the time known solvers of the same problem.

- IGAF algorithms with all expert rules and sub-goals, for the depth of search 5 and 200 defending steps are overperforming the Productivity of min-max algorithm by 14 percent, using for that 6 times less computing time and searching 27 times less nodes of the tree.

## 3.   Problems of Ship Defense Against Air Threats

The scenario involves two parties designated defense and threats, respectively. Each party contains players. Each player responds to the actions taken by the opposite party. The defense party has a single player, i.e., the ship. The threats party may have several players in the form of missiles and aircrafts. The types of threat players can be regrouped into categories, e.g., missiles of type xxx, aircrafts of type yyy. An additional category can be defined for threat players whose type is uncertain.

In the simplified scenario, all the threat players belong to a single category of missiles. Several threat players may attack concurrently. The threat players are generated as follows:

- All threat players are created at the start of the scenario.

- The maximum number of threat players is max threats N = 8.

- The initial position of each threat is uniformly and randomly selected in an area of space satisfying the conditions: - Initial range of 5 to 80 km from own ship, - Polar angle between 0o and 90o (i.e, angle in the vertical plane), - Any azimuthal angle (i.e., angle in the horizontal plane).

Assumptions:

1. It is assumed that the threats are ranked by the defense player. In the simplified scenario, the ranking function is the range: the closer the threat, the higher the rank of the threat.

2. It is assumed that the defense player may bundle up concurrent defense actions. The admissible bundles must satisfy the engagement rules.

3. A bundle of defense actions must ensure that only one defense action per threat is undertaken at any given time. Each action results in a transformation in the scenario. The sets of defense actions, defense bundles, threat actions, and their associated transformation rules are assumed to be finite and known.

The objective of a defense strategy is to prescribe a unique defense bundle for every admissible threat action.

The game tree describes all the admissible sequence of threat and defense responses. The branching in the game tree is generated by the capabilities of the players and the uncertainties in the game, i.e., branches are created for:

- each category of threat and defense players,

- each admissible defense and threat bundle of actions,

- each possible outcome of the transformation rules (when the outcome of a response is uncertain).

With some certain steps applied to defensive actions, the following types of defense actions were revealed:

- launch a long-range surface-air missile,

- shoot the medium-range gun,

- shoot the short-range gun

The proposed scenario for the defense of the ship leads to the following main conclusions for this problem in [15].

For the case when waiting conditions are ignored search time in the NGT for the best strategies is significantly less compared with those for the TABU system [22].

It is shown that the solution of the game tree for deliberative planning maximizes the probability of survival of the own ship with concerning worst-case situation.

Scenarios with up to 8 threats are considered. Monte Carlo simulations are employed to statistically assess the benefits of the proposed deliberative planning.

## 4.   Graphical Language Interpreter for RGT Problems

Human-computer interaction (HCI) has been a pivotal aspect of computer science since its inception, evolving significantly over the decades to accommodate more intuitive and efficient modes of interaction between humans and machines. Initially, computers operated strictly on machine code, a form of communication that was cumbersome and unintuitive for human operators. This barrier was partially alleviated by the introduction of assemblers, which translated more accessible, albeit still technical, instructions into machine code. The development of procedural languages further shifted HCI towards a more human-centric approach, adopting notations akin to those used in mathematics and physics to facilitate a clearer expression of ideas.

The advent of object-oriented programming marked a significant milestone, establishing a new industrial standard that mirrored human thought processes more closely. By organizing software design around concepts, their relationships, and interactions, object-oriented languages enabled programmers to model complex systems in a manner more aligned with human reasoning. The next frontier in HCI aimed to bridge the gap between human and computer communication through natural language processing, epitomized by developments such as ChatGPT [23]. This AI-driven approach has garnered popularity for its ability to understand and generate human-like text, making interactions more seamless and intuitive.

Despite these advancements, the research underscores a crucial aspect of human cognition: visual processing. Humans predominantly interpret and assimilate information through visual means, not just verbal or textual interactions. Consequently, the research emphasizes the importance of visual languages in HCI, advocating for enhanced visual representations of concepts to align more closely with human cognitive processes. This visual approach not only complements the textual and verbal advancements but also enriches the interaction, making it more holistic and reflective of human informational intake and processing.

To combine the existing efforts in the direction and enable utilizing the achievements in a generic Solver of RGT problems, a common graphical interface was developed [24].

By analyzing about 100 chess concepts, about 4 general construction blocks were identified using which it is possible to represent communicable concepts. They are classifiers (primitive, composite), relations, sets and actions.

Classifiers - there can be 2 types of classifiers - primitive and composite.

- Primitive classifiers - extend the initial classifiers by narrowing the range that can be matched.

- Composite classifiers - compose primitive any types of classifiers, sets and actions.

- Relations - units of knowledge that represent general relations between instances of classifiers.

- Sets - units of knowledge that are used for matching several instances of classifiers.

- Actions - units of knowledge that describe transformations of situations and their components

- instances of concepts.

1. The Knowledge Base module of the RGT Solver package is developed that allows representing, modifying and removing classifiers.

2. A graphical language for the graphical representation of construction blocks and their compositions is developed.

3. A graphical user interface, which provides graphical tools for representing the graphical language units is developed.

4. The viability of the approach and program was proved by experimenting with the representation of about 100 chess concepts and by representing chess concepts for the solution plan of Reti Etude. The method can be divided into the following steps:

- The expert analyzes the new concept and finds out the lower-level concepts and relational rules that are enough to represent the original concept.

- As the next step, the expert checks whether the lower-level concepts already exist in the system. If some lower-level concepts are not represented in the system, the expert tries to represent the corresponding concept by decomposing it into more primitive ones. The process continues until all the lower-level concepts are represented.

The framework for representing communicable lexical units for expert strategies of the RGT class was developed:

- For known types of personalized expert strategies of the RGT class the framework for representing and acquisition is developed.

- OOP constructions [25] and software for representing the variety of strategy knowledge of the RGT problems, interaction and modification are developed and realized. The graphical language interpreter and interface for the formation and acquisition of expert strategies in a regular way is designed and realized in extended Java language.

- The viability of the interpreter, interface and substantiation for the RGT problems is experimentally approbated for expert knowledge intensively using chess problems.

## 5. Knowledge Presentation, Acquisition and Matching Algorithms

5.1. In [10], the role and proportion of personalized expertise in comparison to common, communicable expertise were examined using chess, a typical representative of the RGT class. Expert requests to the game storage in natural language were simulated and analyzed to identify winning strategies of specified types. A correspondence was revealed between approximately 300 units of chess vocabulary and the Zermelo classes of chess positions and strategies, which argued for the constructive nature of these vocabulary units, thereby, in principle, allowing for their simulation. However, it was also stated that any real implementation of such content could only approximate the original winning game tree structures, due to the prohibitive computational complexity required to prove the correctness of the majority of the content. This provided a measurable precedent of human expertise specification, where the learned contents of realities that share the same vocabulary are, as a rule, essentially personalized.

5.2. Following successful results in developing generic graphical language and unified mechanisms for RGT problem knowledge interpretation and interface, studies were conducted to provide enhanced and generic knowledge presentation and storage mechanisms, along with matching algorithms. All these elements were designed to be adequate those of experts [18, 19].

A model has been built for the representation of classifiers analogical to Be- Have- Do dimensions of English grammar. Models of knowledge in RGT Solvers can be presented as a network of classifiers. It continuously acquires the defined classifiers into the internal network - Network of classifiers (NCl) by finding and constructing appropriate be-, have- or do connections with already existing nodes of Network.

The acquisition of knowledge leads to having different types of NC nodes:

NT - Nucleus Type, the types of the smallest representation units of knowledge. They compose the set of NA roots. The construction of more complex classifiers is started with them.

NC - Nucleus classifiers, the instances of Nucleus Types with additional restrictions (they represent the subset of the value of the types).

CR1 - Classifiers that hold a level between the nucleus and composite classifiers. In other words, a CR1 represents the description of a position in a space.

CC - Composite Classifiers, the most common form of the classifier representation. They are composed of any other Classifier types and are able to represent all kinds of regularities.

SC - Sets are composed of a single composite classifier element and a rule specifying the number of elements in the group.

Action - The following nodes are the only ones that represent actions in the NCl.

VC - Virtual Classifiers, which have undefined values for their attributes (in parallel with OOP virtual classes). Consequently, they inherit almost all the advantages of OOP interfaces (polymorphism, etc.).

The model for presenting and storing (store of prints) situations has been developed as a list of groups of contiguous nucleus attributes, referred to as CR1 instances. The store of prints has been modeled as a composition of t-prints and delta-prints. The former is a
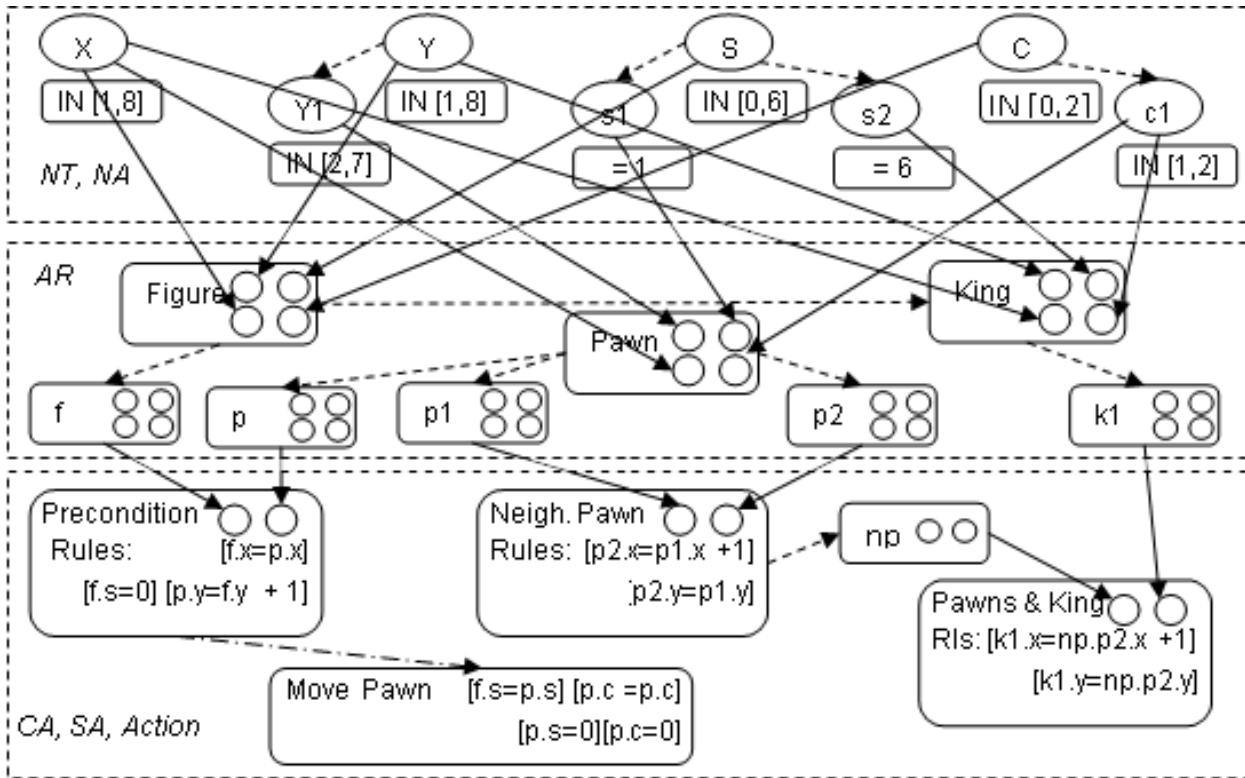
Figure 1: A fragment of a Network of Classifiers for the example of chess representing Be (dense), Have (dashed) and Do (dot-dashed) connections

snapshot of the perceived universe at a time t and is represented as a bunch of cr1 instances, while the latter is the difference between prints at time t+1 and t.

Algorithms have been developed in the generic RGT Solver, which triggers the matching of classifiers to situations by iterative matching of sub-classifiers via processing t-prints constituents over the network of classifiers. It is an adaptation of a classical CSP (constraint satisfaction problem) solving the Rete algorithm [26]. Distinct matching procedures have been developed for different types of nodes categorizing them into filtering and conjunction nodes. 5.3. To transform natural presentations of situations to RGT Solvers symbolic presentation, methods were proposed [27], using Neural Networks for classification and detection [28] of units, applicable to RGT problems, particularly to chess [27] and battlefield [29] scenarios. The chess scenario provides algorithms based on the classifiication and detection of chess units from the given images and the construction of the chess situations, accordingly. The battlefield scenario extends and continues the approach developed in the chess scenario, providing processing and classification of military units on UAV-based images.

## 6.   Decision Making by Personalized Planning and Integrated Testing

Following the approach described in [30, 14] as well as in the above sections, algorithms for decision-making were developed based on personalized planning and integrated testing (PPIT), which enhanced the proposed algorithms making them generic and integrating effective knowledge-based goals searching algorithms of trajectories-zones technique (TZT) as well as initially proposed by Botvinnik [30]. Decision-making is interpreted as strategy

searching and proposing actions for the given RGT situations [16, 31].

Thus, in PPIT decision making algorithms, we deal with plans, which are lists of goals by their priorities, while goals consist of a) precondition describing the situations where the goal can be applied; b) postcondition describing the final situation where the goal is achieved; c) depth describing the depth of the tree to be generated for processing the goal; d) criteria describing the situation after of postcondition to show how good the goal is achieved. PPIT algorithms consist of the following mean steps: Reducing Hopeless Plans (RHP), Choosing Plans with Max Utility (CPMU), Generating Moves by a Plan (GMP).

Action selection with TZT algorithms for a given goal is described in [32] which considers the trajectories of attack and zones of counteractions: a. Generation of a tree of situations with the defined depth that leads to goal achievement, b. Extension of situation chains by all possible counteractions by the opponent, and possible actions to intercept the counteractions, c. Checking if the goal can be achieved and evaluation if defined.

The adequacy of PPIT algorithms was demonstrated on chess etudes suggested by Botvinnik as tests for such decision-making frameworks as well as in other RGT problems, e.g., management, battlefield, testing of programs [32, 33, 41].

The experiments effectively cover the adequacy and effectiveness of the provided package modules described in Chapters 4 and 5, wrapping the main components of the system for generic RGT Solvers.
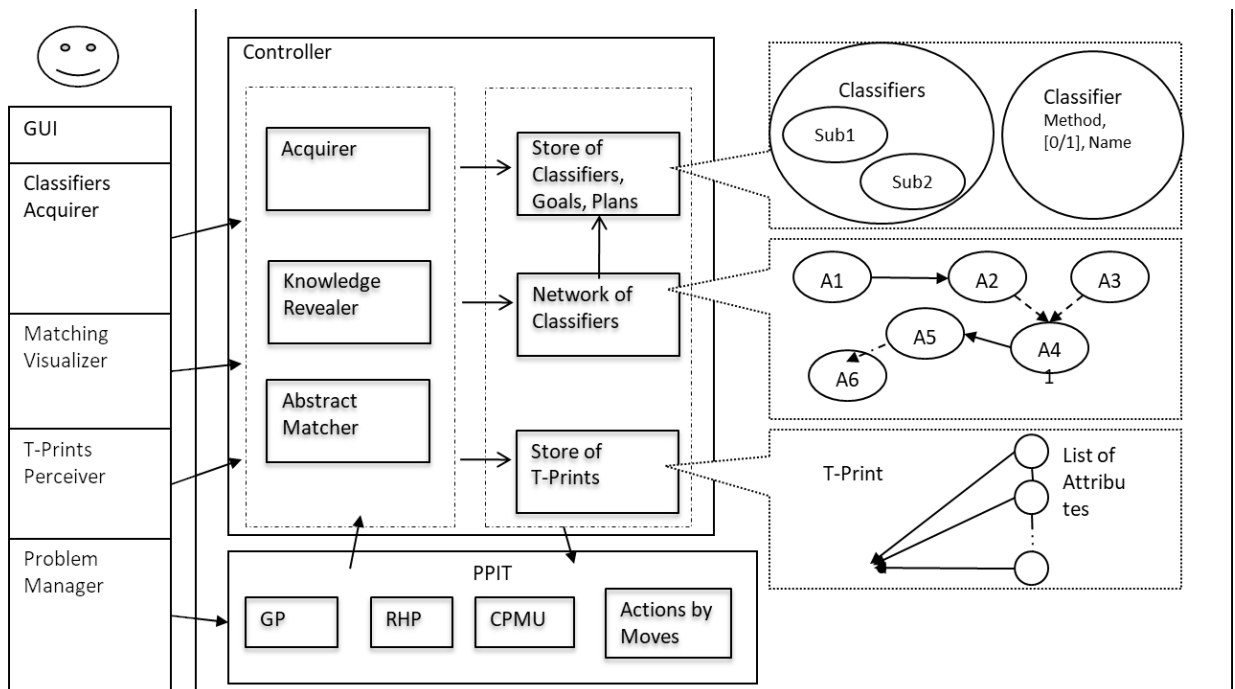


Figure 2: Generic structure of RGT Solvers

## 7.  Testing Programs

The problem of testing programs was reduced to RGT class as follows [33]:

- The actors in software testing are the tested program and the tester.

- The actions are any valid elementary operations that can be performed with the program. While building the game tree, the Solver dynamically combines these actions, creates test cases and executes them depending on the response of the program.

- The situations are the current states of the program. We can estimate the current situations with [0;1] numbers, where 0 means that no bugs were found, 1- that the program is in a critical state and is not usable. The numbers in between 0 and 1 are intermediate values and situations with values closer to 1 are worse than situations with values closer to 0.

In the scope of the research, the following results were achieved:

1. Tools defining types of knowledge testing of the target application were described. The described knowledge was integrated into RGT Solver and used to run test cases and test scenarios with later evaluation of test results.

2. An approach for evaluating the state of the program during the testing was proposed.

3. The adequacy of the proposed approach was experimented with the open-source Blender application.

4. The proposed approach solves the drawbacks of the model-based testing approach [35], namely, allows to generate test cases dynamically.

## 8.  Battlefield Problems

Following achievements in the games of strategy video games and modern UAV-based solutions the research was initiated to transfer battlefield problems into generic RGT Solvers and apply its achievements for decision-making and autonomy integration [29, 41].

The battlefield problems were interpreted as RGT problems as follows:

- The battling sides can be considered as interacting actors

- Military units' movements and attacks can be considered as actions

- The battlefield areas with the military units involved, can be considered as situations

- As goals, different situations can be considered, such as: capturing objects, destroying enemy units, pushing the frontline, holding the defense, etc.

The following results were achieved at the current state of the research:

1. Processing of aerial images to detect 8 military unit classes based on the constructed model. The training dataset of the model represents 8 classes of military unit groups defined by experts.

2. Certain expert-defined classifiers were integrated for proper processing of target selection algorithms.

3. Algorithms were developed to select the target based on input images, objects classified according to them, and the knowledge of the field.

4. Experiments on low-power computing devices demonstrated close to real-time processing efficiency. The solution effectively covers aerial image-based decision-making for a single UAV.

5. Situations for battlefield presentation were provided for RGT Solvers representing a certain composition of battlefield essential nuclear classifier instances.

6. Decision-making algorithms of PPIT and TZT available in RGT Solvers are applied to propose actions for the given situations.

## 9. Communication and Interaction with RGT Solvers

9.1. A group of urgent tasks in RGT Solvers and in expert systems, in general, relate to interaction and communication, particularly problems of acquisition of knowledge from available sources[36], explanation of acquired knowledge, etc. Studies in this direction were conducted. The research concluded in several directions, particularly: 9.2. Tools for testing and correction of the completeness of knowledge acquisition by autistic children were proposed [37], where the peculiarities of 10 years of successful training of an autistic child were considered and some patterns of positive tutoring of children both autistic and ordinary were extracted possible to realize in RGT Solver. The successive approaches to chess-based tutoring and testing were discussed. The assertions on conditions of positive outcomes of tutoring the communalized and personalized meanings of chess concepts were argued and the ways of their implementation by the Solver were considered. Finally, the perspectives of development of the Solver for tutoring the basics of Math, pre chess, testing and tutoring strategy knowledge were discussed.

9.3. Personalized interactive tutors for chess were developed [38, 39] with the following main results:

- Method and software for tutoring chess were developed in the frame of RGT Solvers, external tools were implemented providing students with the following advantages:

  1. The software provides personalized tutoring mechanisms for different types and levels of students and their performances.

  2. The software is interactive making level-by-level tutoring of chess concepts, their testing, with feedback provision and correction with detailed description.

- The designed algorithm and software are validated by testing them on tutoring for chess endgames.

9.4. Algorithms for automating acquisition and explanation of RGT strategy knowledge were developed [40]:

- Algorithms for extracting RGT knowledge from texts were developed and discussed, which included classifiers learning from strictly formatted texts, particularly virtual classifiers, as well as approaches for overcoming strict format restrictions, were discussed and some solutions were shown.

- Meantime enhancement of acquisition of classifiers by examples, using neural networks is performed, which allows adequate demonstration and learning from images, a way

of natural presentation of classifiers, as well as allows using these classifiers to properly demonstrate examples when explaining them.

- Algorithms for explaining acquired by RGT Solvers knowledge by texts were provided, which, based on the HBD model of knowledge presentation allows providing texts for RGT classifiers using have, be and do dimensions of English.

- Experiments to validate the algorithms were conducted for chess classifiers.

9.5. To advance in meaning processing, particularly, Text-Meaning-Text transformations problems, we aim to advance in Learning Expert Meaning Processing (LEMP) and consider this problem in the scope of the RGT class [41].

At first, we consider the interaction with natural language as usage for expert knowledge, and attempt to advance in LEMP in RGT Problems for a kernel RGT problem, e.g., chess. This task includes tasks, such as Natural Language Processing (NLP) for the entire Natural Language reduced to NLP for urgent essential RGT class, then reduced to a seed of RGT (chess) language processing.

9.5.1. The following subtasks are covered for the kernel problem:

- Preparing a Repository of RGT expert classifiers for the kernel RGT problem and ordering them by the complexity of learning by RGT Solvers.

- Advancing in learning expert classifiers by stages 1, 2, ... of their complexity

- Confirming workability of at the time already RGT Solver learned classifiers, particularly by demonstration of abilities of learning, identification of realities, meaning to text to meaning transition.

- Enhancing the versions to identify more realities and to provide better meaning to text to meaning transition.

9.5.2. Focusing on the chess RGT problem, 5 levels of chess classifiers were revealed (initial level and 1-4 main levels) and successfully acquired by RGT Solvers, particularly 1-3 levels of chess classifiers described, particularly, in [7] were acquired by Solvers and matched to chess situations confirming their workability for 100 various chess classifiers.

The initial level of classifiers represents the basic types similar to OOP built-in types, in this case, we start definition with coord x and coord y, figure type, figure color, then expand to field, figure and specific figure types, such as pawn, knight, etc. Some of the other classifiers acquired by the Solvers are:

1st level: vertical, diagonal, phalax of knight and pawn, etc.

2nd level: field under the attack of a pawn (either black or white), passant pawn, doubled pawn, etc.

3rd level: phalax of pawns in the center of the board, hit or defense by a figure (e.g., by knight), etc.

Results demonstrate the adequacy of chess classifiers acquired by the Solver to expert ones and the above-mentioned solutions can be used to transform to texts for explanation.

The successful results then can be used for:

- Expanding to the whole class of RGT.

- Expanding the results of the first and second stages to the natural language content.

## 10. Conclusions

10.1. We have observed some successful applications of our models of cognizing by arguing their adequacy through RGT games, with those achievements mostly occurring since 2003. Particularly, they include:

- Intrusion protection problem: an urgent problem in the field of information technologies, was successfully modeled as an RGT problem and the provided Solvers overcame the existing at the time approaches in providing a successful defense of the network again various types of hacker attacks.

- Single ownship defense: the problem was successfully modeled as an RGT problem and Solvers for the task of defending their own ship against specific known types of missile attacks were developed providing evidence of the approach maximizing the probability of the ownship survival.

- Generic Solver was developed that utilizes the following main components: 1. Advanced graphical language interpreter that allows users to insert RGT classifiers with specified types, 2. A network of classifiers was developed to present and store RGT classifiers in the form of a network based on the HBD language model and matching algorithms were developed to match these classifiers to RGT situations, 3. Decision-making algorithms were developed based on PPIT planning and TZT goal-searching algorithms. Interfaces for various RGT problems were developed.

- Testing of programs was successfully interpreted as an RGT problem, where a new approach for evaluation of testing program state was proposed. The adequacy of the approach was experimented on open-source applications and overcame some drawbacks of the popular model-based testing approach.

- Battlefield problems were interpreted as RGT problems, based on aerial images, where certain classes of military units were defined and the approach demonstrated adequacy to the experts of the field providing effective autonomous decision-making based on expert knowledge utilizing RGT Solver capabilities.

- To enhance the experience of communication with RGT Solvers, problems of communication were researched. 1. A personalized interactive tutor for chess was developed with comprehensive tutoring abilities. 2. Algorithms were developed to extract RGT knowledge from texts and vice versa: to convert RGT knowledge to texts. 3. The LEMP problem was considered as an interpretation of the NLP problem and certain levels of kernel RGT problem classifiers were identified and successfully acquired by the solver, while being adequate to human classifiers, allowing them to transform to human-understandable texts and applying explanation algorithms to interact with humans.

- Many more urgent problems were interpreted and successfully researched as RGT problems, such as the detection of anomalies in big data, problems in marketing and management, diagnoses of specific diseases, etc.

10.2. Note, that some other urgent problems were also interpreted as RGT problems and successfully resolved, including detection anomalies in big data, problems of marketing and management, diagnoses of specific diseases, etc. [20, 12, 37].

10.3.   Future improvements in general Solvers based on these foundations, expanding their capabilities in learning expert meaning processing can allow them to easily acquire domain expert knowledge, evolve into comprehensive assistants that not only search for optimal strategies combinatorial problems of the class but also interact with users across a wide range of domains of the class. Continuous research and development in this direction is in progress.

# References

[1]  T. Burge and H. Enderton, *The Collected Works of Alonzo Church*, MIT Press, Cambridge, MA, USA, 2019.

[2]  A. Turing, "Computing machinery and intelligence," *Mind*, vol. 49, reprinted in *Minds and Machines*, A. Anderson (ed.), Engelwood Cliffs, NJ, 1950.

[3]  J. Flavell, *The Developmental Psychology of Jean Piaget*, D. Van Nostrand Comp. Inc., Princeton, 1962.

[4]  R. Benergji, *Theory of Problem Solving*, Elsevier, 1969.

[5]  J. E. Laird, A. Newell, and P. S. Rosenbloom, "Soar: an architecture for general intelligence," *Artificial Intelligence*, vol. 33, no. 1, pp. 1–64, 1987.

[6]  E. Pogossian, "Adaptation of combinatorial algorithms," *Academy of Sciences of Armenia*, 1983.

[7]  E. Pogossian, *Constructing Models of Being by Cognizing*, Academy of Sciences of Armenia, Yerevan, Armenia, 2020.

[8]  E. Pogossian, "Artificial intelligence: alternating the highest human cognizing," in *Proceedings of International Conference of Computer Science and Information Technologies 2019*, pp. 36–40, Yerevan, Armenia, 2019.

[9]  E. Pogossian, "Specifying adequate models of cognizers," *AIP Conference Proceedings*, vol. 2757, no. 1, article 020003, 2021. doi:10.1063/5.0135909.

[10]  E. Pogossian, "Specifying personalized expertise," in *International Conference of Cognition and Exploratory Learning in Digital Age*, pp. 151–159, Barcelona, Spain, 2006.

[11]  S. Grigoryan, "On validity of personalized planning and integrated testing algorithms in reproducible games," in *Proceedings of International Conference of Computer Science and Information Technologies 2015*, pp. 317–321, Yerevan, Armenia, 2015.

[12]  E. Pogossian, "Focusing management strategy provision simulation," in *Proceedings of International Conference of Computer Science and Information Technologies 2001*, Yerevan, Armenia, 2001.

[13]  E. Pogossian, A. Javadyan, and E. Ivanyan, "Effective discovery of intrusion protection strategies," in *Workshop on Agents and Data Mining*, pp. 263–274, St. Petersburg, Russia, 2005.

[14] E. Pogossian, V. Vahradyan, and A. Grigoryan, "On competing agents consistent with expert knowledge," in *Workshop on Autonomous Intelligent Systems - Agents and Data Mining*, St. Petersburg, Russia, 2007.

[15] E. Pogossian, D. Dionne, A. Grigoryan, J. Couture, and E. Shahbazian, "Developing goals directed search models empowering strategies against single ownship air threats," in *Proceedings of International Conference of Computer Science and Information Technologies 2009*, pp. 155–163, Yerevan, Armenia, 2009.

[16] S. Grigoryan, "Structuring of goals and plans for personalized planning and integrated testing of plans," *Mathematical Problems of Computer Science*, vol. 43, pp. 62–75, 2015.

[17] K. Khachatryan, "Developing algorithms and programs for formation of and search in knowledge bases of competition and combating problems," PhD Thesis, Yerevan, Armenia, 2013.

[18] K. Khachatryan and S. Grigoryan, "Java programs for presentation and acquisition of meanings in SSRGT games," in *SEUA Annual Conference*, pp. 135–141, Yerevan, Armenia, 2013.

[19] K. Khachatryan and S. Grigoryan, "Java programs for matching situations to the meanings of SSRGT games," in *SEUA Annual Conference*, pp. 127–135, Yerevan, Armenia, 2013.

[20] Z. Naghashyan, "Developing software for formation and acquisition lexical units in certain limited languages," PhD Thesis, Yerevan, Armenia, 2010.

[21] E. Pogossian and A. Djavadyan, "A game model for effective counteraction against computer attacks in intrusion detection systems," in *NATO ASI, Data Fusion for Situation Monitoring, Incident Detection, Alert and Response Management*, Tsaghkadzor, Armenia, 2003.

[22] D. E. Blodgett, M. Gendreau, F. Guertin, J. Potvin, and R. Sguin, "A Tabu search heuristic for resource management in naval warfare," *Journal of Heuristics*, vol. 9, pp. 145–169, 2003.

[23] P. P. R. Partha, "ChatGPT: A comprehensive review on background, applications, key challenges, bias, ethics, limitations and future scope," *Internet of Things and Cyber-Physical Systems*, vol. 3, pp. 121–154, 2023.

[24] Z. Naghashyan, "Developing graphical language interpreter for representing communicable knowledge of the concepts," in *SEUA Annual Conference 2010*, Yerevan, Armenia, 2010.

[25] D. Poo, D. Kiong, and S. Ashok, *Object-Oriented Programming and Java*, Springer Science & Business Media, London, 2007.

[26] C. L. Forgy, "Rete: A fast algorithm for the many pattern/many object pattern match problem," *Artificial Intelligence*, vol. 19, pp. 17–37, 1982.

[27] N. Hakobyan, "System for transforming images to symbolic presentation for combinatorial defense and competition problems," *NAS RA and ESUA Series of Technical Sciences*, pp. 199–209, Yerevan, Armenia, 2019.

[28] K. He, S. Ren, J. Sun, and X. Zhang, "Deep residual learning for image recognition," *CoRR*, abs/1512.03385, 2016.

[29] S. Grigoryan and E. Pogossian, "Developing aerial unmanned effective decision makers," *Mathematical Problems of Computer Science*, vol. 58, pp. 52–60, 2022.

[30] M. Botvinnik, *Computers in Chess: Solving Inexact Search Problems*, Springer Series in Symbolic Computation, with Appendixes, Springer-Verlag, New York, 1984.

[31] S. Grigoryan, "Research and development of algorithms and programs of knowledge acquisition and their effective application to resistance problems," PhD Thesis, Yerevan, Armenia, 2016.

[32] S. Grigoryan, N. Hakobyan, and T. Baghdasaryan, "Solvers of combinatorial problems adequate to experts," in *Proceedings of International Conference of Computer Science and Information Technologies 2019*, pp. 29–32, Yerevan, Armenia, 2019.

[33] M. Buniatyan, S. Grigoryan, and E. Danielyan, "Expert knowledge-based RGT solvers for software testing," *Mathematical Problems of Computer Science*, vol. 59, pp. 45–56, 2023.

[34] S. Grigoryan, "Context knowledge-based decisions for battlefields," in *Proceedings of International Conference of Computer Science and Information Technologies 2023*, pp. 42–44, Yerevan, Armenia, 2023.

[35] I. Schieferdecker and A. Hoffmann, "Model-based testing," *IEEE Software*, vol. 29, no. 1, pp. 14–18, 2012.

[36] P. Langley, H. Shrobe, and B. Katz, "Cognitive task analysis of rapid procedure acquisition from written instructions," in *Proceedings of the Ninth Annual Conference on Advances in Cognitive Systems*, 2021.

[37] E. Arakelova and E. Pogossian, "Tools for testing and correction of the completeness of knowledge acquisition by autistic children," in *Proceedings of International Conference of Computer Science and Information Technologies 2011*, pp. 159–165, Yerevan, Armenia, 2011.

[38] S. Grigoryan and L. Berberyan, "Developing interactive personalized tutors in chess," *Mathematical Problems of Computer Science*, vol. 44, pp. 116–132, 2015.

[39] E. Pogossian, S. Grigoryan, and L. Berberyan, "Personalized Interactive Tutoring in Chess," in *London Chess Conference*, December 10–12, 2016.

[40] S. Grigoryan, "Automating acquisition and explanation of strategy knowledge," in *Proceedings of International Conference of Computer Science and Information Technologies 2021*, pp. 21–23, Yerevan, Armenia, 2021.

[41] S. Grigoryan and E. Pogossian, "Learning Expert Meaning Processing," RAU-IIAP Science Comimittee project 2023-2025.

# Իմացության մոդելների ադեկվատությունը և կիրառությունները կոմբինատոր խնդիրներում

## Սեդրակ Վ. Գրիգորյան և Զավեն Հ. Նաղաշյան

ՀՀ ԳԱԱ Ինֆորմատիկայի և ավտոմատացման պրոբլեմների ինստիտուտ, Երևան, Հայաստան
e-mail: sedrak.grigoryan@iiap.sci.am, znaghash@gmail.com

## Ամփոփում

Մենք նպատակ ունենք տրամադրել մարդու կողմից տիեզերքի իմացության կառուցողական և ադեկվատ մոդելներ։ Արձանագրելով, որ կոմբինատոր խաղերը համարժեք մոդելներ են Մարդ-Տիեզերք խնդրի ուսումնասիրության համար, մենք ներկայացնում ենք Վերարտադրվող Խաղային Ծառերի (RGT) կոմբինատոր խաղերի դաս, որն ընդգրկում է ոչ միայն մրցակցային, պաշտպանական և հաղորդակցային խնդիրներ։

Մենք մշակում ենք փորձագիտական գիտելիքահեն RGT Solver ծրագիր, որը ընդհանուր ձևով փնտրում է հնարավոր RGT ռազմավարություններ՝ հիմնավորելով, որ այդ ռազմավարությունները փոխանցելի են RGT ամբողջ դասի մեջ։

Մենք գնահատում ենք իմացական մոդելների ադեկվատությունը, մասնավորապես, RGT խնդիրների լուծման մեջ առաջընթացի միջոցով, միաժամանակ լուծումներ տալով արդի կիրառական խնդիրներին։

Այս աշխատանքում մենք ուրվագծում ենք մեր RGT մոտեցումը՝ փաստելով մարդու ադեկվատությունը իմացական մոդելների հարցում և ներկայացնում դրանից բխող որոշ հաջող կիրառությունները։

**Բանալի բառեր՝** իմացության մոդելավորում, կոմբինատոր խաղեր, պաշտպանություն ներխուժումից, պաշտպանական ռազմավարություններ, մարկետինգ, ուսուցում, իմաստների մշակում։

# Адекватность и применение моделей познания с использованием комбинаторных игр

## Седрак В. Григорян и Заве О.Нагашян

Институт проблем информатики и автоматизации НАН РА, Ереван, Армения
e-mail: sedrak.grigoryan@iiap.sci.am, znaghash@gmail.com

## Аннотация

Мы стремимся предложить конструктивные и адекватные модели человеческого познания Вселенной.

Утверждая, что комбинаторные игры являются адекватными моделями для изучения проблемы человек-Вселенная, мы вводим класс Воспроизводимых Игровых Деревьев (RGT), которые в общем случае не ограничены представлением конкурентных, оборонительных и коммуникационных задач.

Мы разрабатываем основанный на экспертных знаниях RGT Solver для унифицированного поиска возможных стратегий RGT, утверждая, что такие

стратегии могут быть перенесены на весь класс.

Мы оцениваем адекватность моделей познания, в частности, посредством прогресса в решении задач RGT, которые одновременно предоставляют решения для актуальных приложений.

В данной работе мы излагаем наш подход к RGT для аргументации адекватности моделей познания к человеческому и приводим успешные приложения.

**Ключевые слова:** моделирование познания, комбинаторные игры, защита от вторжений, оборонительные стратегии, маркетинг, Обучение, обработка значений..

UDC 519.872

# Advanced Queueing Model of a Multiprocessor Computing System

Artur P. Vardanyan

Institute for Informatics and Automation Problems of NAS RA, Yerevan, Armenia
e-mail: artur.vardanyan@iiap.sci.am

## Abstract

This paper presents an advanced queueing model for a multiprocessor computing system, where tasks require a random number of processors and are subject to constraints on waiting times in the queue. Unlike classical multi-server queueing systems, this model accounts for both resource requirements and queue waiting time restrictions, making it more suitable for real-world computing environments. By incorporating the probabilistic behavior of task arrival, service, and waiting constraints, the expressions are derived for key performance metrics, including the probabilities of task rejection and failure, system throughput, and resource utilization. An algorithm for determining the optimal queue length is also developed to enhance system efficiency by minimizing the probability of task losses. The proposed model provides a framework for analyzing and optimizing resource allocation in multiprocessor systems, improving their capability to handle dynamic and complex workloads.

**Keywords:** Multiprocessor System, Queueing System, Multi-server Queueing System, Waiting Time Restriction, Resource Utilization, System Efficiency, Performance Measures.

## 1. Introduction

In the rapidly evolving field of information technology, distributed and parallel high-speed computing systems have become essential due to advancements in several key areas, including multi-agent intelligent methods for information retrieval, data science for processing and storing vast amounts of data, and scientific research addressing complex challenges[1]. These systems are crucial for scientific and technological modelling, where there is a growing demand for increased accuracy, faster computations, and large-scale calculations.

Multiprocessor systems are often employed to tackle problems requiring large-scale computations that cannot be handled by a single processor. However, this leads to significant challenges in managing the simultaneous execution of multiprocessor tasks while ensuring the efficient utilization of system resources[2]. One of the critical issues in this context is the

development of effective scheduling algorithms for such systems.

Research on efficient scheduling algorithms for multiprocessor systems is a key area in computer science and parallel computing. Modern multiprocessor systems typically consist of heterogeneous processors with varying capabilities and performance characteristics. Additionally, applications are becoming increasingly diverse and dynamic, necessitating adaptive scheduling strategies that can efficiently allocate system resources while optimizing key performance metrics such as system throughput, service latency, and energy efficiency[3, 4].

As the development of scheduling algorithms continues to evolve, there is a growing need to incorporate additional metrics to enhance efficiency[5]. While optimization theory and machine learning tools are often employed to address these challenges, valuable insights can also be gained by analyzing these systems through the framework of queueing theory.

In this study, a multiprocessor system is modeled as a queuing system, where tasks require parallel servicing and constraints on task waiting times in the queue are explicitly considered.

## 2. Queueing Model

A computing system consisting of $m$ processors (cores, cluster nodes, etc.) is modeled as a queueing system ($m \geq 1$). The system can queue a limited number of tasks, constrained by $n$ waiting slots ($n \geq 1$).

Each task in the system is characterized by three random parameters ($\nu, \beta, \omega$):

- $\nu$ represents the number of computing resources (processors, cores, cluster nodes, etc.) required for servicing the task,

- $\beta$ denotes the maximum time needed to service the task,

- $\omega$ is the maximum allowable waiting time for a task in the queue, after which the task leaves the system without being serviced.

The task is either accepted and placed in the service queue or denied service. Service denial may occur if there is no space in the queue or user-defined constraints (e.g., servicing time, waiting time, number of processors) cannot be met. The time required to service a task is partly conditional, meaning it is the maximum allowable value. The actual servicing time is random and may be shorter than the given maximum, allowing the order of service to change as tasks arrive or as services are completed.

The queuing model incorporates the cumulative distribution function of the exponential distribution constraints for task arrivals, servicing, and failures due to waiting time restrictions. These are defined by the intensities: $a$ for the incoming task stream, $b$ for task servicing, and $w$ for task failure within the queue[6]. The model also considers normal distribution constraints for the random variable $\nu$, representing the number of computational resources required to perform a task. The probability distribution is given by:

$$P(\nu = k) = \frac{1}{m}, \quad k = 1, 2, \ldots, m.$$

Tasks are serviced in the order they enter the system, following a FIFO discipline. Tasks that arrive when the queue is full are denied service.

To describe system transitions, the state of the system is defined by the number of tasks $i$

being serviced and $j$ tasks waiting in the queue. The probability of the system being in this state is denoted by $P_{i,j}$. Since the number of possible states is finite, the system eventually reaches a stable operating mode, known as the steady state[7].

A system of equations was derived to describe the steady-state behavior of the queueing model.

A detailed description of the derivation, analysis, and development of a numerical algorithm for solving this system of equations is presented in [6]. This research provides an efficient and accurate method for computing the $P_{i,j}$ steady-state probabilities for the considered multiprocessor queueing system.

## 3. Performance Measures

To analyze the performance measures of the considered queueing system, it is first necessary to determine the effective arrival rate and the service rate of the tasks using the given system parameters and distribution functions for the time between arrivals, the service time, and the permissible waiting time. Unlike classical multi-server queueing systems, in this model, each task requires a specific number of service nodes and is subject to a restriction on queue waiting time. The permissible waiting time $\omega$ is modeled by an exponential distribution, while the number of required computational resources $\nu$ follows a uniform distribution. These considerations significantly impact the system's performance measures, including the probability of task rejection, the probability of queue task failure and the resource utilization factor. However, these considerations do not directly affect the service rate $\mu$, which is based on only service time distribution. Specifically, the service rate $\mu$ is given by $b$ in the considered queueing system.

To understand the real impact of these factors on system performance measures, it is first necessary to calculate the probabilities of task access rejection and task failure (i.e., when a task leaves the queue due to exceeding its waiting time) during system operation.

Upon task arrival, the system will reject access if the number of tasks waiting in the queue reaches its maximum capacity, $n$. In other words, the probability of task access rejection during system operation can be calculated by considering the probabilities of being in all system states where the queue is fully occupied. This probability of task access rejection, denoted by $P_r$, can be expressed as follows:

$$P_r = \sum_{i=0}^{m} \frac{aP_{i,n}}{a + ib + nw},$$

where $a$ represents the arrival rate of tasks, $b$ represents the service rate, $w$ represents the rate at which tasks fail due to waiting too long in the queue, and $P_{i,n}$ for $i = 0, 1, \ldots, m$ are the steady-state probabilities of the system when $i$ tasks are being serviced and the queue is fully occupied.

It is assumed that each task has a maximum allowable waiting time before being serviced, after which it leaves the system without being served. The probability of task failure during system operation, denoted by $P_f$, can be calculated using the system state probabilities. The formula to compute $P_f$ is as follows:

$$P_f = \sum_{i=0}^{m} \sum_{j=1}^{n} \frac{jwP_{i,j}}{a + ib + jw},$$

where, as above, $a$ represents the arrival rate of tasks, $b$ represents the service rate, $w$ represents the rate at which tasks fail due to waiting too long in the queue, and $P_{i,j}$ for $i = 0, 1, \ldots, m$ and $j = 0, 1, \ldots, n$ are the steady-state probabilities of the system when $i$ tasks are being serviced and $j$ tasks are waiting in the queue.

By using the above-obtained probabilities, the effective arrival rate $\lambda$ in the considered queueing system can be calculated as follows:

$$\lambda = aP_a,$$

where $P_a$ is the probability of task abandonment, which represents the likelihood that a task leaves the queue without being serviced, either due to exceeding its permissible waiting time or being rejected by the system because the queue is fully occupied.

Furthermore, $P_a$ is expressed as follows:

$$P_a = (1 - P_r)(1 - P_f).$$

Queuing systems define the system throughput, which is closely related to the effective arrival rate, but they describe different aspects of the system's performance[8]. The system throughput is denoted by $X$ and is defined as:

**Definition 1..** *System Throughput is the rate at which tasks are completed and leave the system.*

In a stable system (where the queue doesn't grow indefinitely over time), the system throughput is typically equal to the effective arrival rate. This is because the system can handle the incoming tasks without accumulating an infinite queue, meaning that every task that arrives is eventually processed. For the considered queueing system, the system throughput is the same as the effective arrival rate:

$$X = \lambda.$$

Next, to derive a formula for the utilization factor $\rho$ in the queueing system under consideration, it is first necessary to define the utilization factor in the context of this multiprocessor queueing system. Since, each task requires a random number of computational resources, which affects how much of the system's total resources are utilized on average, the utilization factor will be defined as follows:

**Definition 2..** *Utilization is defined as the ratio of the service capacity demand to the total service capacity of the system:*

$$\rho = \frac{Service\ Capacity\ Demand}{Total\ Service\ Capacity}$$

As each task requires a random number of processors, the system's effective utilization factor must consider the expected number of processors required by a task, denoted as $E[\nu]$. Thus, the service capacity demand is determined by $\lambda \times E[\nu]$. This accounts for the fact that each task might occupy multiple number computational resources simultaneously.

For a system with $m$ processors, where each processor has a service rate $\mu$, the total service capacity is $m \times \mu$.

Thus, the refined utilization factor formula becomes:

$$\rho = \frac{\lambda E[\nu]}{m\mu}.$$

Given that the distribution of $\nu$ is uniform from 1 to $m$, the expected value $E[\nu]$ is determined as follows:

$$E[\nu] = \sum_{k=1}^{m} kP(\nu = k) = \frac{1}{m}\sum_{k=1}^{m} k = \frac{m+1}{2}.$$

By substituting the derived values for $\lambda$, $\mu$ and $\mathbb{E}[\nu]$, a formula is obtained for the utilization $\rho$:

$$\rho = \frac{a(m+1)P_a}{2mb}.$$

The formula for calculating the utilization factor $\rho$ is refined to be consistent as a measure of system resource usage.

## 4.   Optimal Service Parameters

This section presents the process of determining the optimal configuration for the modeled queueing system based on given parameters and distributions. As discussed in the previous section, for the specified distributions of system parameters, it is possible to evaluate the probabilities of task rejection and task failure while waiting in the queue. This allows for estimating the probability that an incoming task will not be serviced by the system. This probability is a key indicator of the number of tasks unserviced by the system and can be calculated as follows:

$$P_l = P_r + (1 - P_r)P_f,$$

Thus, the question arises as to how this probability can be minimized, which would reduce the number of unserviced tasks by the system. It is evident that the value of $P_l$ depends on the number of processors $(m)$ in the multiprocessor system, the queue length $(n)$, the task arrival rate $(a)$, the service rate $(b)$, and the task failure rate in the queue $(w)$. Considering this, the objective is to minimize $P_l$ by varying the queue length, identifying the queue length at which $P_l$ takes its minimum value for the given system parameters while ensuring that the utilization factor is less than one:

$$\begin{cases} P_l \to \min \\ \rho < 1 \end{cases}$$

It is evident that when there is no queue, the rejection probability $P_r$ has a certain value, while there is no concept of $P_f$ probability(in this case, $P_f$ is assumed to be zero for simplicity). As the queue length increases, the rejection probability $P_r$ tends toward 0, and the failure probability $P_f$ approaches 1, as follows:

| $n = 0$ | $n \to \infty$ |
|---|---|
| $0 < P_r \leq 1$ | $P_r \to 0$ |
| $P_f = 0$ | $P_f \to 1$ |

An algorithm has been developed and implemented in Python, to determine the optimal queue length for a multiprocessor system with a given number of processors, task arrival, service, and failure rates. The algorithm initially sets the queue length to $n = 1$ and calculates the probability $P_l$. At each subsequent step, the calculation is repeated with the queue length increased by one, and the new $P_l$ value is compared to the previous value. If the new value is smaller, the algorithm continues this cycle. When the $P_l$ value from the previous step is smaller than the current step, the queue length is set to the previous value,

and the system utilization factor is calculated for that queue length. If the utilization factor is less than one, the algorithm terminates, setting the current $n$ as the optimal queue length for the given system parameters. If the utilization factor is greater than or equal to one, the algorithm ends with a message indicating that the given parameters don't support effective system performance. Thus, with this queue length, the system can achieve an optimal service configuration, minimizing the probability $P_l$ of unserviced tasks for the given parameters. The pseudocode of the algorithm consists of two blocks and is presented below:

---

**Algorithm 1** System Performance Measures Computation

---

**Input:** $n, m, a, b, w$
**Output:** $P_r, P_f, \rho$

1: $p \leftarrow$ SteadyStateProbabilities$(n, m, a, b, w)$
2: $P_r, P_f \leftarrow 0, 0$
3: $i, j \leftarrow 0, 0$
4: **for** each $x \in p$ **do**
5:      **if** $j == n$ **then**
6:          $P_r \leftarrow P_r + \dfrac{a \cdot x}{a + i \cdot b + j \cdot w}$
7:      **end if**
8:      $P_f \leftarrow P_f + \dfrac{j \cdot w \cdot x}{a + i \cdot b + j \cdot w}$
9:      $j \leftarrow j + 1$
10:      **if** $j == n + 1$ **then**
11:          $j \leftarrow 0$
12:          $i \leftarrow i + 1$
13:      **end if**
14: **end for**
15: $P_a \leftarrow (1 - P_r) \cdot (1 - P_f)$
16: $\rho \leftarrow \dfrac{aP_a \cdot (m + 1)}{2 \cdot m \cdot b}$
17: **return** $P_r, P_f, \rho$

---

---

**Algorithm 2** Optimal Queue Length Computation

---

**Input:** $m, a, b, w$
**Output:** $n_{opt}$ (the optimal queue length)

1: $n_{opt} \leftarrow 1, n \leftarrow 1$
2: $P_r, P_f, \rho_{opt} \leftarrow$ SystemPerformanceMeasures$(m, n, a, b, w)$
3: $M_1 \leftarrow P_r + (1 - P_r) \cdot P_f$
4: $n \leftarrow n + 1$
5: $P_r, P_f, \rho \leftarrow$ SystemPerformanceMeasures$(m, n, a, b, w)$
6: $M_2 \leftarrow P_r + (1 - P_r) \cdot P_f$
7: **while** $M_1 > M_2$ **do**
8:      $n_{opt} \leftarrow n$
9:      $n \leftarrow n + 1$
10:      $M_1 \leftarrow M_2$
11:      $\rho_{opt} \leftarrow \rho$
12:      $P_r, P_f, \rho \leftarrow$ SystemPerformanceMeasures$(m, n, a, b, w)$
13:      $M_2 \leftarrow P_r + (1 - P_r) \cdot P_f$
14: **end while**
15: **if** $\rho_{opt} \geq 1$ **then**
16:      **Raise** "InvalidParameterException: These parameters don't support effective system performance!"
17: **else**
18:      Print "The optimal queue length is $n_{opt}$"
19:      **return** $n_{opt}$
20: **end if**

---

## 5.   Conclusion

The study presented in this paper offers a refined approach to modeling multiprocessor systems using advanced queueing theory and accounting for variability in task requirements and queue constraints. By analyzing the steady-state probabilities and deriving metrics such as task rejection and failure rates, effective arrival rates, and system utilization, insights into optimizing system performance are gained. The proposed algorithm for finding the optimal queue length minimizes task losses while maintaining efficient resource usage. This work contributes to the field of multiprocessor queueing theory, providing tools for better scheduling and resource allocation strategies in high-performance computing environments. Future work may explore extensions of this model to systems with heterogeneous resources or additional performance constraints, further enhancing the model's applicability in real-world scenarios.

## References

[1] L. N. Bhuyan and S.Sinha, "Design of Parallel and Distributed Systems", *Springer, Cham,* pp. 12-250, 2023.

[2] V. Sahakyan and A. Vardanyan, "About the possibility of executing tasks with a waiting time restriction in a multiprocessor system", *AIP Conference Proceedings*, 2757.1, pp. 030003, 2023. DOI: https://doi.org/10.1063/5.0135784.

[3] D.Bertsimas and D.Gamarnik, "Queueing Theory: Classical and Modern Methods", *Dynamic Ideas*, Belmont, pp. 126-586, 2022.

[4] F. P. Kelly, S. Zachary and I.Ziedins, "Stochastic Networks: Theory and Applications", *Clarendon Press*, Oxford, pp. 16-298, 2020.

[5] J. Anamika, J. Madhu, D. Bhardwaj, "Controllable multiprocessor queueing system", *Applications of Mathematical Modeling, Machine Learning, and Intelligent Computing for Industrial Development*, pp. 61-76, 2023.

[6] V. Sahakyan and A. Vardanyan, "A Computational Approach for Evaluating Steady-State Probabilities and Virtual Waiting Time of a Multiprocessor Queuing System", *Programming and Computer Software*, Volume 49, pp. S16S23, 2023. DOI: https://doi.org/10.1134/S0361768823090098.

[7] J. F.Shortle, J. M.Thompson, D. Gross and Harris C. M., *Fundamentals of Queueing Theory*, John Wiley and Sons, New York, pp. 35-475, 2018.

[8] H. Takagi, "Appendix A: Derivation of Formulas by Queueing Theory" *Spectrum Requirement Planning in Wireless Communications*, John Wiley & Sons Ltd, pp. 199-218, 2008. DOI: https://doi.org/10.1002/9780470758946.app1.

# Բազմապրոցեսսորային հաշվողական համակարգի ընդլայնված հերթերի մոդել

## Արթուր Պ. Վարդանյան

ՀՀ ԳԱԱ Ինֆորմատիկայի և ավտոմատացման պրոբլեմների ինստիտուտ, Երևան, Հայաստան

e-mail: artur.vardanyan@iiap.sci.am

### Ամփոփում

Այս հոդվածում ներկայացվում է բազմապրոցեսսորային հաշվողական համակարգի ընդլայնված հերթերի մոդել, որտեղ առաջադրանքները պահանջում են պատահական քանակով պրոցեսորներ և ենթակա են հերթում սպասման ժամանակի սահմանափակումների: Ի տարբերություն դասական բազմասերվերային հերթերի համակարգերի, այս մոդելը հաշվիէառնում ինչպես ռեսուրսների պահանջները, այնպես էլ հերթում սպասման ժամանակի սահմանափակումները, ինչն առավել հարմար է իրական հաշվողական միջավայրերի համար: Ներառելով առաջադրանքների մուտքի, սպասարկման և սպասման սահմանափակումների հավանականային բնույթը, արտածվել են համակարգի կարևոր կատարողական ցուցանիշների՝ առաջադրանքների մերժման և ձախողման հավանականությունների, համակարգի թողունակության և ռեսուրսների օգտագործման գործակցի, գնահատման արտահայտություններ: Մշակվել է նաև հերթի օպտիմալ երկարությունը որոշող ալգորիթմ, որը բարելավումէհամակարգի արդյունավետությունը՝ նվազեցնելով առաջադրանքների կորստի հավանականությունը:

**Բանալի բառեր`** Բազմապրոցեսսորային համակարգ, հերթերի համակարգ, բազմասերվերային հերթերի համակարգ, սպասման ժամանակի սահմանափակում, ռեսուրսների օգտագործում, համակարգի արդյունավետություն, կատարողականության չափեր:

# Расширенная модель очередей многопроцессорной вычислительной системы

## Артур П. Варданян

Институт проблем информатики и автоматизации НАН РА, Ереван, Армения

e-mail: artur.vardanyan@iiap.sci.am

### Аннотация

В данной статье представлена расширенная модель очередей для многопроцессорной вычислительной системы, где задачи требуют случайного количества процессоров и подчиняются ограничениям на время ожидания в очереди. В отличие от классических многосерверных систем очередей, эта модель учитывает как требования к ресурсам, так и ограничения на ожидание в очереди, что делает её более подходящей для реальных вычислительных сред. С использованием вероятностного подхода к моделированию поступления, обслуживания задач и ограничениям на ожидание были получены выражения для ключевых показателей производительности, включая вероятности отказа и сбоя задач, пропускную способность системы и загрузку ресурсов.

Также был разработан алгоритм для определения оптимальной длины очереди, позволяющий повысить эффективность системы за счёт минимизации вероятности потерь задач.

**Ключевые слова:** Многопроцессорная система, система очередей, многосерверная система очередей, ограничение времени ожидания, использование ресурсов, эффективность системы, показатели производительности.

# On Sub-Gaussianity in Banach Spaces

George J. Giorgobiani, Vakhtang V. Kvaratskhelia and Vazha I. Tarieladze

Muskhelishvili Institute of Computational Mathematics of the Georgian Technical University,
Tbilisi, Georgia
e-mail: giorgobiani.g@gtu.ge, v.kvaratskhelia@gtu.ge, v.tarieladze@gtu.ge

**Abstract**

We show that if $X$ is a Banach space and a weakly sub-Gaussian random element in $X$ induces the 2-summing operator, then it is $T-$sub-Gaussian, provided that $X$ is a reflexive type 2 space. Using this result, we obtain a characterization of weakly sub-Gaussian random elements in a Hilbert space which are $T-$sub-Gaussian.

**Keywords:** Sub-Gaussian random variable, Gaussian random variable, weakly sub-Gaussian random element, $T-$sub-Gaussian random element, Banach space, Hilbert space.

**Article info:** Received 7 October 2024; sent for review 15 October 2024; accepted 26 November 2024.

**Acknowledgment:** The work was partially supported by the European Union's HORIZON EUROPE Grant Project GAIN.

## 1 Introduction

Let $(\Omega, \mathcal{A}, \mathbf{P})$ be a probability space. Following [8], we call a real-valued measurable function $\xi : \Omega \to \mathbb{R}$ a sub-Gaussian random variable if there exists a real number $a \geq 0$ such that for every real number $t$ the following inequality is valid

$$\mathbb{E}\, e^{t\xi} \leq e^{\frac{1}{2}a^2 t^2},$$

where $\mathbb{E}$ stands for the mathematical expectation.

To each random variable $\xi$, there corresponds a parameter $\tau(\xi) \in [0, +\infty]$ defined as follows (we agree $\inf(\emptyset) = +\infty$):

$$\tau(\xi) = \inf\left\{ a \geq 0 : \quad \mathbb{E}\, e^{t\xi} \leq e^{\frac{1}{2}a^2 t^2}, \quad t \in \mathbb{R} \right\}.$$

A random variable $\xi$ is sub-Gaussian if and only if $\tau(\xi) < +\infty$ and $\mathbb{E}\xi = 0$. Moreover, if $\xi$ is a sub-Gaussian random variable, then for every real number $t$

$$\mathbb{E}\, e^{t\xi} \leq e^{\frac{1}{2}\tau^2(\xi)t^2}$$

and
$$\left(\mathbb{E}\xi^2\right)^{\frac{1}{2}} \leq \tau(\xi).$$

If $\xi$ is a Gaussian random variable with $\mathbb{E}\xi = 0$, then $\xi$ is sub-Gaussian and

$$\left(\mathbb{E}\xi^2\right)^{\frac{1}{2}} = \tau(\xi).$$

**Remark 1.1** *[3, Example 1.2]. If $\xi$ is a bounded random variable, i.e., if for some constant $c \in \mathbb{R}$ with $1 \leq c < +\infty$, we have $|\xi| \leq c$ a.s. and $\mathbb{E}\xi = 0$, then $\xi$ is sub-Gaussian and $\tau(\xi) \leq c$.*

Denote by $\mathcal{SG}(\Omega, \mathcal{A}, \mathbb{P})$, or in short, by $\mathcal{SG}(\Omega)$ the set of all sub-Gaussian random variables defined on a probability space $(\Omega, \mathcal{A}, \mathbb{P})$. $\mathcal{SG}(\Omega)$ is a vector space over $\mathbb{R}$ with respect to the natural point-wise operations; moreover, the functional $\tau(\cdot)$ is a norm on $\mathcal{SG}(\Omega)$ (provided that random variables that coincide almost surely are identified) and $(\mathcal{SG}(\Omega), \tau(\cdot))$ is a Banach space [2]. For $\xi \in \mathcal{SG}(\Omega)$ instead of $\tau(\xi)$ we will write also $\|\xi\|_{\mathcal{SG}(\Omega)}$.

More information about the sub-Gaussian random variables can be found, for example, in [6].

**Remark 1.2** *[3, Theorem 1.3] (see also[14, Proposition 2.9]). For a sub-Gaussian random variable $\xi$, we have*
$$\vartheta(\xi) = \sup_{n \geq 1} \frac{\left(\mathbb{E}\,\xi^{2n}\right)^{1/2n}}{n^{1/2}} < +\infty,$$

*the functional $\vartheta$ is a norm on the vector space $\mathcal{SG}(\Omega)$ and the norms $\tau$ and $\vartheta$ are equivalent, i.e., there exist positive constants $a_1$ and $a_2$ such that for every $\xi \in \mathcal{SG}(\otimes)$ we have*

$$a_1 \vartheta(\xi) \leq \tau(\xi) \leq a_2 \vartheta(\xi).$$

In an infinite dimensional Banach space there are several notions of sub-Gaussianity. The aim of the paper is to show that these concepts are different in general. We also give some sufficient conditions for their equivalence.

Let $X$ be a Banach space over $\mathbb{R}$ with a norm $\|\cdot\|$ and $X^*$ be its dual space. The value of the linear functional $x^* \in X^*$ at an element $x \in X$ is denoted by the symbol $\langle x^*, x\rangle$.

Following [15, p. 88], a mapping $\xi : \Omega \to X$ is called a random element (vector) in $X$ if $\langle x^*, \xi\rangle$ is a random variable for every $x^* \in X^*$.

If $0 < p < \infty$, then a random element $\xi$ in a Banach space $X$:

- has *a strong $p$-th order*, if $\|\xi\|$ is a random variable and $\mathbb{E}\,\|\xi\|^p < \infty$;

- has *a weak $p$-th order*, if $\mathbb{E}\,|\langle x^*, \xi\rangle|^p < \infty$ for every $x^* \in X^*$;

- is *centered*, if $\xi$ has a weak first order and $\mathbb{E}\,\langle x^*, \xi\rangle = 0$ for every $x^* \in X^*$.

To each weak second-order centered random element $\xi$ in a separable Banach space $X$, there corresponds a mapping $R_\xi : X^* \to X$ such that

$$\langle y^*, R_\xi x^*\rangle = \mathbb{E}\,\langle y^*, \xi\rangle\langle x^*, \xi\rangle, \quad \text{for every} \quad x^*, y^* \in X^*,$$

which is called *the covariance operator of $\xi$* [15, Corollary 2 (p.172)].

A random element $\xi : \Omega \to X$ is called *Gaussian*, if for each functional $x^* \in X^*$, the random variable $\langle x^*, \xi \rangle$ is Gaussian.

A mapping $R : X^* \to X$ is said to be *a Gaussian covariance* if there exists a Gaussian random element in $X$, the covariance operator of which is $R$.

A random element $\xi : \Omega \to X$ will be called *weakly sub-Gaussian* [13] if for each $x^* \in X^*$, the random variable $\langle x^*, \xi \rangle$ is sub-Gaussian.

A random element $\xi : \Omega \to X$ will be called $T-sub$-$Gaussian$ (or $\gamma-$sub-Gaussian [5]) if there exists a probability space $(\Omega', \mathcal{A}', \mathbf{P}')$ and a centered Gaussian random element $\eta : \Omega' \to X$ such that for each $x^* \in X^*$

$$\mathbb{E}\,e^{\langle x^*, \xi \rangle} \leq \mathbb{E}\,e^{\langle x^*, \eta \rangle}. \tag{1.1}$$

**Theorem 1.3** (*a*) *If $X$ is a finite-dimensional Banach space, then every weakly sub-Gaussian random element in $X$ is $T-sub$-Gaussian.*

(*b*) *If $X$ is a infinite-dimensional separable Banach space, then there exists a weakly sub-Gaussian random element in $X$, which is not $T-sub$-Gaussian.*

**Proof.**

(*a*) See [14, Proposition 4.9].

(*b*) According to [13] (see also [14, Theorem 4.5]), we can find and fix a weakly sub-Gaussian random element $\xi$ in $X$, such that $\mathbb{E}\|\xi\| = \infty$. Such a random element cannot be $T-sub$-Gaussian, because as stated in [5, Theorem 3.4] every such random element must be "exponentially integrable". $\blacksquare$

To every weakly sub-Gaussian random element $\xi : \Omega \to X$, we associate *the induced linear operator*

$$T_\xi : X^* \to \mathcal{SG}(\Omega)$$

defined by the equality:

$$T_\xi x^* = \langle x^*, \xi \rangle \qquad \text{for all} \quad x^* \in X^*.$$

Let $X$ and $Y$ be Banach spaces, $L(X, Y)$ be the space of all continuous linear operators acting from $X$ to $Y$. An operator $T \in L(X, Y)$ is called 2-(absolutely) summing if there exists a constant $C > 0$ such that for each natural number $n$ and for every choice $x_1, x_2, \ldots, x_n$ of elements from $X$, we have

$$\left( \sum_{k=1}^{n} \|T x_k\|^2 \right)^{1/2} \leq C \sup_{\|x^*\|_{X^*} \leq 1} \left( \sum_{k=1}^{n} |\langle x^*, x_k \rangle|^2 \right)^{1/2}. \tag{1.2}$$

For a 2-summing $T : X \to Y$, we denote the minimum possible constant $C$ in (1.2) by $\pi_2(T)$.

We say that a Banach space $X$ has type 2 if there exists a finite constant $C \geq 0$ such that for each natural number $n$ and for every choice $x_1, x_2, \ldots, x_n$ of elements from $X$, we have

$$\left( \int_0^1 \left\| \sum_{k=1}^{n} r_k(t) x_k \right\|^2 dt \right)^{1/2} \leq C \left( \sum_{k=1}^{n} \|x_k\|^2 \right)^{1/2},$$

where $r_1(\cdot), \ldots, r_n(\cdot)$ are Rademacher functions on $[0, 1]$. An example of a type 2 space is a Hilbert space as well as the spaces $l_p, L_p([0, 1]), 2 \leq p < +\infty$.

## 2 Main results

The following theorem is a slightly corrected version of [9, Theorem 1.7].

**Theorem 2.1** *Let $X$ be a separable Banach space. For a weakly sub-Gaussian random element $\xi : \Omega \to X$, consider the assertions:*

*(i) $\xi$ is $T-$sub-Gaussian.*

*(ii) $T_\xi : X^* \to \mathcal{SG}(\Omega)$ is a 2-summing operator.*

*Then:*

*(a) (i) $\Longrightarrow$ (ii);*

*(b) The implication (ii) $\Longrightarrow$ (i) is true provided that $X$ is a reflexive Banach space of type 2.*

**Proof.**

(a) (i) implies that there exists a centered Gaussian random element $\eta : \Omega' \to X$ such that for each $x^* \in X^*$ the relation (1.1) holds. This implies that

$$\tau(T_\xi x^*) \leq \tau(T_\eta x^*) \qquad \text{for all} \quad x^* \in X^*.$$

Thus, as $\eta$ is a Gaussian random element in $X$, the operator $T_\eta$ is 2-summing (see, for example, [4]). Hence, we conclude that (ii) holds.

(b) Since $\xi$ is a weakly sub-Gaussian random element, for every $x^* \in X^*$, we can write:

$$\mathbb{E}\, e^{\langle x^*, \xi \rangle} \leq e^{\frac{1}{2}\|T_\xi x^*\|^2_{\mathcal{SG}(\Omega)}}.$$

Taking into account that the operator $T_\xi$ is 2-summing and $X$ is reflexive, by Pietsch domination theorem (see [10] or [15, Theorem 2.2.2]), there exists a probability measure $\mu$ defined on the $\sigma(X, X^*)$-Borel sigma-algebra of the unit ball $B_X \subset X$ such that

$$\|T_\xi x^*\|^2_{\mathcal{SG}(\Omega)} \leq \pi_2^2(T_\xi) \int\limits_{B_X} \langle x^*, x \rangle^2 \, \mu(dx), \quad x^* \in X^*.$$

If we consider $\mu$ as a probability measure in $X$ concentrated on $B_X$, then for every $x^* \in X^*$

$$\int\limits_{B_X} \langle x^*, x \rangle^2 \, \mu(dx) = \int\limits_{X} \langle x^*, x \rangle^2 \, \mu(dx) = \langle R_\mu x^*, x^* \rangle,$$

where $R_\mu$ is the covariance operator of $\mu$. As $\mu$ is concentrated on the bounded set, it clearly has a strong second order, and taking into account the fact that $X$ is a type 2 space, we obtain that $R_\mu$ is a Gaussian covariance (see [4, Theorem 3.1]). Denoting $\pi_2^2(T)R_\mu = R$, we get

$$\mathbb{E}\, e^{\langle x^*, \xi \rangle} \leq e^{\frac{1}{2}\langle Rx^*, x^* \rangle}, \qquad x^* \in X^*,$$

and, thus, $\xi$ is a $T-$sub-Gaussian random element as $R$ is a Gaussian covariance. ∎

**Problem 2.2** *Problem. Prove that the reflexivity condition for $X$ in Theorem 2.1(b) can be removed.*

Consider now the case when $X = H$, where $H$ denotes an infinite-dimensional separable Hilbert space with the inner product $\langle \cdot, \cdot \rangle$. As usual we identify $H^*$ with $H$ by means of the equality $H^* = \{\langle \cdot, y \rangle : y \in H\}$.

From Theorem 2.1, we will derive now the following result, which is related to a similar assertion contained in [1, Proposition 3.1].

**Theorem 2.3** *Let $H$ be an infinite-dimensional separable Hilbert space. For a weakly sub-Gaussian random element $\xi : \Omega \to H$, the following statements are equivalent:*

*(i) $\xi$ is $T-$sub-Gaussian.*

*($ii_m$) For each orthonormal basis $(\varphi_k)$ of $H$,*

$$\sum_{k=1}^{\infty} \tau^2(\langle \varphi_k, \xi \rangle) < \infty . \tag{2.1}$$

**Proof.**     The implication $(i) \Longrightarrow (ii_m)$ follows from Theorem 2.1 $(a)$.

The implication $(ii_m) \Longrightarrow (i)$ follows from Theorem 2.1 $(b)$ as $H$ is a type 2 space and according to [11], the condition $(ii_m)$ implies that the condition $(ii)$ of Theorem 2.1 is satisfied as well. ∎

In connection with Theorem 2.3, the following question naturally arises: is it possible to replace the condition $(ii_m)$ by the following (weaker) condition?

*($ii_w$) There is an orthonormal basis $(\varphi_k)$ of $H$ such that*

$$\sum_{k=1}^{\infty} \tau^2(\langle \varphi_k, \xi \rangle) < \infty .$$

In [1, Remark 4.3], it is claimed that the answer to this question *is positive.*

At the end, we pose another interesting question related to Theorem 2.3: does there exist a bounded centered random element $\xi$ in a separable infinite-dimensional Hilbert space $H$ such that

$$\sum_{k=1}^{\infty} \tau^2(\langle \psi_k, \xi \rangle) = \infty$$

for *every* orthonormal basis $(\psi_k)$ of $H$?

## 3   Conclusion

We have shown that in an infinite dimensional Banach space, the notions of weak sub-Gaussianity and $T$-sub-Gaussianity do not coincide. Sufficient conditions for their equivalence in a general, infinite-dimensional Banach space is given in terms of 2-summing induced operators.

We are very grateful to the referees for the comments and the careful reading of the paper.

# References

[1] R. G. Antonini, "Subgaussian random variables in Hilbert spaces", *Rend. Sem. Mat. Univ. Padova*, vol. 98, pp. 89–99, 1997.

[2] V. V. Buldygin and Yu. V. Kozachenko, "Sub-Gaussian random variables", *Ukrainian Mathematical Journal*, vol. 32, pp. 483–489, 1980.

[3] V. V. Buldygin and Yu. V. Kozachenko, *Metric Characterization of Random Variables and Random Processes*. American Mathematical Soc., 2000.

[4] S. A. Chobanjan and V. I. Tarieladze, "Gaussian characterizations of certain Banach spaces", *J. Multivariate Anal.*, vol. 7, no. 1, pp. 183–203, 1977.

[5] R. Fukuda, "Exponential integrability of sub-Gaussian vectors", *Probab. Theory Relat. Fields*, vol. 85, no. 4, pp. 505–521, 1990.

[6] G. Giorgobiani, V. Kvaratskhelia and M. Menteshashvili, "Unconditional Convergence of Sub-Gaussian Random Series", *Pattern Recognition and Image Analysis*, vol. 34, no. 1, pp. 92–101, 2024.

[7] G. Giorgobiani, V. Kvaratskhelia and V. Tarieladze, "Notes on sub-Gaussian random elements", *In Applications of Mathematics and Informatics in Natural Sciences and Engineering: AMINSE 2019*, Tbilisi, Georgia, pp. 197–203, Springer International Publishing, 2020.

[8] J. P. Kahane, "Proprietes locales des fonctions a series de Fourier aleatoires", *Studia Math.*, 19, pp. 1–25, 1960.

[9] V. Kvaratskhelia, V. Tarieladze and N. Vakhania, "Characterization of $\gamma$-Subgaussian Random Elements in a Banach Space", *Journal of Mathematical Sciences*, vol. 216, no. 4, pp. 564–568, 2016.

[10] A. Pietsch, "Absolute $p$-summierende abbildugen in normierten raumen", *Studia Math.*, vol. 28, pp. 333–353, 1967.

[11] W. Slowikowski, "Absolutely 2-summing mappings from and to Hilbert spaces and a Sudakov Theorem", *Bull. Acad. Polon. Sci. Ser. Sci. Math. Astronom. Phys.*, vol. 17, pp. 381–386, 1969.

[12] M. Talagrand, "Regularity of gaussian processes", *Acta Math.*, vol. 159, no. 1-2, pp. 99–149, 1987.

[13] N. Vakhania, "On subgaussian random vectors in normed spaces", *Bull. Georgian Acad. Sci.*, vol. 163, no. 1, pp. 8–11, 2001.

[14] N. N. Vakhania, V. V. Kvaratskhelia and V. I. Tarieladze, "Weakly sub-Gaussian random elements in Banach spaces", *Ukrainlan Math. J.*, vol. 57, no.9, 1387–1412, 2005.

[15] N. N. Vakhania, V. I. Tarieladze and S. A. Chobanyan, *Probability distributions on Banach spaces*. Dordrecht: Reidel, 1987.

# Բանախի տարածություններում ենթագաուսականության մասին

Ջորջ Դ. Գիորգոբիանի, Վախտանգ Վ. Կվարացխելիա և Վաժա Ի. Տարիելաձե

Վրաստանի տեխնիկական համալսարանի հաշվողական մաթեմատիկայի Մուսխելիշվիլու ինստիտուտ
Թբիլիսի, Վրաստան
e-mail: giorgobiani.g@gtu.ge, v.kvaratshelia@gtu.ge, v.tarieladze@gtu.ge

## Ամփոփում

Մենք ցույց ենք տալիս, որ եթե $X$-ը Բանախի տարածություն է, և թույլ ենթագաուսյան պատահական տարրը $X$-ում առաջացնում է 2-ամփոփիչ օպերատորը, ապա այն $T^*$ ենթագաուսյան է՝ պայմանով, որ $X$-ը ռեֆլեքսիվ 2 տիպի տարածություն է: Օգտագործելով այս արդյունքը, մենք ստանում ենք թույլ ենթագաուսյան պատահական տարրերի բնութագրում Հիլբերտյան տարածության մեջ, որոնք $T^*$ ենթագաուսյան են:

**Բանալի բառեր`** ենթագաուսյան պատահական մեծություն ն, Գաուսյան պատահական մեծություն, թույլ ենթագաուսյան պատահական տարր, $T^*$ ենթագաուսյան պատահական տարր, Բանախի տարածություն, Հիլբերտի տարածություն:

# О субгауссовости в банаховых пространствах

Георгий Д. Гиоргобиани, Вахтанг В. Кварацхелия и Важа И. Тариеладзе

Институт вычислительной математики Мусхелишвили Грузинского технического университета,
Тбилиси, Грузия
e-mail: giorgobiani.g@gtu.ge, v.kvaratshelia@gtu.ge, v.tarieladze@gtu.ge

## Аннотация

Мы показываем, что если $X$ - банахово пространство и слабо субгауссовский случайный элемент в $X$ индуцирует оператор 2-суммирования, то оно $T^*$-субгауссово при условии, что $X$ - рефлексивное пространство типа 2. Используя этот результат, мы получаем характеристику слабо субгауссовских случайных элементов в гильбертовом пространстве, которые являются $T^*$ субгауссовыми.

**Ключевые слова:** субгауссовская случайная величина, гауссовская случайная величина, слабо субгауссовский случайный элемент, $T^*$ субгауссовский случайный элемент, банахово пространство, гильбертово пространство.

# Approach and Challenges of Training an Armenian Version of BERT Language Model

Mikayel K. Gyurjyan and Andranik G. Hayrapetyan

Institute for Informatics and Automation Problems of NAS RA, Yerevan, Armenia
e-mail: mikayelg@gmail.com, andranik.h89@gmail.com

## Abstract

Training and deploying BERT models for specific languages, especially low-resource ones, presents a unique set of challenges. These challenges stem from the inherent data scarcity associated with languages like Armenian, the computational demands of training BERT models, often requiring extensive resources, and the inefficiencies in hosting and maintaining models for languages with limited digital traffic. In this research, we introduce a novel methodology that leverages the Armenian Wikipedia as a primary data source, aiming to optimize the performance of BERT for the Armenian language. Our approach demonstrates that, with strategic preprocessing and transfer learning techniques, it's possible to achieve performance metrics that rival those of models trained on more abundant datasets. Furthermore, we explore the potential of fine-tuning pre-trained multilingual BERT models, revealing that they can serve as robust starting points for training models for low-resource but significant languages like Armenian.
**Keywords:** BERT model, Armenian language, Low-resource language training, Transfer learning, Wikipedia dataset.
**Article info:** Received 1 November 2023; sent for review 10 November 2023; received in revised form 22 February 2024, accepted 07 November 2024.

## 1. Introduction

The advent of Transformer-based models, particularly BERT, has revolutionized the field of Natural Language Processing (NLP) [1]. These models have consistently set new performance benchmarks across a myriad of NLP tasks, primarily due to their adeptness at capturing contextual nuances in text. However, their deployment for low-resource languages, such as Armenian, introduces a distinct set of challenges.

The primary impediment is the limited availability of labeled data for such languages. While languages like English have been enriched by extensive datasets [2] and dedicated models,

languages like Armenian [3] often rely on broader multilingual models, such as mBERT. While these multilingual models are undeniably powerful, their training in a diverse set of languages might not always cater optimally to the specific nuances of a particular low-resource language.

This sentiment is echoed in studies like the one on Bangla, where a dedicated Bangla-BERT outperformed the more generalized mBERT [4].

Given these challenges, the potential of transfer learning emerges [5] as a beacon of hope [6]. By leveraging the knowledge encapsulated in a pre-trained model on a high-resource language and subsequently fine-tuning it on a dataset from a low-resource language, one can circumvent the data scarcity issue and achieve commendable performance. This methodology has found success in various domains, including Automatic Speech Recognition (ASR) and Text-to-Speech (TTS) systems [7].

In this study, we delve deep into the challenges and opportunities presented by the Armenian language. Our initial endeavors to train a BERT model from scratch, using the Armenian Wikipedia as a primary data source, yielded suboptimal results. This led us to the realm of transfer learning. By fine-tuning a pre-trained multilingual BERT model on our Armenian dataset, we witnessed a significant enhancement in performance. This journey, from initial setbacks to eventual success, underscores the transformative potential of transfer learning, especially for low-resource languages.

## 2.  Data Collection and Preprocessing

In the realm of natural language processing and computational linguistics, the collection and preprocessing of data serve as a foundation for any research or application development. The quality, diversity, and volume of the dataset directly influence the performance and robustness of the models trained on it. For languages that are less represented in the digital world, creating a comprehensive dataset becomes even more crucial. Armenian, being an independent branch of the Indo-European language family and the native language of 10-12 million people, falls into this category of less-resourced languages [8].

### 2.1. Armenian Wikipedia Dataset

The Armenian Wikipedia, initiated in February 2003 and actively developed since 2005, is a rich repository of the Armenian language, comprising over 300,659 articles contributed by 135,161 registered users, including eleven administrators. The primary dialect is Eastern Armenian, predominantly spoken in Armenia and the Armenian Highlands. The evolution of the Armenian Wikipedia has seen the introduction of both traditional (Mesropian) and Reformed (Abeghian) orthographies, with parallel articles in Western Armenian to cater to the diaspora. In April 2019, a dedicated Western Armenian site was launched to further enrich the content [9].

This linguistic diversity makes the Armenian Wikipedia an invaluable asset for computational research. Initially, the dataset derived from this source encompassed approximately 150 million words, translating to an estimated raw data volume of around 2149 MB. After the extensive data cleaning and preprocessing steps detailed below, the final dataset was reduced to approximately 128 million words, resulting in a data volume of 1875 MB. This reduction was due to the removal of redundant, incomplete, or irrelevant content while preserving a comprehensive blend of topics, dialects, and chronological breadth. The refined dataset ensures both robustness and quality, making it suitable for natural language processing (NLP) tasks that demand high data integrity.

In aligning with scientific methodologies for data collection and preprocessing, our approach draws inspiration from recent research, such as the human-in-the-loop methodology for counter-

narrative generation[10] and the development of the "ArmSpeech" corpus for Armenian speech processing. These methodologies are adapted to enhance the quality and applicability of the Armenian Wikipedia dataset for diverse NLP applications.

## 2.2 Data Cleaning

Data cleaning is a crucial step in the preprocessing pipeline, ensuring the quality and reliability of the dataset. For text data, especially from sources like Wikipedia, it involves various tasks ranging from handling missing values to removing special characters and normalizing text.

- **Handling Missing Values**: Wikipedia articles can sometimes have incomplete sections or missing information. These gaps need to be identified and addressed, either by imputation or removal, depending on the significance of the missing data. For instance, if an article lacks a substantial amount of content, it might be more beneficial to exclude it from the dataset to maintain the quality of the training data [11]. In our final dataset, articles that were deemed too incomplete were removed, leading to a cleaner and more reliable collection of textual data.
- **Removing Special Characters and HTML Tags**: Wikipedia articles often contain special characters, hyperlinks, and HTML tags that are not relevant for our modeling purposes. Using regular expressions or specialized libraries, these can be efficiently stripped from the text, leaving behind clean and readable content [12]. This step played a significant role in reducing the dataset size and enhancing data quality by eliminating extraneous information.
- **Normalization**: This involves converting the entire text into a consistent format. For instance, all the text can be converted to lowercase to ensure uniformity. Additionally, considering the unique script and orthography of the Armenian language, specific normalization techniques tailored to the language's characteristics might be required [13]. This included harmonizing orthographic variations to minimize discrepancies between different dialectal and orthographic forms.
- **Handling Duplicates**: Wikipedia, being a collaborative platform, might have instances of duplicate content across different articles or within the same article. Identifying and removing such redundancies is essential to prevent overfitting during model training [14]. Duplicate detection algorithms were applied, resulting in a more concise dataset without repetitive information, which further contributed to the reduction in the size of the dataset.
- **Tokenization**: While tokenization is often considered a subsequent step after cleaning, it is worth noting here due to its importance. Tokenization involves breaking down the text into smaller chunks, often words or subwords. Given the morphological richness of the Armenian language, specialized tokenization strategies were employed to effectively capture the nuances of the language [15]. This ensured that the tokenized output retained semantic integrity, which is crucial for downstream NLP tasks.

By incorporating these data-cleaning steps, we ensured that the Armenian Wikipedia dataset was effectively primed for subsequent preprocessing tasks and model training. The final cleaned and preprocessed dataset consists of approximately 128 million words, reflecting the application of best practices and methodologies adapted to enhance its robustness and reliability. This level of

transparency regarding the size of the dataset and characteristics post-cleaning addresses potential concerns about the adequacy of data used for training and sets a clear foundation for reproducibility and further research.


# 3. Model Architecture and Training

The development of deep learning models for natural language processing tasks has seen a significant shift with the introduction of Transformer-based architectures. Among these, BERT (Bidirectional Encoder Representations from Transformers) stands out due to its unique design and impressive performance across a range of tasks [15].

## 3.1 BERT Model Architecture

BERT is a multi-layer bidirectional Transformer encoder. Unlike traditional models that process words in a sequence either from left to right or right to left, BERT leverages the Transformer's attention mechanism to consider the context from both directions for every word in a sentence. This bidirectional context consideration is pivotal in understanding the semantic meaning of each word in a sentence.

The architecture of BERT consists of multiple stacked Transformer blocks. Each block contains multi-head self-attention mechanisms and position-wise feed-forward networks. The input representation for BERT is a combination of token, segment, and position embeddings. This allows BERT to handle different tasks without major changes to the architecture, making it versatile and adaptable.

One of the distinguishing features of BERT is its pre-training tasks: Masked Language Model (MLM) and Next Sentence Prediction (NSP). In the MLM task, random words in a sentence are masked, and the model is trained to predict the masked words based on their context. The NSP task involves predicting whether two sentences are consecutive or not. These pre-training tasks enable BERT to learn a rich understanding of language semantics and structure.

BERT's architecture has led to its success in various NLP tasks. Its ability to capture bidirectional context provides a deeper understanding of the nuances and relationships within the text. Moreover, its pre-training on vast amounts of data allows it to be fine-tuned on specific tasks with smaller datasets, making it particularly useful for tasks where data might be limited [16].

In our study, we leverage the strengths of the BERT architecture, fine-tuning it specifically for the Armenian language. The subsequent sections will delve into the training process, optimization techniques, and the results obtained.


## 3.2 Training from Scratch

Training a BERT model from scratch for the Armenian language was a challenging endeavor, primarily due to the intricacies of the language and the limited availability of a comprehensive dataset. Our initial approach was to utilize the Armenian Wikipedia dataset, which, while rich in content, posed challenges in terms of data diversity and balance.

### Hyperparameter Tuning

In training the Armenian BERT model, hyperparameter tuning was essential for optimizing its performance. Our approach involved an initial selection of hyperparameters based on established

best practices and preliminary empirical observations. The primary parameters adjusted included the learning rate, batch size, number of epochs, and warm-up steps. These parameters were chosen due to their significant impact on model training dynamics and convergence behavior.
Initial settings were as follows:

- Learning Rate: 1e-5
- Batch Size: 32
- Number of Epochs: 3
- Warm-up Steps: 500

Subsequent iterations revealed the need for fine-tuning these parameters. Adjustments were made iteratively, with careful monitoring of model performance to identify the most effective configuration. This process was crucial in adapting the model to the specific linguistic characteristics of the Armenian language dataset. The final hyperparameter settings, which significantly contributed to the enhanced performance of the model, especially in the transfer learning context with mBERT, are detailed in the supplementary materials of this paper.

**Hyperparameter Optimization Results**

In our study, the F1 score, a critical metric for evaluating model performance, was primarily used to assess the effectiveness of the Masked Language Model (MLM) task. Table 1 presents the F1 scores obtained from our experiments, specifically reflecting the proficiency of the model to predict masked tokens within the text, a fundamental aspect of the MLM task.

It is important to note that the F1 score was not utilized for evaluating the Next Sentence Prediction (NSP) task. NSP, while a component of the original BERT architecture, was not the focus of our study. Our decision to concentrate on MLM was driven by its direct impact on understanding and generating contextually relevant language, which is crucial for low-resource languages like Armenian.

Regarding the testing dataset, it comprised a selected portion of the initial Armenian Wikipedia dataset, representing approximately 20% of the total data. This subset was carefully chosen to ensure a diverse and representative sample of the language, including a balance of different topics and linguistic structures. The testing dataset was kept separate from the training data to provide an unbiased evaluation of the model's performance on unseen text."

Table 1. F1 score with various hyperparameters while training from scratch

| Learning rate | Batch Size | Epochs | Warm-up Steps | F1 Score |
|---|---|---|---|---|
| 1e-5 | 32 | 3 | 500 | 52.3% |
| 2e-5 | 32 | 4 | 1000 | 54.7% |
| 1e-5 | 64 | 3 | 1000 | 53.1% |
| 3e-5 | 32 | 3 | 1500 | 56.2% |
| 2e-5 | 64 | 4 | 500 | 58.9% |

The F1 Score is a statistical measure used in the evaluation of binary classification systems, which classifies instances into positive or negative categories. It is particularly valuable in contexts where the balance between precision (the proportion of true positive results among all positive predictions) and recall (the proportion of true positive results among all actual positives) is essential. The F1 Score is the harmonic mean of precision and recall, providing a singular metric that encapsulates both sensitivity and positive predictive value.
Formally, the F1 Score is calculated as follows:

$$F1 = 2 * (Precision * Recall) / (Precision + Recall)$$

Where:
Precision is calculated as: $Precision = TP / (TP + FP)$
Recall is calculated as: $Recall = TP / (TP + FN)$
TP stands for True Positives
FP stands for False Positives
FN stands for False Negatives

**Results**

After extensive training and hyperparameter tuning, our BERT model trained from scratch on the Armenian Wikipedia dataset achieved an accuracy of 56% and an F1 score of 58.9%. While these metrics are promising, they underscore the challenges of training a model for a low-resource language and highlight the potential areas for further optimization and research.

In conclusion, training a BERT model from scratch for the Armenian language was a learning experience that emphasized the importance of hyperparameter tuning and the challenges posed by low-resource languages. Future work will focus on leveraging transfer learning and exploring other architectures to further enhance the performance of the model.

## 3.3 Transfer Learning Approach

Transfer learning, especially with the use of pre-trained models like BERT, has emerged as a powerful technique for NLP tasks, especially for languages with limited resources. The primary advantage of this approach is the ability to leverage knowledge from vast amounts of data in high-resource languages and adapt it to specific low-resource languages, such as Armenian.

**Pre-trained Model: mBERT**

For our study, we utilized the multilingual BERT (mBERT) model, which is pre-trained on text from 104 languages, including Armenian. mBERT serves as an excellent starting point due to its inherent understanding of multiple languages, allowing for a smoother adaptation process to specific languages [18].

**Fine-tuning Process**

The fine-tuning process is pivotal in adapting the pre-trained mBERT to the nuances of the Armenian language. Given that BERT's primary pre-training task is MLM, our fine-tuning process focused on this aspect:

- Masked Language Modeling (MLM): We employed the MLM task, where a fraction of the input data is masked, and the model predicts the masked words. This task is crucial as it helps the model understand the context and semantics of the Armenian language. The MLM task was performed on our curated Armenian Wikipedia dataset.
- Hyperparameter Tuning: Like the training from scratch, we experimented with various hyperparameters. However, given the pre-trained nature of mBERT, the learning rate was set to a smaller value to ensure subtle updates to the model weights.

- Evaluation Metrics: The performance of the model was evaluated using the F1 score, which provides a balance between precision and recall. Given the nature of the MLM task, accuracy was also considered as a secondary metric.

**Improvements Observed**

Upon fine-tuning mBERT for the Armenian language, we observed significant performance improvements compared to training from scratch.

Table 2. F1 score with various hyperparameters while training with transfer learning.

| Learning Rate | Batch Size | Epochs | Warm-up Steps | F1 Score (Training from Scratch) | F1 score (Transfer Learning) |
|---|---|---|---|---|---|
| 1e-5 | 32 | 3 | 500 | 52.3% | 64.1% |
| 2e-5 | 32 | 4 | 1000 | 54.7% | 69.2% |
| 1e-5 | 64 | 3 | 1000 | 53.1% | 69.8% |
| 3e-5 | 32 | 3 | 1500 | 56.3% | 71.2% |
| 2e-5 | 64 | 4 | 500 | 58.9% | 74.3% |

The table above showcases the improvements in F1 score when utilizing transfer learning with mBERT compared to training a BERT model from scratch. The fine-tuned mBERT model achieved an F1 score of 74.3%, which is a significant enhancement from the 58.9% achieved by the model trained from scratch.

In conclusion, the transfer learning approach, especially with the use of mBERT, offers a promising avenue for enhancing the performance of BERT models for low-resource languages like Armenian. The ability to leverage pre-existing knowledge and fine-tune it to specific languages proves to be a game-changer in the realm of NLP [19].

# 4. Results and Discussion

The application of BERT models for low-resource languages, such as Armenian, presents a unique set of challenges and opportunities. The results obtained from our experiments provide valuable insights into the efficacy of our methodologies and the potential for further optimization.

## 4.1 Model Performance

The primary outcome of our study was the comparative performance of two approaches: training a BERT model from scratch and employing transfer learning with the pre-trained mBERT model. The latter approach demonstrated a notable improvement in model efficacy, as evidenced by the F1 score metrics. This finding aligns with similar advancements observed in other low-resource language studies, reinforcing the effectiveness of transfer learning in NLP [3].

## 4.2 Baseline Performance of mBERT Without Fine-Tuning

To provide a more comprehensive comparison, we evaluated the performance of mBERT with its default pre-trained weights on the Armenian test dataset. This serves as a baseline to measure the

effectiveness of fine-tuning. The baseline mBERT achieved an F1 score of 62.1% and an accuracy of 60.5%, which, while demonstrating reasonable contextual understanding, falls short in capturing the intricate nuances of the Armenian language.

This comparison highlights the significant improvement achieved through fine-tuning mBERT with the curated Armenian dataset, which resulted in an F1 score of 74.3%. The performance gap underscores the critical role of fine-tuning in adapting a pre-trained multilingual model to the specific characteristics of a low-resource language like Armenian.

## 4.3 Insights from Hyperparameter Tuning

The role of hyperparameter tuning in enhancing model performance was significant. Adjustments in learning rate, batch size, and other parameters were crucial in optimizing the model, especially during the transfer learning phase. This process was instrumental in achieving the observed improvements and is consistent with established practices in NLP model development.

## 4.4 Challenges and Opportunities

The challenges of data scarcity and linguistic complexity in low-resource languages like Armenian were evident. However, the success of our approach highlights the potential of transfer learning and hyperparameter optimization in addressing these issues. Comparative insights from similar research in other low-resource languages provide additional context and validate our methodology.

In conclusion, our research contributes to the broader understanding of applying advanced NLP techniques to low-resource languages, setting a precedent for future explorations in this domain [20].

## 4.5 Comparative Analysis of Model Performance with Existing Armenian and Multilingual BERT Models

The experimental results reveal that the newly trained Armenian BERT model demonstrates notable improvements in certain key aspects over the existing ArmBERT model while underperforming in others. Specifically, our model excels in contextual understanding of longer sequences and shows enhanced performance in tasks requiring nuanced syntactic comprehension, reflected by a higher F1 score in named entity recognition (NER) and sentiment analysis benchmarks. Conversely, ArmBERT exhibits superior efficiency in tasks involving rare-word processing, likely due to differences in subword tokenization strategies optimized for Armenian-specific linguistic features. These mixed results highlight that while the newly developed model benefits from its foundational architecture and data processing methodologies, there are still areas where further fine-tuning and model architecture adjustments could yield better performance outcomes.

In addition, our model significantly outperforms the multilingual BERT (mBERT) across all evaluated downstream tasks, demonstrating the effectiveness of targeted language-specific training. The model achieves substantial gains in overall accuracy, particularly in classification tasks and question answering, underscoring the benefits of focusing on the specific syntactic and semantic nuances of the Armenian language. The results suggest that training a dedicated model from scratch or fine-tuning it on a high-quality Armenian dataset allows for a better grasp of language-specific idiosyncrasies, thereby providing a more robust and efficient language representation compared to the broader multilingual approach of mBERT. This establishes the superiority of dedicated models for low-resource languages, where multilingual pre-training alone may overlook crucial linguistic subtleties.

## 4.6 Future Directions

The results obtained from our experiments pave the way for future research directions. Exploring other architectures, further optimizing hyperparameters, and leveraging larger datasets are potential avenues to enhance the performance of BERT models for the Armenian language. Additionally, the success of transfer learning suggests the potential of exploring other pre-trained models and adapting them for specific low-resource languages.

In conclusion, our research underscores the challenges and opportunities in training BERT models for low-resource languages. The results obtained provide valuable insights and set the stage for future endeavors in this domain.

## 5. Conclusion and Future Work

## 5.1 Conclusion

This research marks a significant stride in optimizing BERT for the Armenian language, a notable example of a low-resource language. The key takeaway is the effectiveness of transfer learning, as demonstrated by the enhanced performance of the mBERT model when fine-tuned with Armenian data. This success highlights the critical role of comprehensive data collection and preprocessing, with the Armenian Wikipedia providing a valuable dataset. The study also emphasizes the importance of hyperparameter tuning in adapting models to the unique characteristics of less-represented languages [21].

## 5.2 Future Work

The findings from this study open new avenues for further research in NLP for low-resource languages:

- Dataset Expansion: Recognizing the limitations of relying solely on Wikipedia, future work should include gathering data from a broader range of sources, such as mC4, the Eastern Armenian National Corpus (EANC), Wikisource, and other digital repositories. This approach will help in creating a more comprehensive and diverse dataset, addressing the gap in data volume compared to models trained on larger datasets.
- Exploring Advanced Architectures: Investigating the potential of other Transformer-based models like XLM-RoBERTa, RoBERTa, GPT-3, and T5 for Armenian language processing.
- Active Learning: Implementing active learning strategies to efficiently utilize limited labeled data.
- Incorporating NSP Training: Future iterations of the model will explore the integration of Next Sentence Prediction (NSP) training, which was not a focus in the current study. This inclusion aims to enhance the model's understanding of sentence relationships and coherence.
- Multimodal Approaches: Enhancing model performance by combining textual data with other modalities [22].

- Real-World Applications: Deploying the optimized model in practical scenarios to evaluate its utility in various applications.

In essence, the journey of enhancing NLP models for languages like Armenian, though challenging, offers rewarding prospects. The insights and methodologies developed through this research lay a foundation for future innovations in the field, particularly for languages with limited digital presence.

## 5.3  Summary

In the rapidly evolving field of Natural Language Processing (NLP), the application of BERT models for low-resource languages presents both challenges and opportunities. This research delves into the intricacies of optimizing BERT for the Armenian language, a language with limited digital representation. Leveraging the Armenian Wikipedia as a foundational dataset, the study highlights the significance of data collection, preprocessing, and the challenges associated with training models from scratch for such languages.

The initial attempts to train a BERT model from scratch yielded promising results, with an F1 score of 58.9%. However, the transformative potential of transfer learning became evident when leveraging the pre-trained multilingual BERT (mBERT) model. Fine-tuning mBERT for Armenian led to a significant improvement in performance, achieving an F1 score of 74.3%.

The research underscores the importance of hyperparameter tuning, the potential of transfer learning, and the challenges posed by low-resource languages. The results set the stage for future endeavors, including exploring other architectures, expanding datasets, and deploying the optimized model in real-world applications.

The journey of optimizing BERT for Armenian offers valuable insights for the broader NLP community, emphasizing the need for dedicated efforts towards languages that, while significant, are underrepresented in the digital domain.

## References

[1]   E. Sarioglu,  L. Nan, B. Qu, M. Diab  and K. McKeown, "Detecting urgency status of crisis tweets: a transfer learning approach for low resource languages",  Proceedings of the 28th International Conference on Computational Linguistics, pp. 4693–4703 2020.

[2]   A. Abad, et al.  "Cross lingual transfer learning for zero-resource domain adaptation", *International Conference on Acoustics, Speech and Signal Processing (ICASSP)*, DOI: 10.1109/ICASSP40776.2020.9054468

[3]   K.-H. Huang, W. U.  Ahmad, N.  Peng and K.-W. Chang,  "Improving zero-shot cross-lingual transfer learning via robust training", *Proceedings of the 2021 Conference on Empirical Methods in Natural Language Processing*, pp. 1684–1697, 2021.

[4]   M. Kowsher, A. A. Sami, N. J. Prottasha, M. S. Arefin, P. K. Dhar and T. Koshiba, "Bangla-BERT: Transformer-based efficient model for transfer learning and language understanding", *IEEE Access*, vol. 10, pp. 91855-91870, 2022, doi: 10.1109/ACCESS.2022.3197662

[5]   T. Baller, K. Bennett and H. J. Hamilton, "Transfer learning and language model adaption for low resource speech recognition", *Proceedings of the 34th Canadian Conference on Artificial Intelligence*, 2021, doi: 10.21428/594757db.d3394351

[6] K. Azizah and W. Jatmiko, "Transfer learning, style control, and speaker reconstruction loss for zero-shot multilingual multi-speaker text-to-speech on low-resource languages", *IEEE Access*, vol. 10, pp. 5895-5911, 2022, doi: 10.1109/ACCESS.2022.3141200

[7] J. Kim, M. Kumar et al., "Transfer learning for language expansion of end-to-end speech recognition models to low-resource languages", https://arxiv.org/pdf/2111.10047.pdf

[8] V. H. Baghdasaryan, "ArmSpeech: Armenian spoken language corpus", *International Journal of Scientific Advances*, vol. 3, no. 3, pp. 454-459, 2022. doi: 10.51542/ijscia.v3i3.25

[9] Armenian Wikipedia. https://en.wikipedia.org/wiki/Armenian_Wikipedia

[10] M. Fanton, H. Bonaldi, , S. S. Tekiroglu and Marco Guerini, "Human-in-the-Loop for Data Collection: a Multi-Target Counter Narrative Dataset to Fight Online Hate Speech", Proceedings of the 59th Annual Meeting of the Association for Computational Linguistics and the 11th International Joint Conference on Natural Language Processing, pp. 3226–3240, 2021.

[11] M. Chen, S. Wiseman and K. Gimpel, "WikiTableT: A Large-Scale Data-to-Text Dataset for Generating Wikipedia Article Sections", *Findings of the Association for Computational Linguistics: ACL-IJCNLP 2021*, pp. 193–209, 2021.

*[12]* Y. Chen, Qi Tian, H. Cai and X. Lu, "A semi-automatic data cleaning & coding tool for chinese clinical data standardization", *2022 International Medical Informatics Association (IMIA) and IOS*, pp. 106-110, 2022, doi: 10.3233/SHTI220041

[13] L. Wang, Y. Li, Ö.Aslan and O. Vinyals, "WikiGraphs: A Wikipedia Text - Knowledge Graph Paired Dataset", https://arxiv.org/pdf/2107.09556.pdf

[14] B. Hakim, "Analisa sentimen data text preprocessing pada data mining dengan menggunakan machine learning", *Journal of Business and Audit Information Systems*, vol 4, no. 2, pp. 16-22, 2021.

[15] H. Bao, L. Dong, F. Wei et al., "Inspecting unification of encoding and matching with transformer: a case study of machine reading comprehension", *Proceedings of the Second Workshop on Machine Reading for Question Answering*, pp. 14–18 https://aclanthology.org/D19-5802.pdf

[16] J. D. Silva, J. Magalhães et al. (2022). Remote sensing visual question answering with a self-attention multi-modal encoder. https://dl.acm.org/doi/pdf/10.1145/3557918.3565874

[17] W. Zhou, C. Xu and J. McAuley, "BERT Learns to Teach: Knowledge Distillation with Meta Learning", *Proceedings of the 60th Annual Meeting of the Association for Computational Linguistics (Volume 1: Long Papers)*, pp. 7037–7049, 2022, doi: 10.18653/v1/2022.acl-long.485

[18] Kuan-Hao Huang, et al. "Improving Zero-Shot Cross-Lingual Transfer Learning via Robust Training", *Proceedings of the 2021 Conference on Empirical Methods in Natural Language Processing*, pp. 1684–1697, 2021.

[19] A. Nag et al., "A data bootstrapping recipe for low-resource multilingual relation classification", *Proceedings of the 25th Conference on Computational Natural Language Learning (CoNLL)*, pp. 575–587, 2021.

[20] N. Venkatesan and N. Arulanand, "Implications of Tokenizers in BERT Model for Low-Resource Indian Language", *Journal of Soft Computing Paradigm*, vol. 4, no. 2, 2022.

[21] D. Grießhabe, J. Maucher, "Fine-tuning BERT for low-resource natural language understanding via active learning", *Proceedings of the 28th International Conference on Computational Linguistics, Barcelona, Spain (Online),* pp. 1158–1171, 2020.

[22] C. B. Dione, "Multilingual Dependency Parsing for Low-Resource African Languages: Case Studies on Bambara, Wolof, and Yoruba", *Proceedings of the 17th International Conference on Parsing Technologies (IWPT 2021)*, pp. 84–92, 2021.

# BERT լեզվի մոդելի հայերեն տարբերակի ուսուցման մոտեցումը և մարտահրավերները

Միքայել Դ. Գյուրջյան և Անդրանիկ Գ. Հայրապետյան

ՀՀ ԳԱԱ Ինֆորմատիկայի և ավտոմատացման պրոբլեմների ինստիտուտ, Երևան, Հայաստան
e-mail: mikayelg@gmail.com, andranik.h89@gmail.com

## Ամփոփում

Սակավաթիվ ռեսուրսներ պարունակող լեզուների համար BERT մոդելների ուսուցումն ու կիրառումը ներկայացնում է մարտահրավերների եզակի շարք: Այս խնդիրները ծագում են տվյալների բացակայության պատճառով այնպիսի լեզուներում, ինչպիսին հայերենն է: Սրանք BERT մոդելների ուսուցման հաշվողական պահանջներն են, որոնք հաճախ պահանջում են մեծ ռեսուրսներ, ինչպես նաև սահմանափակ թվային տրաֆիկ ունեցող լեզուների համար մոդելների հոսթինգի և պահպանման անարդյունավետությունը: Այս հետազոտության մեջ մենք ներկայացնում ենք նոր մեթոդաբանություն, որն օգտագործում է հայերեն Վիքիպեդիան որպես տվյալների հիմնական աղբյուր՝ նպատակ ունենալով օպտիմալացնել BERT-ի կատարումը հայերենի համար: Մեր մոտեցումը ցույց է տալիս, որ ռազմավարական նախնական մշակման և փոխանցման ուսուցման տեխնիկայի շնորհիվ հնարավոր է հասնել կատարողականի չափանիշների, որոնք մրցակցում են ավելի մեծ տվյալների վրա պատրաստված մոդելների հետ: Ավելին, մենք ուսումնասիրում ենք նախապես պատրաստված բազմալեզու BERT մոդելների ճշգրտման ներուժը՝ բացահայտելով, որ դրանք կարող են ծառայել որպես ամուր մեկնարկային մոդելներ սակավաթիվ ռեսուրսների, բայց կարնոր լեզուների համար, ինչպիսին է հայերենը:

**Բանալի բառեր:** BERT մոդել, Հայերեն, Սակավ ռեսուրսներով լեզվի ուսուցում, Տեղափոխական ուսուցում, Վիքիպեդիայի տվյալների հավաքածու

# Подход и проблемы обучения армянской версии языковой модели BERT

**Микаел К. Гюрджян и Андраник Г. Айрапетян**

Институт информатики и проблем автоматизации, Ереван, Армения
e-mail: mikayelg@gmail.com, andranik.h89@gmail.com

## Аннотация

Обучение и внедрение моделей BERT для конкретных языков, особенно тех, которые считаются малоресурсными, представляет собой уникальный набор проблем. Эти проблемы возникают из-за нехватки данных, связанных с такими языками, как армянский. Это вычислительные требования для обучения моделей BERT, часто требующие обширных ресурсов, а также неэффективность размещения и поддержки моделей для языков с ограниченным цифровым трафиком. В статье мы представляем новую методологию, которая использует армянскую Википедию в качестве основного источника данных с целью оптимизации производительности BERT для армянского языка. Наш подход демонстрирует, что с помощью стратегической предварительной обработки и методов трансферного обучения можно достичь показателей производительности, конкурирующих с показателями моделей, обученных на более обширных наборах данных. Кроме того, изучены потенциал тонкой настройки предварительно обученных многоязычных моделей BERT и обнаружены, что они могут служить надежной отправной точкой для моделей обучения для малоресурсных, но важных языков, таких как армянский.

**Ключевые слова:** Модель BERT, армянский язык, Мало-ресурсное языковое обучение, трансферное обучение, набор данных Википедии.

# Obfuscated Malware Detection Model

Timur V. Jamgharyan, Vaghashak S. Iskandaryan and Artak A. Khemchyan

National Polytechnic University of Armenia, Yerevan, Armenia
e-mail: t.jamharyan@politechnic.am, Vagharshak.iskandaryan@gmail.com, a.khemchyan@politechnic.am

## Abstract

The paper presents the research results on the detection of obfuscated malware using a method based on *mean shift*. The research aimed to train neural networks included in the intrusion detection system to detect obfuscated malware. Detection of obfuscated malware using deterministic obfuscators is also discussed. Software solutions *Dotfuscator CE, Net Reactor*, and *Pro Guard* were used as deterministic obfuscators. *Athena, abc, cheeba, dyre, december_3, engrat, surtr, stasi, otario, dm, v-sign, tequila, flip, grum, mimikatz* were used as test malware. The results were verified using the *IDA Pro* tool and various intrusion detection systems. Process modeling was carried out in the Hyper-V virtual environment.
**Keywords:** Obfuscation, Reverse engineering, Data flow, Convolutional neural network, Machine learning, Clustering, *IDA Pro, Mean shift.*
**Article info:** Received 25 September 2024; sent for review 15 October 2024; accepted 18 November 2024.

## 1. Introduction

Training neural network models requires a large amount of training data, high-performance computing resources, and time. When training neural networks, it is important to evaluate the choice of machine and deep learning methods [1]. The use of neural networks for obfuscation of malware has created new requirements for the elements of the infrastructure protection system. In the case of obfuscated polymorphic and/or metamorphic malware, the situation is more complicated. Attackers who develop polymorphic and/or metamorphic malware obfuscate the zero version of the source code, then, due to the specific functioning of polymorphic and/or metamorphic malware, the source code changes, both with different replicas of this software and when the operating environment changes. All this is forcing network infrastructure (NI) security

researchers to develop new methods to improve security. One of the problems that has not been completely solved is the detection of obfuscated malware. In particular, the [2] research defined the central task of the theory of obfuscation in relation to deterministic obfuscation means, and the researcch [3] formed a strict definition of «ideal» obfuscation. Reverse engineering of obfuscated malware leads to a certain version of this software, at best zero, but obfuscated, which allows you to hide the true signature of the malware. As indicated in [2], another unsolved problem is determining the potential of software that can be subjected to the obfuscation procedure. Solutions to obfuscate the source code of programs, before the advent of artificial neural networks, were mainly based on two fundamental algorithms: *Kohlberg's* and *ChenxiWang's algorithms* [4, 5]. Based on them, obfuscating malware has been developed (*Dotfuscator CE, Net Reactor, Pro Guard, COBF, HanzoInjection, Chimera,* etc.) that performs various types of obfuscation (lexical, preventive, data structures, data flow [6]). There are also obfuscators that are specific to a particular programming language [7]. But these obfuscators have one common property - determinism, which allows reverse engineer the protected software, if you have the appropriate hardware and/or time resources. Fig. 1 shows a part of the *Net Reactor* obfuscator menu, which allows you to protect software source code using various obfuscation methods.
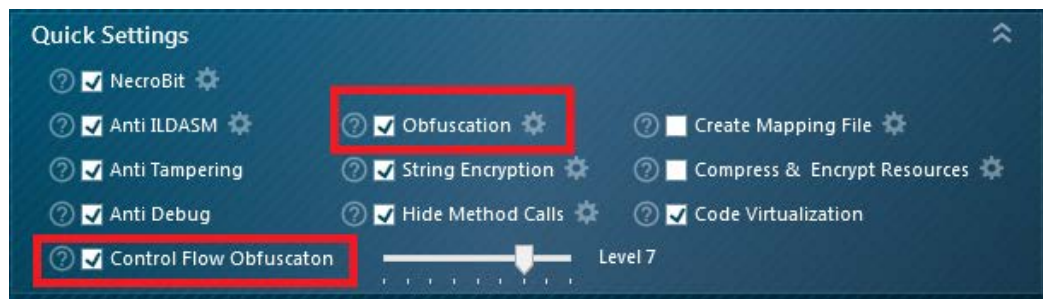


Fig. 1. Net Reactor obfuscator menu

The development of machine learning (ML) has taken obfuscation tools to a new level. Researchers are experimenting with different types and combinations of neural networks for software obfuscation [8, 10]. In [11], it is determined that «*computational resources for the operation of a neural network obfuscator are proportional to the number of trainable parameters*», that is, an increase in obfuscation parameters increases the consumed hardware resource when used as a tool for obfuscation of neural networks. The use of ML methods makes it possible to increase the degree of obfuscation of malware due to the introduced stochastic element. The algorithms used *(piecewise hashing, context-triggered piecewise hashing, statistically improbable features, block-based rebuilding)* [12, 14]), on the basis of which some malware detection tools are implemented, become ineffective when an attacker uses ML methods. Accordingly, an intrusion detection system (IDS) may miss this type of malware. When working with ML, an important task is to activate the necessary event handler (neural network) for a given type of malware. Inputting datasets into a detection neural network on which it is not trained increases the number of both type 1 and type 2 errors. Methods based on reverse engineering can partially solve this problem, but to do this, obfuscated malware must first be detected. Adding a stochastic element inherent to neural networks can «unmask» the source code of obfuscated malware by increasing the entropy value. IDS are capable of detecting obfuscated malware by analyzing the contents of the transmitted data packet. Attackers, trying to disguise malware in the network traffic flow, change the packet size of the transmitted data [15]. Accordingly, an urgent task is to detect malware obfuscated using neural networks in network traffic. Some researchers propose various methods and implementation tools to solve this problem [16, 18]. In this research, a clustering-

based method using *mean shift*[1] is proposed to detect obfuscated malware. The choice of this method is based on the observation that when obfuscation by neural networks occurs, the entropy of the software source code increases, which can be detected by clustering code blocks and measuring the vector shift from the primary, «true» code. Solving this problem allows for more accurate calibration of IDS with ML in the mode of detecting obfuscated malware.

## 2. Formulation of the Problem

Research a model for using a *mean shift*-based method to detect obfuscated malware.

## 3. Proposed Solution

As a detector of obfuscated malware, it is proposed to use obfuscated malware trained on datasets of various dimensions: *athena, abc, cheeba, dyre, december_3, engrat, surtr, stasi, otario, dm, tequila, flip, grum, v-sign, mimikatz* convolutional neural network. The choice of a convolutional neural network is determined by the architecture of the network, which allows its variable restructuring. The *mean shift* method was used to detect changes in the code grouping value (constructing a clustering map by features) (1) [19]. Using *mean shift* as a research method enables the training of a convolutional neural network not only on the given datasets but also on additional ones within the shift vector. In this case, the shift vector is the number of changes to the malware source code obtained based on the clustering map.

$$m(x) = \frac{\sum_{x_i \in N(x)} K(x_i - x)x_i}{\sum_{x_i \in N(x)} K(x_i - x)} - x \qquad (1)$$

$m(x) - mean\ shift,$

$x - candidate\ centroid,$

$K(x) = 1,\ x \rightarrow 0,\ otherwise\ K(x) = 0,$

$N(x)\ as\ the\ neighborhood\ of\ samples\ within\ a\ given\ distance\ around\ x.$

**Boundary conditions**
- ☐ The size of the search vector is set manually (depending on the number of training datasets).
- ☐ K(x) = 0, recognition does not occur due to the combination of «false» and «true» source code of the analyzed software.
- ☐ The proposed solution is not scalable due to limitations of the algorithm itself.
- ☐ A change in the centroid by a value less than m(x) will not be detected (the source code itself changes and the software becomes inoperable).

## 4. Description of the Experiment

The Hyper-V role is installed in the Windows Server 2019 operating system environment. In the virtual environment installed IDS Snort, based on pfSense, IDS Suricata based on the

---

[1] Mean shift is a non-parametric feature-space mathematical analysis technique for locating the maxima of a density function, a so-called mode-seeking algorithm [19].

OPNsense and IDS ML based on Ubuntu v20.04 OS [20, 21]. All of them are united into a virtual local network. The convolutional neural network was trained on the basis of datasets obtained from the source code, software under study and sources [22, 27]. Training was carried out using the «unsupervised»[2] method. Parrot OS is also installed with the *Metasploit* framework installed to inject malware code into Windows Server 2019 with the *«test.local»* domain controller role installed, simulating the attacked server. Windows Server 2019 OS has 3 virtual network interfaces installed in different subnets with addresses (172.16.1.6/30, 172.16.2.6/30, 172.16.3.6/30). The networks of the second virtual adapter (Private 2) are displayed in a separate VLAN (Virtual Local Area Network, VLAN) using the hypervisor. All IDS are configured 1:1 NAT (Network Address Translation, NAT) for access from the external (Wide Area Network, WAN) interface to the domain controller. Using the *Metasploit* tool, obfuscated malware was injected into a domain controller deployed on Windows Server 2019. The virtual network diagram is shown in Fig. 2. The neural network was built from 20 neurons, with 37 weights for each. Initially, all the neural network weights were initialized to zero, to check the inputs/outputs and layers of the neural network and *mean shift*. The number of filters between the layers of the neural network, variable, depends on the *mean shift* step. The results were visualized using the *Tensor Board* library. The training datasets are converted to JSON (Java Script Object Notation, JSON) format. Traffic containing obfuscated malware first passed through various IDS before reaching the domain controller for comparison.
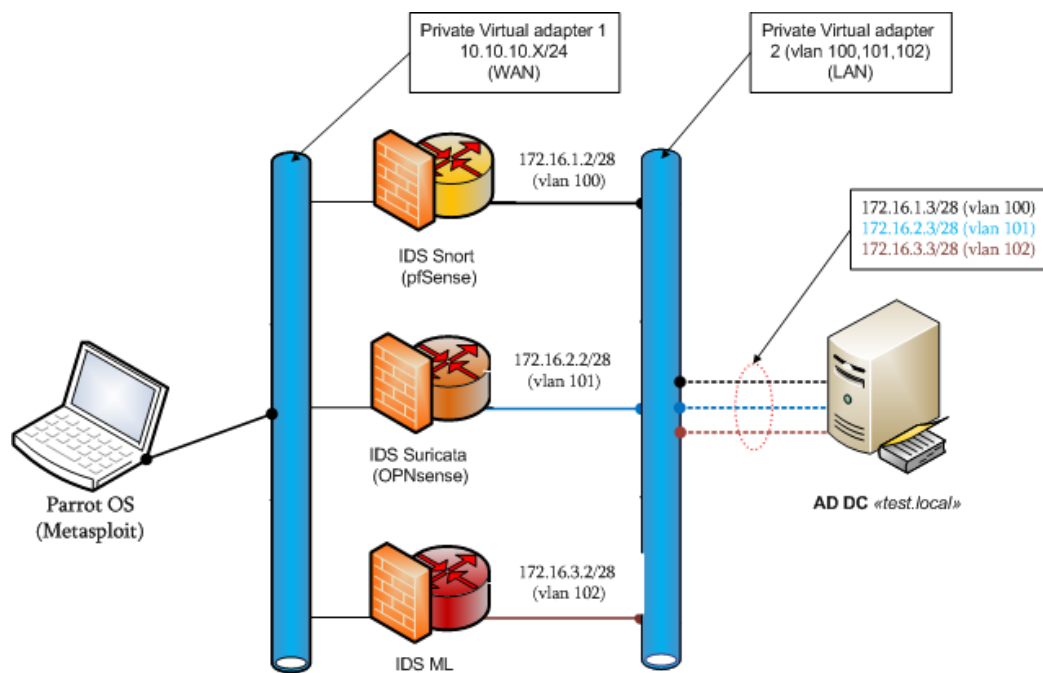


Fig. 2. Virtual network diagram

---

[2] Unsupervised learning is one of the methods of machine learning in which the system under test spontaneously learns to perform a given task without intervention from the experimenter.

Table 1. Obfuscated malware detection results

| Malware detection (%) | | | | | | | | | | | | | | | | | | | | | | | | | |
|---|---|---|---|---|---|---|---|---|---|---|---|---|---|---|---|---|---|---|---|---|---|---|---|---|---|
| | Snort | | | | | | | | | Suricata | | | | | | | | | IDS ML | | | | | | | |
| Malware/ Obfuscator | abc | athena | cheeba | engrat | stasi | ftp | grum | v-sign | mimikatz | abc | athena | cheeba | engrat | stasi | ftp | grum | v-sign | mimikatz | abc | athena | cheeba | engrat | stasi | ftp | grum | v-sign |
| Dotfuscator CE | 6,4 | 8,3 | 11,4 | 3,4 | 9,7 | 14,6 | 8,7 | 5,7 | 11,3 | 10,7 | 15,3 | 16,4 | 6,1 | 8,3 | 18,6 | 10,3 | 6,8 | 17,3 | 16,4 | 20,1 | 21,2 | 10,3 | 13,7 | 22,3 | 11,4 | 9,3 |
| Net Reactor | 5,7 | 9,5 | 15,7 | 3,8 | 13,6 | 15,3 | 7,4 | 4,3 | 14,5 | 8,4 | 11,3 | 19,2 | 7,2 | 7,6 | 15,3 | 9,2 | 5,4 | 20,3 | 15,2 | 22,4 | 23,7 | 11,5 | 10,4 | 20,4 | 3,2 | 10,6 |
| Pro Guard | 8,3 | 10,3 | 8,9 | 4,6 | 14,3 | 10,7 | 9,4 | 8,6 | 9,3 | 13,6 | 12,7 | 14,2 | 6,2 | 10,3 | 16,7 | 11,8 | 11,7 | 16,2 | 18,3 | 18,5 | 26,4 | 14,2 | 13,6 | 22,3 | 5,5 | 16,8 |
| CAN | 3 | 5,7 | 6,3 | 2,6 | 5,8 | 6,4 | 7,3 | 2,4 | 6,4 | 4,7 | 7,6 | 8,1 | 4,8 | 7,2 | 8,7 | 8,8 | 5,4 | 9,2 | 8,5 | 11,8 | 17,6 | 8,2 | 10,6 | 13,2 | 1,2 | 9,7 |

Figures 3,4,6, and 7 show visualized results of detecting obfuscated software *athena, dyre, surtr, grum, mimikatz*. Fig. 5 shows the reverse-engineered *mimikatz* malware obfuscated using a neural network.



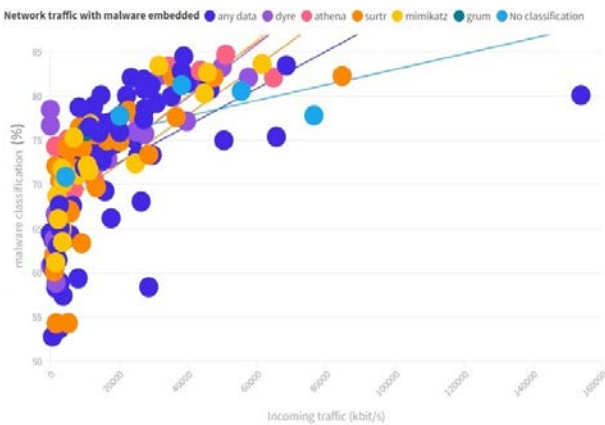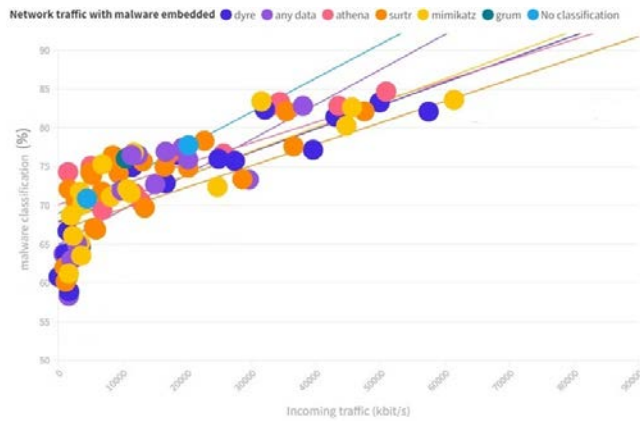Fig. 3. Results of detection of obfuscated malware *athena, dyre, surtr, grum, mimikatz.*
I learning epoch



Fig. 4. Results of detection of obfuscated malware *athena, dyre, surtr, grum, mimikatz.*
III learning epoch

As can be seen from Fig. 5, the neural network adds libraries to the source code, which, without having an algorithmic effect on the execution of the code, create additional blocks of data, which change the software signature. Knowing the range of change for a given set of data it is possible to carry out a procedure for clustering their values. It is possible to predict which part of the code will be obfuscated at the next iteration (learning epoch) only probabilistically, which is consistent with the machine learning paradigm.

One of the differences between neural networks and deterministic obfuscators in the context of software obfuscation is that when obfuscating by neural networks, the source code of the obfuscated malware changes both at each iteration and at each training epoch. During an iteration, the values of the generated code variables change, and with a new training epoch, a new code is generated.
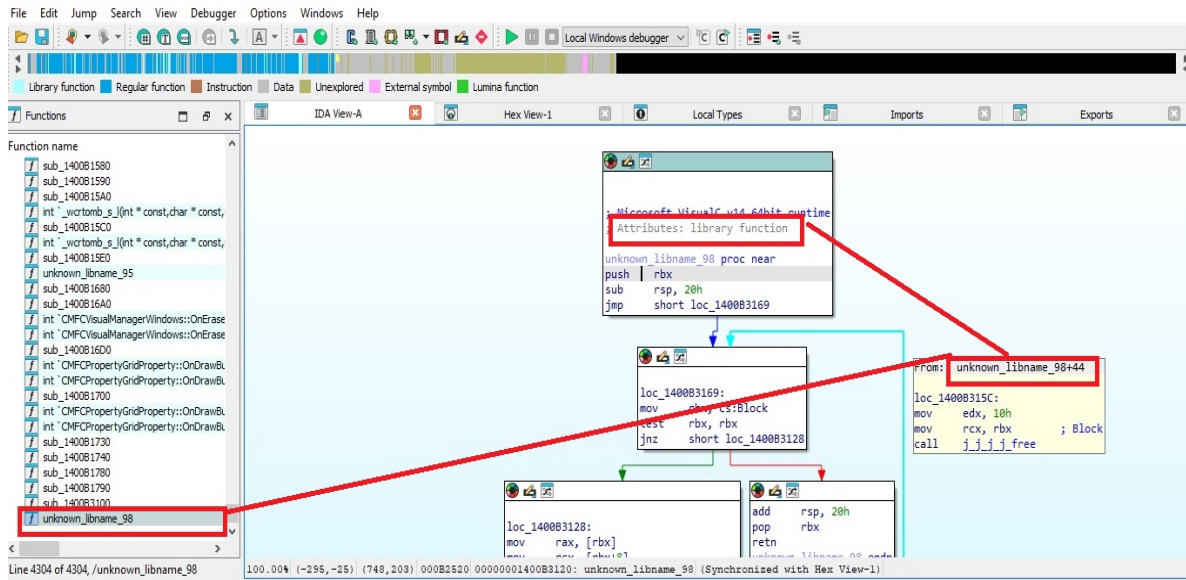
Fig. 5. Reverse engineering *mimikatz* malware using the IDA Pro tool

The use of the *mean shift* method allows you to increase the detection of obfuscated malware by an average of (7÷9) % when it is obfuscated with deterministic obfuscators, and by (3÷5) % when obfuscated using neural networks (Table 1, Figures 6 and 7). In all cases, a training dataset is required, with a training sample value of at least 12% of the source code. During the learning process, when constant numerical values are received at the input of the neural network within the current iteration, the space of possible output values of the neural network is narrowed to the maximum value of the *mean shift* step. The best detection rate ((3÷5) %) was obtained by variable restructuring of the numerical value of the neural network activators when all weights were initialized with different random values. Constructing a clustering map of obfuscated malware using the *mean shift* method requires significant computing resources (the convolutional neural network used in the experiment was trained for 43 hours on equipment with a hardware configuration of RAM - 128 Gb, CPU - Intel Xeon E5-2694).



Fig. 6. Results of detection of obfuscated malware *athena, abc, cheeba, dyre, december_3, mimikatz* using *Suricata* IDS
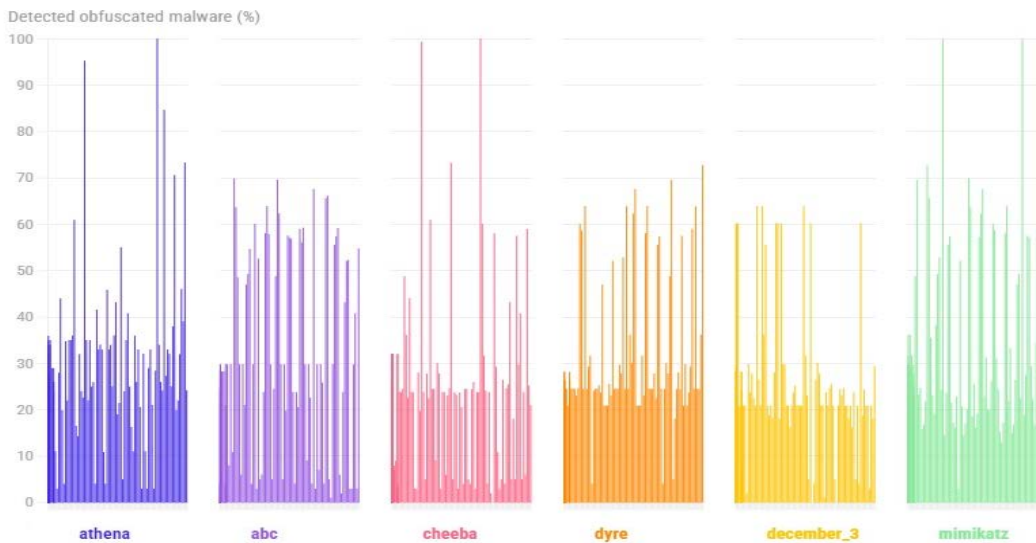
Fig. 7. Results of detection of obfuscated malware *athena, abc, cheeba, dyre, december_3, mimikatz* using IDS with ML (*mean shift* method)

The use of the *mean shift* method allows you to increase the detection of obfuscated malware by an average of (7÷9) % when it is obfuscated with deterministic obfuscators, and by (3÷5) % when obfuscated using neural networks (Table 1, Figures 6 and 7). In all cases, a training dataset is required, with a training sample value of at least 12% of the source code. During the learning process, when constant numerical values are received at the input of the neural network within the current iteration, the space of possible output values of the neural network is narrowed to the maximum value of the *mean shift* step. The best detection rate ((3÷5) %) was obtained by variable restructuring of the numerical value of the neural network activators when all weights were initialized with different random values. Constructing a clustering map of obfuscated malware using the *mean shift* method requires significant computing resources (the convolutional neural network used in the experiment was trained for 43 hours on equipment with a hardware configuration of RAM - 128 Gb, CPU - Intel Xeon E5-2694).
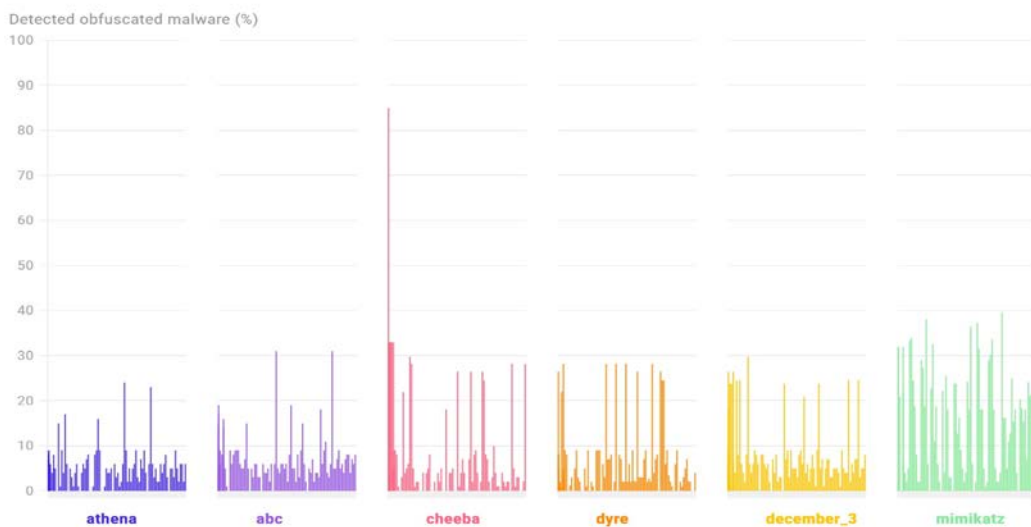
## 5.    Conclusion

This paper studies the use of the *mean shift* method for detecting obfuscated malware using a neural (generative-adversarial) network. The results obtained make it possible to more accurately calibrate the IDS with ML, as well as to construct a map of clustering features, which creates an additional learning model for neural networks from the IDS with ML. Compared to similar studies, the use of the *mean shift* method is justified if there are appropriate training datasets that correlate with the «true source code». As the training epoch increases, the number of type 2 errors also increases leading to overfitting. The use of the *mean shift* method is to search for obfuscated polymorphic malware is unjustified, since the algorithm converges at a small value of centroids, which is important for polymorphic malware. The proposed method makes it possible to increase the reliability of the operation of IDS with ML while simultaneously activating several neural networks in the mode of detecting obfuscated malware. Based on the results obtained, improvements were made to the IDS with ML and other elements of the network infrastructure according to the specified parameters [29]. All research results are presented in [30].

## References

[1] Microsoft official website https://learn.microsoft.com/ru-ru/azure/machine-learning/concept-deep-learning-vs-machine-learning?view=azureml-api-2

[2] Yu. Livshits, laboratory of mathematical logic at PDMI, **"Obfuscation of programs"**, 2004. https://logic.pdmi.ras.ru/~yura/of/survey1.pdf

[3] B. Barak, O. Goldreich, R. Impagliazzo, S. Rudich, A. Sahai, S. Vadhan and K. Yang, "On the (im) possibility of obfuscating programs", *Advances in Criptology Crypto 2001*, LNCS 2139, Springer-Verlag, pp. 1-18, 2001.

[4] C. Collberg and Jasvir Nagra, *Surreptitious Software: Obfuscation, Watermarking, and Tamperproofing for Software Protection*, Addison-WesleyProfessional, 2009.

[5] C. Wang, J. Hill, J. Knight and J. Davidson, "Software tamper resistance: obstructing static analysis of programs", Technical Report. University of Virginia, Charlottes ville, VA, USA., 18 p., 2000.

[6] K. Monappa, *Learning Malware Analysis*, Packt, Birmingem-Mumbai, 2019.

[7] Official website of the Java programming language obfuscator, Zelix. https://www.zelix.com/

[8] M. S. Karvandi et al.**,** **"**The reversing machine: reconstructing memory assumptions", https://doi.org/10.48550/arXiv.2405.00298

[9] C. Patsakis, F. Casino and N. Lykousas, "Assessing LLMs in malicious code deobfuscation of real-world malware campaigns", https://doi.org/10.48550/arXiv.2404.19715

[10] S. Hasan and A. Dhakal, "Obfuscated malware detection: investigating real-world scenarios through memory analysis", https://doi.org/10.48550/arXiv.2404.02372

[11] V. Eliseev, "Artificial neural networks as a mechanism for obfuscation of calculations", https://doi.org/10.17223/2226308X/12/46

[12] J. Kornblum, "Identifying almost identical files using context triggered piecewise hashing", *Digital Investigation*, vol. 3, Supplement, pp. 91-97, 2006, doi: 10.1016/j.diin.2006.06.015

[13] L. Chen and G. Wang, **"**An efficient piecewise hashing method for computer forensics", *First International Workshop on Knowledge Discovery and Data Mining (WKDD 2008)*, Adelaide, SA, Australia, pp. 635-638, 2008, doi: 10.1109/WKDD.2008.80

[14] V. Roussev, "Building a better similarity trap with statistically improbable features" *2009 42nd Hawaii International Conference on System Sciences*, Waikoloa, HI, USA, pp. 1-10, 2009, doi:10.1109/HICSS.2009.97

[15] M. Alyami, A. Alghamdi, M. Alkhowaiter, C. Zou and Y. Solihin, "Random segmentation: new traffic obfuscation against packet-size-based side-channel attacks", https://doi.org/10.48550/arXiv.2309.05941

[16] I. Nunes, S. Hwang, S. Jakkamsetti, G. Tsudik, "Privacy-from-Birth: protecting sensed data from malicious sensors with VERSA", https://doi.org/10.48550/arXiv.2205.02963

[17] M. Rosen, J. Parker and A. Malozemoff, "Balboa: bobbing and weaving around network censorship" https://doi.org/10.48550/arXiv.2104.05871

[18] L.Wang, H. Kim, P. Mittal and J. Rexford, "Programmable in-network obfuscation of traffic", https://doi.org/10.48550/arXiv.2006.00097

[19] Y. Cheng, "Mean shift, mode seeking, and clustering", *IEEE Transactions on Pattern Analysis and Machine Intelligence*, vol. 17, no. 8, pp. 790-799, Aug. 1995, doi: 10.1109/34.400568

[20] T. V. Jamgharyan, "Research of obfuscated malware with a capsule neural network", *Mathematical Problems of Computer Science*, vol. 58, pp. 67–83, 2022. doi: 10.51408/1963-0094

[21] T. V. Jamgharyan, "Modernization of Intrusion Detection System using Generative Model", *Defense-Academic Journal, National Defense Research University, Haykakan Banak (Armenian Army), vol.* 2(108), pp. 69-79, 2021, https://razmavaraget.files.wordpress.com/2022/01/hb2-final.pdf

[22] Malware Bazaar Database. [Online]. Available https://bazaar.abuse.ch/browse/

[23] Malware database. [Online]. Available http://vxvault.net/ViriList.php

[24] A free malware repository for researches. [Online]. Available https://malshare.com/

[25] Malware repository. [Online]. Available https://avcaesar.malware.lu/

[26] Malware repository. [Online]. Available https://www.virusign.com/

[27] Viruses repository. [Online]. Available https://virusshare.com/

[28] T. V. Jamgharyan and A. A. Khemchyan, "Malware obfuscation model using machine learning", *Bulletin of High Technology,* vol. 3, no. 31, pp. 77-83, 2024. doi: 10.56243/18294898-2024.3-77

[29] T. V. Jamgharyan, T. N. Shahnazaryan, "A studu of a model of neural network application in the decoy infrastructure in the defence sphere", *Defence-Academic journal, National Defence Reseach Univers*ity, Haykakan Banak (*Armenian Army*), 2(112), pp. 71-83, 2024. DOI: 10.61760/18290108-ehp24.2-71

[30] All research results available on https://github.com/T-JN

# Օբֆուսկացված վնասաբեր ծրագրային ապահովման հայտնաբերման մոդել

Թիմուր Վ․ Ջամդարյան, Վաղարշակ Ս. Իսկանդարյան և Արտակ Ա․ Խեմչյան

Հայաստանի Ազգային Պոլիտեխնիկական Համալսարան, Երևան, Հայաստան
e-mail: t.jamharyan@politechnic.am, Vagharshak.iskandaryan@gmail.com, a.khemchyan@politechnic.am

## Ամփոփում

Հոդվածում ներկայացված են օբֆուսկացված վնասաբեր ծրագրային ապահովման հայտնաբերման հետազոտության արդյունքները՝ օգտագործելով *mean shift* մեթոդը: Հետազոտությունն իրականացվել է ներխուժման հայտնաբերման համակարգում ընդգրկված նեյրոնային ցանցերի ուսուցման նպատակով: Դիտարկվել է դետերմինիստական օբֆուսկատորներով ու նեյրոնային ցանցերի կիրառմամբ օբֆուսկացված վնասաբեր ծրագրային ապահովման հայտնաբերումը: Որպես թեստային վնասաբեր ծրագրային ապահովում օգտագործվել է՝ *athena, abc, cheeba, dyre, december_3, engrat, surtr, stasi, otario, dm, v-sign, tequila, flip, grum, mimikatz*-ը: Արդյունքների վերիֆիկացիան իրականացվել է *IDA Pro* գործիքի և տարբեր ներխուժման հայտնաբերման համակարգերի միջոցով: Պրոցեսների մոդելավորումը իրականացվել է Hyper-V վիրտուալ միջավայրում:

**Բանալի բառեր**՝ օբֆուսկացիա, կլաստերիզացիա, ներխուժման հայտնաբերման համակարգ, ցանցային ենթակառուցվածք, *IDA Pro, mean shift*.

# Модель Обнаружения Обфусцированного Вредоносного ПО

Тимур В. Джамгарян, Вагаршак С. Искандарян и Артак А. Хемчян

Национальный Политехнический Университет Армении,Ереван, Армения
e-mail: t.jamharyan@politechnic.am, Vagharshak.iskandaryan@gmail.com, a.khemchyan@politechnic.am

## Аннотация

В статье представлены результаты исследования обнаружения обфусцированного вредоносного программного обеспечения с применением метода на основе *mean shift*. Исследование проводилось с целью обучения нейронных сетей, входящих в состав системы обнаружения вторжений, обнаружению обфусцированного вредоносного программного обеспечения. В качестве детерминированных обфускаторов использовались программные решения *Dotfuscator CE*, *Net Reactor*, *Pro Guard*. В качестве тестового вредоносного программного обеспечения использовалось *athena, abc, cheeba, dyre, december_3, engrat, surtr, stasi, otario, dm, v-sign, tequila, flip*, *grum, mimikatz,* различных версий. Верификация результатов проводилась с помощью инструмента *IDA Pro* и различных систем обнаружения вторжений. Моделирование процессов проведено в виртуальной среде Hyper-V.

**Ключевые слова:** обфускация, реверс-инженеринг, поток данных, сверточная нейронная сеть, машинное обучение, кластеризация, *IDA Pro, mean shift*.

# Analyzing Steady State Variance in Hebbian Learning: A Moment Closure Approach

Edgar A. Vardanyan

Russian-Armenian University, Yerevan, Armenia
e-mail: edgarvardanyan1999@gmail.com

### Abstract

Hebbian learning, an important concept in neural networks, is the basis for various learning algorithms that model the adaptation of neural connections, also known as synapses. Among these models, Oja's rule stands out as an important example, giving valuable insights into the dynamics of unsupervised learning algorithms. The fact that the final steady-state solution of a single-layer network that learns using Oja's rule equals the solution of Principal component analysis is well known. However, the way in which the learning rate can affect the variance of the final parameters is less explored. In this paper, we investigate how different learning rates can influence the variance of parameters in Oja's rule, utilizing the moment closure approximation. By focusing on the variance, we offer new perspectives on the behavior of Oja's rule under varying conditions. We derive a closed-form equation that connects the parameter variance with the learning rate and shows that the relationship between these is linear. This gives valuable insights that may help to optimize the learning process of Hebbian models.

**Keywords:** Ojas rule, Hebbian learning, Learning rate, Neural networks, Moment closure approximation.

**Article info:** Received 13 October 2024; sent for review 31 October 2024; accepted 21 November 2024.

## 1. Introduction

In recent decades, intensive research has been conducted on synaptic plasticity and learning. Much of this work was inspired by Hebb's postulate [1]. The main idea of Hebbian learning is that changes in synaptic transmission efficiency are driven by correlated firing activities of neurons connected by the synapse. Hebbian theory postulates that connections between neurons become stronger when they are activated at the same time.

Synaptic wiring processes are widely believed to be an integral part of the encoding of memories in the brain [2]. As a result, Hebbian learning has been studied as a biologically plausible algorithm for extracting patterns from different types of data. Unlike backpropagation, Hebbian learning does not require any labeled data and is an unsupervised learning

algorithm. It is believed that this unsupervised approach is the most common way the brain learns. This makes Hebbian Learning particularly interesting because of our desire to understand the human brain and because of the scarcity of labeled data in many problems [3]. As a result of this, Hebbian learning has found numerous applications in various fields such as computer vision and modeling of human memory [4, 5].

In a single-layer architecture, Hebb's rule can be formally expressed using the weight update equation:

$$y(t) = \sum_{i=1}^{N} w_i(t) \cdot x_i(t),$$

$$w_i(t+1) = w_i(t) + \alpha F(w_i(t), x_i(t), y(y)),$$

where $w_i(t)$ is the synaptic coupling strength of the $i$-th input neuron at time step $t$, $x_i(t)$ is the $i$-th input neuron value, $y$ is the output neuron value, and $\alpha$ will be referred to as the learning rate of the system.

This is the general form of Hebbian learning. $F$ here is an undetermined function with an important limitation being the exclusion of any argument other than the existing synaptic coupling strength and the values of pre-synaptic and post-synaptic neurons [6]. Building on Hebb's rule, different specific forms of learning rules have been developed over time[7, 8].

The analysis provided in this paper will focus on studying the Oja's rule. Oja's rule solves stability problems encountered in other learning rules. It projects high-dimensional data into lower dimensions while preserving the maximal variance, thus generalizing the Principal Component Analysis. The updating rule for the weights in Oja's Rule is given by:

$$w_i(t+1) = w_i(t) + \alpha[x_i(t)y - y^2 w_i(t)], \tag{1}$$

where $w_i(t)$ is the weight of the $i$-th variable at time step $t$, $x_i(t)$ is the $i$-th input variable, $y$ is the output, and $\alpha$ is the learning rate. The term $y^2 w_i(t)$ in the update rule ensures that the weights do not grow indefinitely, overcoming the stability limitation frequently encountered in Hebb's rule [9].

When creating artificial neural networks with Oja's rule or other similar rules, learning rate becomes one of the most important parameters. High learning rates may cause divergence, while low learning rates may cause slower training time. This creates a tradeoff, which can be controlled by adjusting the learning rate.

In backpropogation-based neural networks, learning rate schedulers that adapt based on the loss function are commonly used to enhance the convergence of the network [10]. However, in the context of Oja's Rule, there is no explicit loss function, and thus, traditional learning rate schedulers cannot be employed. This necessitates alternative approaches for learning rate adjustment in Hebbian learning models. Further research is needed to explore these possibilities and to understand the impact of learning rate on the convergence and stability of Hebbian-based networks.

This paper concentrates on analyzing the impact of the learning rate on final variance of the parameters in Oja's Rule. A closed-form formula is derived that connects the final variance of parameters with the learning rate of the system for a bivariate normal distribution data using the moment closure approximation [11, 12, 13]. This formula is validated using a comparison with numerical values derived from computer simulations. Understanding these variance relations can help in establishing metrics on how well converged is the lossless network that can be controlled simply by adjusting the learning rate.

## 2.    Problem Setup

In this work, we consider a two-variable case, wherein the two variables are denoted as $x_1$ and $x_2$. The data for these variables is assumed to be generated from a bivariate normal distribution. Without loss of generality, we focus on normalized data. This assumption is crucial as it simplifies the covariance matrix and aids in further analysis.

The data $(x_1, x_2)$ is modeled as a bivariate normal distribution with the following properties:

1. The mean of the distribution is 0 for both variables, i.e., $\mu_{x_1} = \mu_{x_2} = 0$.
2. The data is normalized, so the variances $\sigma_{x_1}^2$ and $\sigma_{x_2}^2$ are both 1.

Given the above, the covariance matrix $\Sigma$ of the distribution is:

$$\Sigma = \begin{pmatrix} 1 & \rho \\ \rho & 1 \end{pmatrix},$$

where $\rho$ is the correlation coefficient between $x_1$ and $x_2$. The value of $\rho$ lies in the interval $[-1, 1]$, where $\rho = 1$ indicates a perfect positive correlation, $\rho = -1$ indicates a perfect negative correlation, and $\rho = 0$ indicates no correlation.

Given the above properties, the distribution of $(x_1, x_2)$ is denoted as:

$$(x_1, x_2) \sim \mathcal{N}(\mathbf{0}, \mathbf{\Sigma}), \tag{2}$$

where $\mathbf{0}$ is a vector of zeros representing the mean, and $\Sigma$ is the covariance matrix as defined previously.

The specific structure of the covariance matrix has significant implications for learning in neural networks employing Oja's Rule. It has been shown that Oja's rule extracts principal components from the data, trying to create the signal with the highest variance [9]. As the data comes from a normalized distribution with known correlations, the learning dynamics and, as we will see in Section 4, the final variance of the parameters in Oja's Rule can be analyzed as a function of the learning rate $\alpha$ and the correlation coefficient $\rho$.

## 3.    Steady State Solution

It is known that the stable steady state solution of Oja's rule matches with the solution of the Principal Component Analysis(PCA), meaning that our weight vector will be an eigenvector of the covariance matrix that corresponds to the biggest eigenvalue (other eigenvectors are non-stable solutions, which means that if you move $w$ a little away from this solution, it won't come back)[14, 15, 16, 9].

A sketch of the proof will be provided, and the exact stable solutions for the bi-variate case will be calculated in this section. Let's first define $\mathbf{x}$ and $\mathbf{w}$ as:

$$\mathbf{x} = \begin{bmatrix} x_1 \\ x_2 \\ \vdots \\ x_n \end{bmatrix}, \quad \mathbf{w} = \begin{bmatrix} w_1 \\ w_2 \\ \vdots \\ w_n \end{bmatrix}$$

Now we can derive the steady state solution by asserting that the expected value of the change of the weights is equal to zero.

$$y = w^T x = x^T w$$

$$\frac{1}{\alpha}E[\Delta w(t)] = E[yx - y^2 w]$$
$$= E[xy - y^2 w]$$
$$= E[(xx^T)w - (w^T x)(x^T w)w]$$
$$= E[(xx^T)]w - (w^T E[xx^T]w)w$$
$$= \Sigma w - (w^T \Sigma w)w = 0$$

From this, we have that at the steady state $w$ is an eigenvector of $\Sigma$, whose eigenvalue $\lambda$ is equal to $(w^T \Sigma w)$. From this we can derive the $L^2$ norm of the steady state solution.

$$\lambda = (w^T \Sigma w) = w^T \lambda w = \lambda w^T w$$
$$w^T w = 1$$
$$\|w\|_2^2 = 1$$

This will allow us to find the steady state solution for our bi-variate case. If our correlation $\rho$ is positive, the largest eigenvalue will be $\lambda = 1 + \rho$, and the steady state solution will be

$$w = \pm \begin{bmatrix} \frac{\sqrt{2}}{2} \\ \frac{\sqrt{2}}{2} \end{bmatrix}.$$

If $\rho$ is negative, we will have $\lambda = 1 - \rho$ and

$$w = \pm \begin{bmatrix} \frac{\sqrt{2}}{2} \\ -\frac{\sqrt{2}}{2} \end{bmatrix}.$$

The sign of the steady state solution will depend solely on the initial values of the weights.

## 4. Variance of the weights at the Steady State

Let's define the mean and the variance of the weights during the steady state solution.

$$\mu_i(t) = E[w_i(t)]$$
$$V_i(t) = E[(w_i(t) - \mu_i(t))^2]$$
$$V_{ij}(t) = E[(w_i(t) - \mu_i(t))(w_j(t) - \mu_j(t))]$$
$$\hat{\mu}_i = \lim_{t\to\infty} \mu_i(t) = \frac{\sqrt{2}}{2}$$
$$\hat{V}_i = \lim_{t\to\infty} V_i(t), \quad \hat{V}_{ij} = \lim_{t\to\infty} V_{ij}(t) \tag{3}$$

From this point on, we will do the calculations only for the positively correlated pairs. The same calculations will hold if $\rho$ is negative as well. Let's introduce auxiliary variables $\bar{w}_1$ and $\bar{w}_2$ for describing the state of our system as the difference between the weights and their steady state solutions.

$$\bar{w}_1 = w_1 - \frac{\sqrt{2}}{2}$$
$$\bar{w}_2 = w_2 - \frac{\sqrt{2}}{2} \tag{4}$$

This notation is natural as the variances whose steady state solution we are trying to calculate can be expressed by these variables using (4) and (3) as $V_1 = E[\bar{w}_1{}^2]$, $V_2 = E[\bar{w}_2{}^2]$ and $V_{12} = E[\bar{w}_1\bar{w}_2]$. According to (1), those variables will be updated at each step by the following rule.

$$\bar{w}_1(t+1) = \bar{w}_1(t) + \alpha \left[ x_1(t)y(t) - y(t)^2 w_1(t) \right] \tag{5}$$
$$\bar{w}_2(t+1) = \bar{w}_2(t) + \alpha \left[ x_2(t)y(t) - y(t)^2 w_2(t) \right]$$

If we substitute the values of $y$, $w_1$ and $w_2$ in this by their representations through $x_1$, $x_2$, $\bar{w}_1$ and $\bar{w}_2$, we get the following update rule for our auxiliary variables after the expansion of (5)[1].

$$
\begin{aligned}
\bar{w}_1 \leftarrow \bar{w}_1 \; + \; &\alpha\bigg( \left( \frac{1}{2\sqrt{2}} - \frac{\bar{w}_1}{2} - \frac{3\bar{w}_1{}^2}{\sqrt{2}} - \bar{w}_1{}^3 \right) x_1^2 \\
&+ \; \left( -\frac{1}{2\sqrt{2}} - \frac{\bar{w}_1}{2} - \bar{w}_2 - \sqrt{2}\bar{w}_1\bar{w}_2 - \frac{\bar{w}_2{}^2}{\sqrt{2}} - \bar{w}_1\bar{w}_2{}^2 \right) x_2^2 \\
&+ \; \left( -2\bar{w}_1 - \sqrt{2}\bar{w}_1{}^2 - 2\sqrt{2}\bar{w}_1\bar{w}_2 - 2\bar{w}_1{}^2\bar{w}_2 \right) x_1 x_2 \bigg) \tag{6}
\end{aligned}
$$

$$
\begin{aligned}
\bar{w}_2 \leftarrow \bar{w}_2 \; + \; &\alpha\bigg( \left( \frac{1}{2\sqrt{2}} - \frac{\bar{w}_2}{2} - \frac{3\bar{w}_2{}^2}{\sqrt{2}} - \bar{w}_2{}^3 \right) x_2^2 \\
&+ \; \left( -\frac{1}{2\sqrt{2}} - \frac{\bar{w}_2}{2} - \bar{w}_1 - \sqrt{2}\bar{w}_2\bar{w}_1 - \frac{\bar{w}_1{}^2}{\sqrt{2}} - \bar{w}_2\bar{w}_1{}^2 \right) x_1^2 \\
&+ \; \left( -2\bar{w}_2 - \sqrt{2}\bar{w}_2{}^2 - 2\sqrt{2}\bar{w}_2\bar{w}_1 - 2\bar{w}_2{}^2\bar{w}_1 \right) x_1 x_2 \bigg) \tag{7}
\end{aligned}
$$

From the symmetry of the problem, it is obvious that $\hat{V}_1 = \hat{V}_2$. This means, that to calculate the steady state variances tracking the expected values of $\bar{w}_1{}^2$ and $\bar{w}_1\bar{w}_2$ is sufficient. Rules of their update can be calculated by multiplying (6) with itself and with (7). After these multiplications, we will have the following update rule.

$$
\begin{aligned}
\bar{w}_1^2 \leftarrow \quad & \bar{w}_1^2 + \alpha^2 \left( \frac{x_1^4}{8} - \frac{x_1^2 x_2^2}{4} + \frac{x_2^4}{8} \right) + \alpha^2 \bar{w}_2{}^2 \left( -\frac{1}{2}x_1^2 x_2^2 + \frac{3x_2^4}{2} \right) \\
+ \quad & \bar{w}_1\bar{w}_2 \left( -2\alpha x_2^2 + \alpha^2 (-2x_1^3 x_2 + 6x_1 x_2^3 + 2x_2^4) \right) \\
+ \quad & \bar{w}_1^2 \bigg( \alpha \left( -x_1^2 - 4x_1 x_2 - x_2^2 \right) \\
+ \quad & \alpha^2 \left( -\frac{5x_1^4}{4} + x_1^3 x_2 + 6x_1^2 x_2^2 + 3x_1 x_2^3 + \frac{x_2^4}{4} \right) \bigg) \\
+ \quad & \bar{w}_1 f_1(x_1, x_2) + \bar{w}_2 f_2(x_1, x_2) + \sum_{i+j\geq 3} \left( w_1^i w_2^j f_{ij}(x_1, x_2) \right) \tag{8}
\end{aligned}
$$

---

[1] For simplicity from now on we will use $F(w_1, w_2) \leftarrow G(w_1, w_2, x_1, x_2)$ to notate update rules of the form $F(w_1(t+1), w_2(t+1)) = G(w_1(t), w_2(t), x_1(t), x_2(t))$.

$$\bar{w}_1\bar{w}_2 \leftarrow \qquad \bar{w}_1\bar{w}_2 + \alpha^2\left(-\frac{x_1^4}{8} + \frac{x_1^2 x_2^2}{4} - \frac{x_2^4}{8}\right)$$

$$+ \qquad \bar{w}_1{}^2\left(-\alpha x_1^2 + \alpha^2\left(x_1^4 + \frac{5x_1^3 x_2}{2} - \frac{x_1 x_2^3}{2}\right)\right)$$

$$+ \qquad \bar{w}_2{}^2\left(-\alpha x_2^2 + \alpha^2\left(x_2^4 + \frac{5x_1 x_2^3}{2} - \frac{x_1^3 x_2}{2}\right)\right)$$

$$+ \qquad \bar{w}_1\bar{w}_2\bigg(\alpha\left(-x_1^2 - 4x_1 x_2 - x_2^2\right)$$

$$+ \quad \alpha^2\left(-\frac{x_1^4}{4} + 2x_1^3 x_2 + \frac{13x_1^2 x_2^2}{2} + 2x_1 x_2^3 - \frac{x_2^4}{4}\right)\bigg)$$

$$+ \qquad \bar{w}_1 g(x_1, x_2) + \bar{w}_2 g(x_1, x_2) + \sum_{i+j\geq 3}\left(w_1^i w_2^j g_{ij}(x_1, x_2)\right) \qquad (9)$$

Here $f_1$, $f_2$, $f_{ij}$, $g_1$, $g_2$, and $g_{ij}$ are polynomial functions of two variables. To estimate the steady state variances we must calculate the expected values of both sides of the above equations at the limit of $t \to \infty$. In order to complete these calculations we must take into account the following.

- At the limit of $t \to \infty$ we conclude from the symmetry of our multivariate Gaussian data distribution that $\hat{V}_1 = \hat{V}_2$. We will notate this variance using $\hat{V}$.

- Since $\bar{w}_i(t)$ and $x_j(t)$ are independent for any i and j

$$E\left[F\left(x_1(t), x_2(t)\right)G\left(\bar{w_1}(t), \bar{w_2}(t)\right)\right] = E\left[F\left(x_1(t), x_2(t)\right)\right]E\left[G\left(\bar{w_1}(t), \bar{w_2}(t)\right)\right]$$

- $x_1(t)$ and $x_2(t)$ are coming from a multivariate normal distribution, their moments can be calculated using Isserlis' theorem[17, 18].

$$\begin{aligned}
E[x_1(t)] = E[x_2(t)] &= 0 \\
E[x_1^3(t)] = E[x_2^3(t)] &= 0 \\
E[x_1^2(t)x_2(t)] = E[x_2^2(t)x_1(t)] &= 0 \\
E[x_1^2(t)] = E[x_2^2(t)] &= 1 \\
E[x_1(t)x_2(t)] &= \rho \\
E[x_1^2(t)x_2^2(t)] &= 1 + 2\rho^2 \\
E[x_1^3(t)x_2(t)] = E[x_2^3(t)x_1(t)] &= 3\rho \\
E[x_1^4(t)] = E[x_2^4(t)] &= 3
\end{aligned}$$

For calculating the expected values of polynomials involving $\bar{w}_1$ and $\bar{w}_2$ we will use the second-order moment closure approximation [11, 12, 13]. We will also keep in mind that at the limit of $t \to \infty$ expected values of $\bar{w}_1$ and $\bar{w}_2$ are equal to zero.

$$E[F(\bar{w}_1\bar{w}_2)] \approx \frac{1}{2}\left(\frac{\partial F(\bar{w}_1\bar{w}_2)}{\partial^2 \bar{w}_1} + \frac{\partial F(\bar{w}_1\bar{w}_2)}{\partial^2 \bar{w}_2}\right)V + \left(\frac{\partial F(\bar{w}_1\bar{w}_2)}{\partial \bar{w}_1 \partial \bar{w}_2}\right)V_{12}$$

Thus, we may obtain the following equations for the expected values of polynomials involving $\bar{w}_1$ and $\bar{w}_2$

$$
\begin{aligned}
E[\bar{w}_1] = E[\bar{w}_2] &= 0 \\
E[\bar{w}_1^2] &= V_1 \\
E[\bar{w}_2^2] &= V_2 \\
E[\bar{w}_1 \bar{w}_2] &= V_{12} \\
\text{If } i + j \geq 3, \text{ then } E[\bar{w}_1^i \bar{w}_2^j] &= 0
\end{aligned}
$$

Now we can finally calculate the expected values of both the right-hand sides and the left-hand sides of the update rules described in (8,9). We will do all calculations for the limit of $t \to \infty$.

$$
\begin{aligned}
\alpha(\frac{1}{2} - \frac{\rho^2}{2}) + (-2 - 4\rho + \alpha(7 + 12\rho + 11\rho^2))\hat{V} + (-2 + \alpha(6 + 12\rho))\hat{V}_{12} &= 0 \\
\alpha(-\frac{1}{2} + \frac{\rho^2}{2}) + (-2 + \alpha(6 + 12\rho))\hat{V} + (-2 - 4\rho + \alpha(5 + 12\rho + 13\rho^2))\hat{V}_{12} &= 0
\end{aligned}
$$

These two equations will allow us to calculate the steady state solutions $\hat{V}$ and $\hat{V}_{12}$. Since $\alpha \ll 1$, $\hat{V} \ll 1$ and $\hat{V}_{12} \ll 1$, we can neglect all terms that include $\alpha\hat{V}$ or $\alpha\hat{V}_{12}$. Thus, we obtain the following closed-form formula for calculating the variances at the steady state.

$$
\hat{V} = \alpha \frac{1 - \rho^2}{8|\rho|}, \tag{10}
$$

$$
\hat{V}_{12} = -\hat{V}. \tag{11}
$$

As we can see after sufficiently long iterations the correlation between $w_1$ and $w_2$ is equal to $-1$. This means that they jump around the steady state solutions, always being on the different sides of it. Their individual variance is proportional to the learning rate, which means that the decaying learning rate once the steady state is reached will also proportionally decrease the variance of the parameters, thus attributing to the better convergence of the model.

## 5.  Experiments

To validate the results of (10) and (11), we have created a simple experimental setup. Initially, we set $w_1 = 0$ and $w_2 = 1$. At each iteration, we generate a new data point from the bi-variate Gaussian distribution (2). Then we train for sufficiently long iterations until the steady state distribution is reached. We repeat this training process from scratch 500 times, save the final weights after each training process and calculate the variance of these 500 weights[2]. Then we repeat this same process for different learning rates to capture the relation between the final variance of the weights and the learning rate $\alpha$.

---

[2]Since the sign of the steady state solution depends on the initial weights every time we set the same value for the weights at the beginning. The same variance will be obtained for other initial conditions as well, while the mean steady state value may differ in sign.
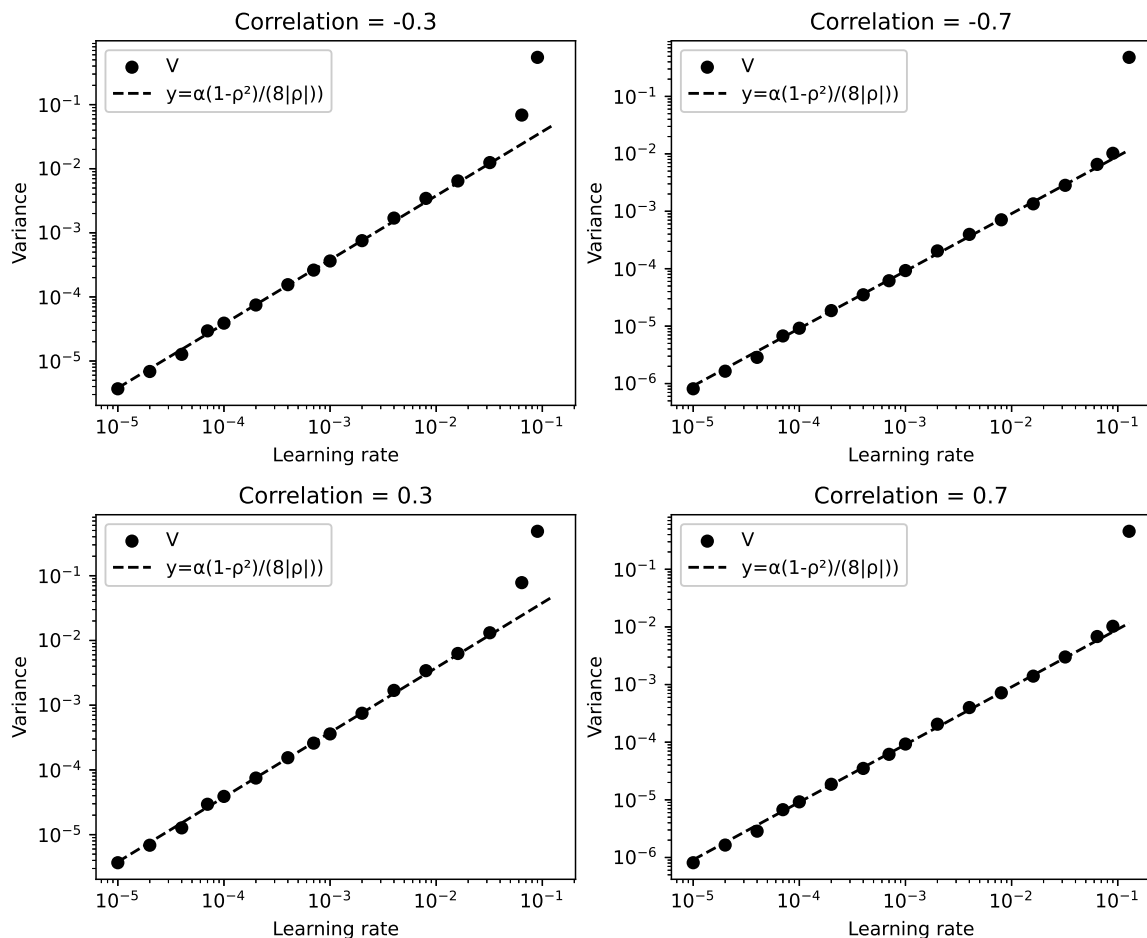
Fig. 1. If we train the system from scratch many times and calculate the variance of the final weight $w_1$, it will be very close to the analytically calculated value of (10) for learning rates that are sufficiently small for converging. Here it is checked for 4 different correlation coefficients, both positive and negative.

This same process is repeated for different sets of data points generated from multivariate normal distribution with different correlation coefficients $\rho$ to check the dependence of variance on correlation found in (10). Comparisons of the variances with the analytic values obtained in the previous section are represented in Fig. 1. [3]

## 6.  Conclusion

This article proposes an analysis of parameter variance in Oja's Rule using moment closure approximation. The steady state variance is studied, leading to a closed-form equation connecting variance to the learning rate by a linear relation.

---

[3]The results of those experiments can be reproduced by following the steps at https://github.com/edgarvardanyan/oja_variance.

A key finding is the linear relationship between parameter variance and learning rate, showing that variance measures convergence. For small learning rates, variance is directly proportional to the learning rate, derived from a simple closed-form equation and validated through simulations across various input correlations.

These results have potential applications in optimizing learning rate schedulers and algorithms by controlling variance, thus improving convergence efficiency without extra computational cost. This can guide unsupervised learning models based on the Ojas Rule in achieving better results without a loss function.

As we can see, once the learning rate is small enough for the convergence of the model(usually achieved with $\alpha < 0.1$ for the provided synthetic data), our closed-form formula is able to estimate the final variance of parameters with good enough accuracy.

# References

[1] D. O. Hebb, *The Organization of Behavior: A Neuropsychological Theory*. Wiley, New York, 1949.

[2] S. Nabavi, R. Fox, C. D. Proulx, J. Y. Lin, R. Y. Tsien, and R. Malinow, "Engineering a memory with LTD and LTP," *Nature*, vol. 511, pp. 348–352, 2014.

[3] E. Kuriscak, P. Marsalek, J. Stroffek, and P. G. Toth, "Biological context of Hebb learning in artificial neural networks: A review," *Neurocomputing*, vol. 152, pp. 27–35, 2015.

[4] G. Amato *et al.*, "Hebbian learning meets deep convolutional neural networks," in *Image Analysis and Processing – ICIAP 2019*, E. Ricci *et al.*, Eds. Springer International Publishing, Cham, pp. 324–334, 2019.

[5] J. P. Johansen *et al.*, "Hebbian and neuromodulatory mechanisms interact to trigger associative memory formation," *Proceedings of the National Academy of Sciences*, vol. 111, no. 51, pp. E5584–E5592, 2014.

[6] T. J. Sejnowski and G. Tesauro, "The Hebb rule for synaptic plasticity: Algorithms and implementations," in *Neural Models of Plasticity*, J. H. Byrne and W. O. Berry, Eds. Academic Press, pp. 94–103, 1989.

[7] E. L. Bienenstock *et al.*, "Theory for the development of neuron selectivity: Orientation specificity and binocular interaction in visual cortex," *Journal of Neuroscience*, vol. 2, no. 1, pp. 32–48, 1982.

[8] T. J. Sejnowski, "Storing covariance with nonlinearly interacting neurons," *Journal of Mathematical Biology*, vol. 4, no. 4, pp. 303–321, 1977.

[9] E. Oja, "A simplified neuron model as a principal component analyzer," *Journal of Mathematical Biology*, vol. 15, no. 3, pp. 267–273, 1982.

[10] L. N. Smith, "Cyclical learning rates for training neural networks," in *Proceedings of the IEEE Winter Conference on Applications of Computer Vision (WACV)*, pp. 464–472, 2017.

[11] E. Vardanyan and D. B. Saakian, "The analytical dynamics of the finite population evolution games," *Physica A: Statistical Mechanics and its Applications*, vol. 553, p. 124233, 2020.

[12] E. Vardanyan, E. Koonin, and D. B. Saakian, "Analysis of finite population evolution models using a moment closure approximation," *Journal of the Physical Society of Japan*, vol. 90, no. 1, p. 014801, 2021.

[13] V. Galstyan and D. B. Saakian, "Quantifying the stochasticity of policy parameters in reinforcement learning problems," *Physical Review E*, vol. 107, p. 034112, 2023.

[14] E. Oja, "Principal components, minor components, and linear neural networks," *Neural Networks*, vol. 5, no. 6, pp. 927–935, 1992.

[15] A. Hyvrinen and E. Oja, "Independent component analysis: Algorithms and applications," *Neural Networks*, vol. 13, no. 4–5, pp. 411–430, 2000.

[16] W. Gerstner, W. M. Kistler, R. Naud, and L. Paninski, *Neuronal Dynamics: From Single Neurons to Networks and Models of Cognition*. Cambridge University Press, 2014.

[17] L. Isserlis, "On a formula for the product-moment coefficient of any order of a normal frequency distribution in any number of variables," *Biometrika*, vol. 12, no. 1–2, pp. 134–139, 1918.

[18] L. Isserlis, "On certain probable errors and correlation coefficients of multiple frequency distributions with skew regression," *Biometrika*, vol. 11, no. 3, pp. 185–190, 1916.

## Հեբբյան ուսուցման կայուն վիճակի դիսպերսիայի վերլուծություն՝ մոմենտների փակման մոտարկմամբ

Էդգար Ա. Վարդանյան

Հայ-Ռուսական համալսարան, Երևան, Հայաստան
e-mail: edgarvardanyan1999@gmail.com

### Ամփոփում

Հեբբյան ուսուցումը, որը նեյրոնային ցանցերի կարևոր գաղափար է, հանդիսանում է տարբեր ուսուցման ալգորիթմների հիմքը, որոնք մոդելավորումեն նեյրոնային կապերի, այսպես կոչված սինապսների, ադապտացիան: Այս մոդելներից մեկն է Օյայի կանոնը, որը կարևոր օրինակ է՝ ապահովելով արժեքավոր պատկերացումներ ինքնասովորեցման ալգորիթմների դինամիկայի մասին: Լավ հայտնի է այն փաստը, որ միաշերտ ցանցի վերջնական կայուն վիճակի լուծումը, որը սովորում է Օյայի կանոնի կիրառմամբ, համընկնում է հիմնական բաղադրիչների վերլուծության լուծման հետ: Սակայն այն, թե ինչպես կարող է ուսուցման արագությունը ազդել վերջնական պարամետրերի տատանմման վրա, քիչ է ուսումնասիրված: Այս հոդվածում մենք ուսումնասիրում ենք, թե ինչպես տարբեր ուսուցման արագություններ կարող են ազդել Օյայի կանոնի պարամետրերի դիսպերսիայի վրա՝ օգտագործելով մոմենտների փակման մոտարկումը: Կենտրոնանալով տատանմման վրա՝ մենք առաջարկումենք նոր հեռանկարներ Օյայի կանոնի վարքագծի վերաբերյալ՝ տարբեր պայմաններում: Մենք ստանումենք փակ տեսքով հավասարում, որը կապում է պարամետրերի տատանմման մեծությունը ուսուցման արագության հետ և ցույց է տալիս,

որ դրանց միջև հարաբերությունը գծային է: Սա արժեքավոր պատկերացումներ է տալիս, որոնք կարողեն օգնել օպտիմալացնել Հեբբյան մոդելների ուսուցման գործընթացը:

**Բանալի բառեր`** Հեբբյանի ուսուցում, ուսուցման արագություն, նեյրոնային ցանցեր, մոմենտների փակման մոտեցում:

# Анализ устойчивой дисперсии в обучении Хебба: подход моментного замыкания

Едгар А. Варданян

Институт проблем информатики и автоматизации НАН РА, Ереван, Армения
e-mail: edgarvardanyan1999@gmail.com

## Аннотация

Обучение Хебба, важное понятие в нейронных сетях, является основой для различных алгоритмов обучения, моделирующих адаптацию нейронных соединений, также известных как синапсы. Среди этих моделей выделяется правило Ойи, которое предоставляет ценные сведения о динамике алгоритмов обучения без учителя. Хорошо известно, что итоговое устойчивое состояние однослойной сети, обучающейся по правилу Ойи, совпадает с решением метода главных компонент. Однако влияние скорости обучения на дисперсию конечных параметров изучено недостаточно. В данной работе мы исследуем, как различные скорости обучения влияют на дисперсию параметров в правиле Ойи, используя подход моментного замыкания. Сфокусировавшись на дисперсии, мы предлагаем новые взгляды на поведение правила Ойи в разных условиях. Мы выводим аналитическое уравнение, связывающее дисперсию параметров со скоростью обучения, и показываем, что эта зависимость является линейной. Это предоставляет ценные данные, которые могут помочь в оптимизации процесса обучения моделей Хебба.

**Ключевые слова:** правило Ойи, обучение Хебба, скорость обучения, нейронные сети, подход моментного замыкания.

# A Multispectral Decomposition and Frequency-Based Framework for Salient Object Detection in Remote Sensing Images

Hayk. A. Gasparyan

Yerevan State University, Yerevan, Armenia
e-mail: hayk.gasparyan@ysu.am

## Abstract

Salient object detection (SOD) aims to identify the most visually prominent objects in images, crucial for tasks like image segmentation, visual tracking, autonomous navigation, and photo cropping. While SOD has been extensively studied in natural scene RGB images, detecting salient objects in remote sensing images remains underexplored due to varying spatial resolutions and complex scenes.

This paper presents a novel framework for SOD called Multispectral Decomposition Network (**MSD-Net**) in remote sensing 3-band RGB images, combining Multispectral Decomposition and Frequency-based Saliency detection. The framework includes three key steps: (i) Multispectral Decomposition: Decomposing a 3-band RGB image into 32 multispectral bands to enhance feature capture across spectral domains; (ii) Synthetic RGB Reconstruction: Using a new entropy-based measure to select the most informative bands in salient regions by analyzing frequency domain and constructing synthetic RGB image; and (iii) Saliency Fusion and Object Detection: training a segmentation network on the fusion of synthetic RGB image and input image for improved accuracy. Comprehensive evaluations of public datasets demonstrate that the proposed method performs better than state-of-the-art (SOTA) models and offers a robust solution for detecting salient objects in complex remote sensing images by integrating multispectral and frequency-based techniques.

Automatic monitoring systems utilizing remote sensing technologies, such as satellite and UAV imagery, have encountered significant challenges in recent years. Remote sensing image processing [1] has numerous applications, including environmental monitoring, surveillance, military operations, autonomous navigation, and visual tracking. Image content analysis is critical across all these applications, encompassing object detection, localization, segmentation, and classification. The complexities and challenges in these tasks stem from varying environmental conditions, inconsistent image quality, and the diverse range of objects or regions requiring analysis. To address these challenges, recent approaches have leveraged properties of the human visual system. Humans possess an innate ability to automatically identify regions of interest within complex scenes through the visual attention mechanism. Inspired by this capability, salient object detection (SOD) enables computers to simulate this behavior, allowing them to detect the most prominent and important objects or regions in a scene automatically. SOD's adaptability and efficiency make it valuable in various applications, including foreground annotation, image enhancement, segmentation, image quality assessment, and video summarization.
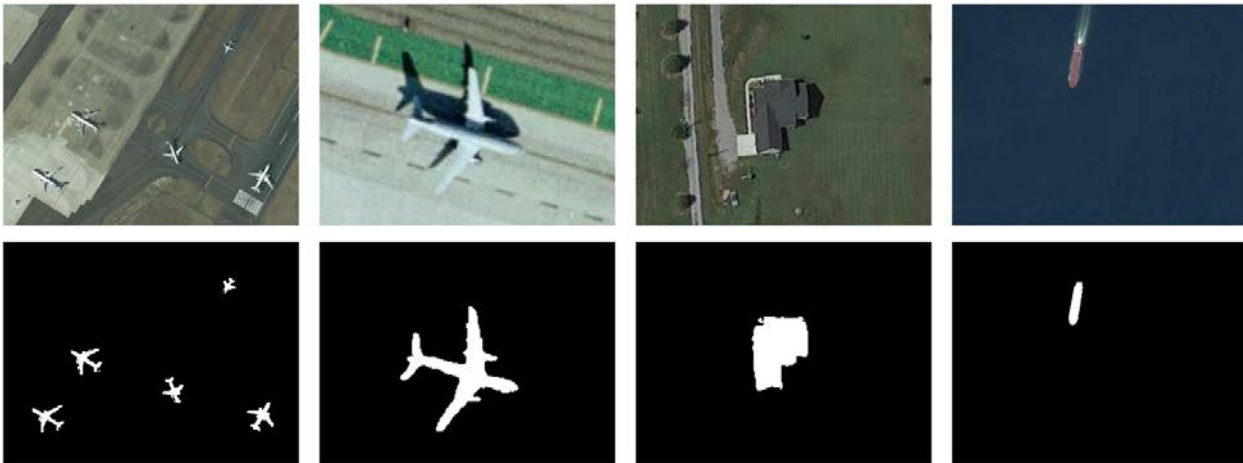


Fig. 1. Examples of SOD. Input and expected outputs are in the first and second rows, respectively.

While recent advances in signal processing have somehow solved these issues by allowing systems to detect predefined classes of objects with high accuracy, a more intricate problem arises in saliency object detection (SOD). Unlike standard detection tasks, where the system is searching for known objects, SOD involves identification of unknown objects or regions of interest [2]. Some example images of salient objects and their corresponding masks are illustrated in Figure 1. In [3], the authors have conducted an excellent review of the challenges in SOD and existing solutions, as well as their pros and cons. While SOD has been extensively studied in natural scene images, its application in remote sensing images brings more challenges, such as varying spatial resolutions, highly heterogeneous and complex scenes, and the presence of background clutter and noise in an image.

Early studies in salient object detection (SOD) showed promising results by using basic, handcrafted features like image contrast and background information to identify important regions in images. These early methods provided a foundation for the development of SOD techniques, and a detailed review of these non-deep learning approaches can be found in [4]. An interesting method proposed by [5] involved extracting spectral residuals from the frequency domain by analyzing the log spectrum of the image. This process helped to create a saliency map in the spatial domain. However, these methods had some limitations: (i) they struggled with complex textures

and fine details, which led to blurred results, and (ii) it was sensitive to noise and image artifacts, which affected their accuracy. Another recent algorithm, based on image contrast, was proposed by [6]. This method used global contrast to detect saliency by separating large objects from their surroundings. It assigned similar saliency values to similar regions, which allowed the entire object to be highlighted evenly. The saliency of each region was mainly based on its contrast with nearby areas, while distant contrasts had less influence. Although this method had difficulties with low image contrast, it was hard to distinguish objects from their backgrounds. These early methods were limited, especially in handling complex textures and low-contrast images. Further advancements were needed to improve their effectiveness and reliability.

With the success of deep learning technologies in computer vision, an increasing number of deep learning-based SOD methods [7] have emerged. Early deep SOD models generally utilized multi-layer perceptron (MLP) classifiers to predict saliency scores based on deep features extracted from individual pixels. These models significantly outperformed traditional, non-deep learning SOD methods. However, the MLP-based models were limited in their ability to capture spatial information effectively, as they lacked the structure to account for spatial dependencies across the image.

Table 1. Existing methods and limitations.

| | SRS | GCR | Conv-NN | ViT | MSD-Net |
|---|---|---|---|---|---|
| Simple and efficient | + | + | - | - | + |
| Can handle complex structures | - | + | + | + | + |
| Robust to noise and contrast variations | + | - | + | + | + |
| High accuracy | - | - | + | + | + |
| Does not require large training data | + | + | - | - | + |
| Low computational complexity | + | + | + | - | + |

Inspired by the success of fully convolutional networks (FCNs) [8] in semantic segmentation, more recent deep SOD methods have shifted toward using FCN-based architectures. These approaches incorporate advanced backbones like VGGNet [9], ResNet [10], and MobileNet [11], allowing end-to-end spatial saliency representation learning. By leveraging the strengths of these convolutional networks, modern SOD models can efficiently predict saliency maps while maintaining spatial coherence, significantly improving both accuracy and computational efficiency compared to earlier methods. Visual transformer-based architectures, such as ViT [13], have recently demonstrated significant potential in segmentation tasks. Several methods have leveraged these architectures to propose transformer-based saliency detection approaches [14]. Furthermore, novel advancements in convolutional networks have emerged, achieving state-of-the-art (SOTA) performance in salient object detection. For instance, GSANet [15] introduced the Semantic Detail Embedding Module (SDEM), which explores the relationships between multi-level features. It adaptively combines shallow texture details with deeper semantic information to efficiently aggregate information entropy in salient regions. Despite these advancements, these architectures have limitations, such as the quadratic computational complexity of visual transformers and the dependency on large-scale pixel-wise human annotations, making them less practical in specific scenarios. To develop effective SOD methods, it is crucial to address the complexities of feature extraction, minimize irrelevant data, and enhance precision in challenging environments such as low-light conditions, complex backgrounds, or high-noise environments. Table 1 summarizes the limitations of existing approaches.

This paper aims to overcome the primary limitations of current SOD methods by improving feature extraction and precision to provide a robust solution for saliency detection across diverse and complex environments. The key contributions of our work include:

1. Novel **Entropy-Based Band Selection Measure** to quantify the information within each spectral band regarding salient objects. It guides the reconstruction of a synthetic RGB image, enhancing the visibility and clarity of salient objects compared to the original image.

2. **Novel Framework for** salient object detection in remote sensing applications, leveraging multispectral decomposition and spectral frequency analysis. Specifically:

   a. We employ a multispectral decomposition technique to distribute the image's information across various spectral bands, effectively filtering out irrelevant details such as noise, background clutter, or non-salient objects and retaining only pertinent information for the segmentation process.

   b. We integrate the selected spectral bands with a segmentation network fused with the original image, improving the network's capacity to identify and delineate salient objects accurately.

3. **The presented Method** has been rigorously evaluated against several SOTA approaches using performance metrics and benchmark datasets. Furthermore, we tested its performance on additional image sets, demonstrating the framework's generalization capability across different domains and environmental conditions.

This comprehensive evaluation provides (i) strong evidence of the developed saliency detection method's effectiveness and robustness and (ii) demonstrates improved precision and adaptability in various contexts. This adaptability ensures that MSD-Net can be effectively applied in diverse and complex environments.

## 2. Framework for Image Enhancement and Segmentation

The proposed framework begins with a histogram equalization-based enhancement applied to the input image to improve its contrast, followed by gamma correction to adjust the brightness by raising the pixel values to the power of gamma. This pre-processing step enhances visibility and prepares the image for further analysis.

The core algorithm is divided into two main branches. The first branch generates a guidance saliency map, which provides high-level information about potential object locations and shapes while guiding further processing. The second branch decomposes the image into multiple spectral bands, distributing information across different bands to facilitate the selection of relevant data while minimizing noise or irrelevant details that could hinder the detection task. The next phase involves band selection, where the framework measures the similarity between the guidance saliency map and each spectral band. The top three bands from the "R," "G," and "B" spectrums are selected based on their relevance and combined to create a synthetic RGB image. This synthesized image is then summed with the original input image and passed to the segmentation network, which produces the final output mask, indicating the segmented regions of interest.

 Fig. 2 illustrates the overall workflow of the framework. The following chapters explain each component's role in image enhancement and segmentation.

## 2.1 Preprocessing Step: Enhancement of an Image

The goal of image enhancement techniques is to improve the characteristics and quality of an image so that the resulting image looks better than the original when evaluated against specific criteria. Image enhancement is crucial in various image processing applications, including digital photography, medical image analysis, computer vision, remote sensing, object recognition, optical character recognition, fingerprint recognition, industrial automation, face recognition, and scientific visualization. It serves as a vital preprocessing step for numerous image-processing applications and vision systems [16]. Several image enhancement algorithms have been developed recently [16-24], which can be categorized into two main classes: spatial-domain processing and transform-domain processing. **Spatial-domain methods** operate directly on pixel values. Representative methods in this category include gray-level histogram techniques, histogram equalization, adaptive histogram equalization like Contrast Limited Adaptive Histogram Equalization (CLAHE), adaptive gamma correction, human visual system-based methods, unsharp masking, ratio image methods, fuzzy entropy approaches, empirical mode decomposition-based methods, partitioned iterated function systems, linear filters, among others (see details in [25]).
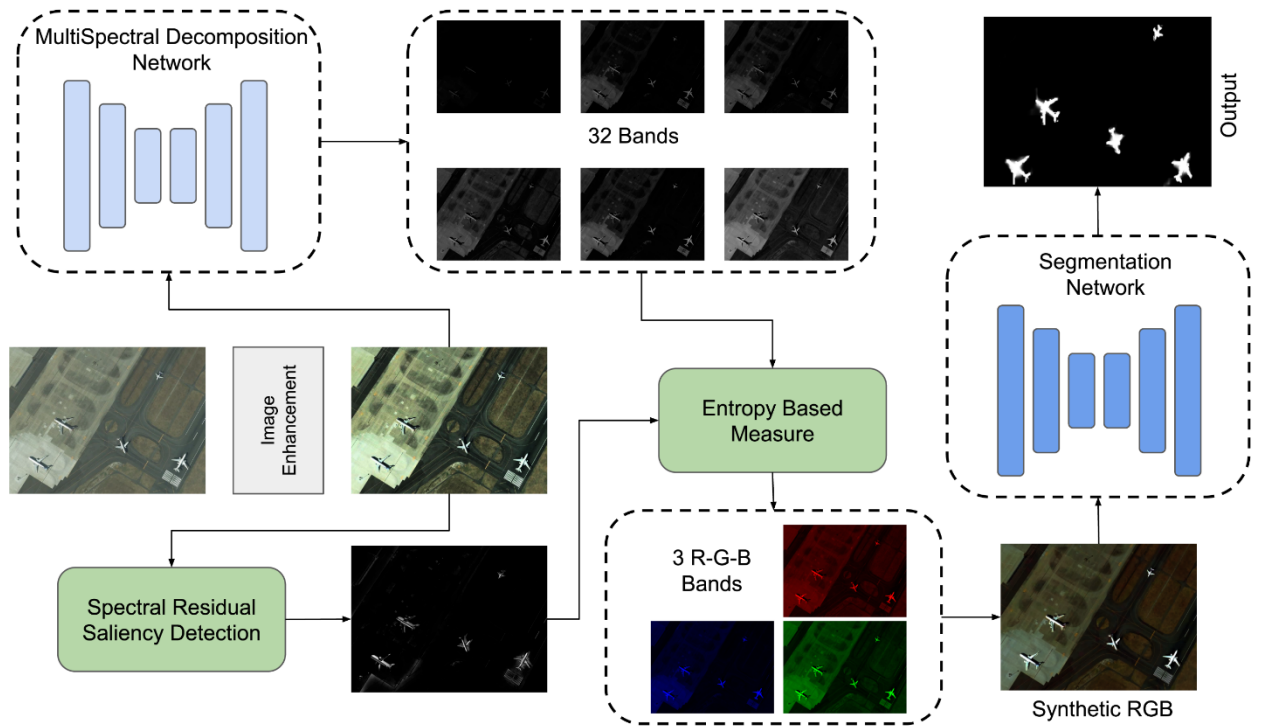


Fig. 2. Overall architecture and workflow of MSD-Net.

This article uses a combined **CLAHE and gamma correction method** as a preprocessing step.

$$I_{enh} = \big(CLAHE(I)\big)^{\gamma} \ where \ \gamma = 1.5.$$

where $I$ is the input image, and $I_{enh}$ is the enhanced output. This approach leverages the strengths of both techniques to enhance image quality effectively:

1. **Contrast Limited Adaptive Histogram Equalization (CLAHE) [25]:** CLAHE improves local contrast by applying histogram equalization to small regions (tiles) of the image rather than the entire image. This method limits contrast amplification to prevent noise enhancement, making fine details more visible without over-saturating the image.
2. **Gamma Correction [26]**: Gamma correction adjusts the brightness of an image by applying a non-linear transformation to the pixel intensity values. It corrects the non-linear way humans perceive light and color, ensuring that the image has appropriate luminance levels—neither too dark nor too bright.

**Combined benefit:** By integrating CLAHE and gamma correction, we aim to enhance both the local contrast and overall brightness of the image:

- **Step 1**: Apply CLAHE to the input image to enhance local contrast. This step emphasizes edge details and textures, making subtle features more discernible.
- **Step 2**: Perform gamma correction on the CLAHE-processed image. Adjust the gamma value to fine-tune the image brightness according to the application's specific requirements.
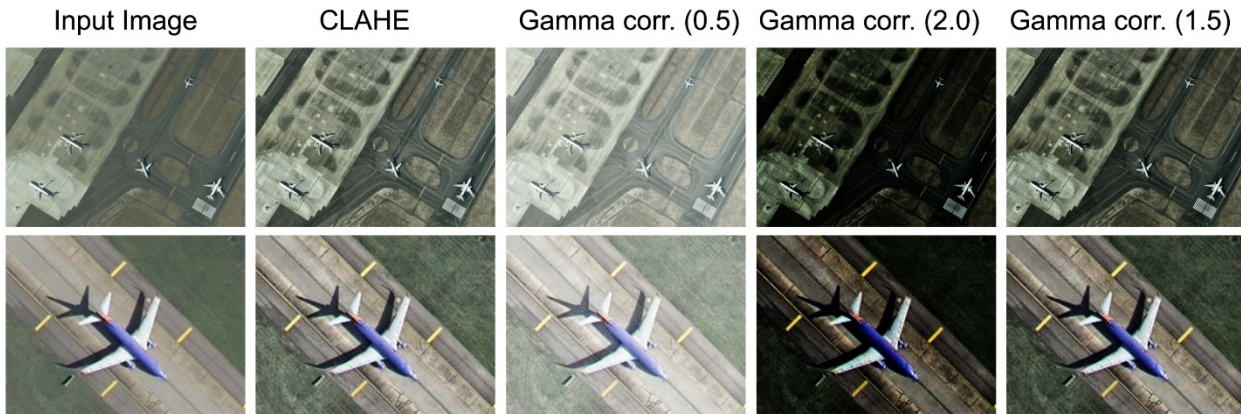


Fig. 3. Input image; CLAHE enhanced; gamma corrected with different gamma parameters.

This combined method enhances fine details while maintaining proper brightness and contrast levels, making an image more suitable for further processing or analysis information during decomposition and more accurate detection of proposal regions by the spectral residual algorithm. Figure 3 demonstrates the effect of CLAHE and gamma correction with different gamma parameters. Experiments showed the best gamma to be selected 1.5, as it does not over-enhance or under-enhance the image. In Fig. 4, spectral residual saliency algorithm is used before (b) and after enhancement (c). We can observe the difference of saliency masks compared to ground truth masks. This difference shows the effect of the enhancement preprocessing part.

## 2.2 Spectral Residual Saliency Object Detection

The algorithm [5] is designed to detect salient regions in an image by analyzing its spectral properties. The key intuition behind this approach is that salient regions are distinguished from the surrounding background in terms of their spectral characteristics. By working in the spectral domain (using the Fourier Transform), the algorithm can efficiently highlight these regions by identifying and manipulating the spectral residual, which captures the unique, non-redundant

information in the image. The algorithm begins with median blurring with kernel size 5 to reduce noise while preserving edges. Next is the Fourier Transform step: the image $I(x,y)$ is transformed into the frequency domain:

$$F(u,v) = F\big(I(x,y)\big)$$

yielding complex values with amplitude and phase information. A logarithm transformation is applied to the magnitude spectrum, followed by smoothing kernel convolution.

$$A(u,v) = |F(u,v)|$$

$$L(u,v) = log\big(A(u,v)\big)$$

$$S(u,v) = h * L(u,v)$$



Fig. 4. Spectral residual saliency (SRS) detection: (a) input image, (b) output of SRS w/o enhancement, (c) output of SRS after enhancement, (d) ground-truth mask.

The spectral residual is computed by subtracting the smoothed spectrum from the original and is exponentiated and combined with the original phase to reconstruct the frequency domain:

$$R(u, v) = L(u, v) - S(u, v),$$

$$M(u, v) = e^{R(u,v)}, \quad F'(u, v) = M(u, v) \cdot e^{j\theta(u,v)},$$

$$Output(u, v) = g(x) \cdot F^{-1}\big(F'(u, v)\big).$$

An inverse Fourier transform followed by a gaussian filter $g(x)$ with ($\sigma = 8$) generates the **Saliency Map**. There is a final optional step, which subtracts saliency map from original image to get an anomaly map, but we do not use that step in our article. Fig. 4 illustrates some examples of spectral residual algorithms.

## 2.3 Multispectral Decomposition

Multispectral and hyperspectral images play a crucial role in understanding the physical attributes of objects in an image. While RGB images are limited to three channels (red, green, and blue),
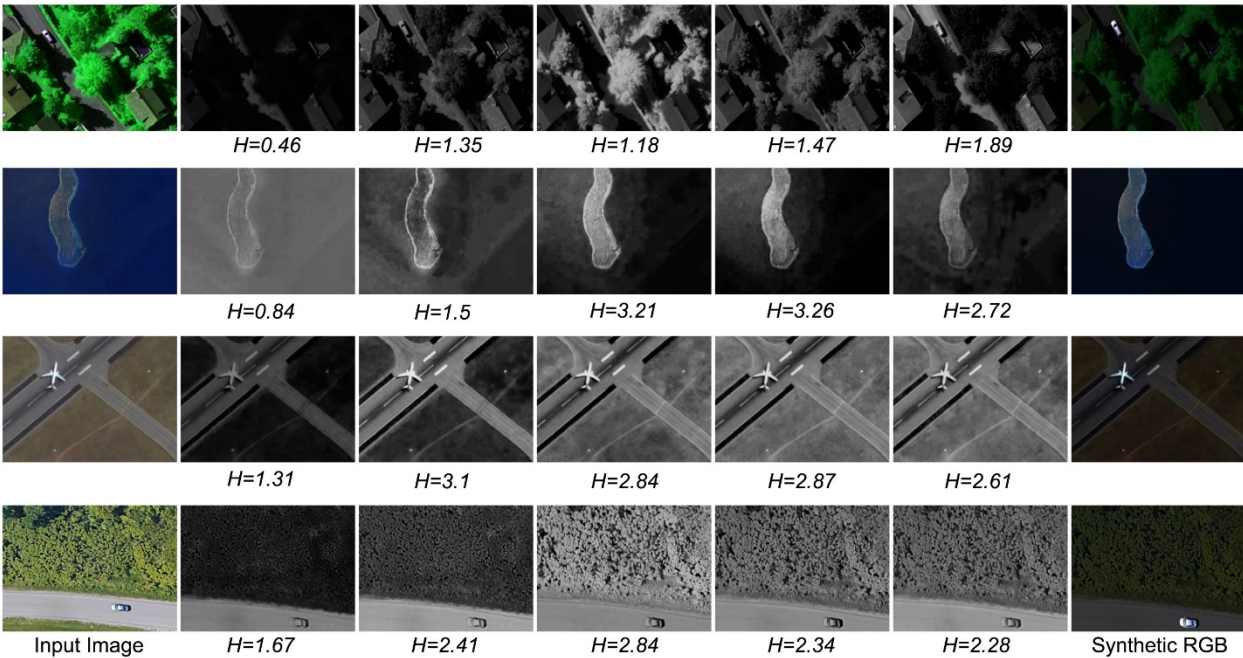


Fig. 5. From left to right: input image, multispectral decomposition bands (indices 1, 7, 15, 22, 30) with entropy measures below, Synthetic reconstructed RGB

multispectral images capture data across a broader range of wavelengths, typically tens to hundreds of spectral bands. This expanded range allows for a more detailed analysis of material properties, surface textures, and object distinctions that might not be visible in standard RGB images.

As obtaining multispectral images can be costly, a significant amount of research aimed at developing methods to predict multispectral information from standard RGB images. Therefore, considerable interest has been in constructing datasets that facilitate RGB-to-multispectral conversions (predictions) through deep learning and other techniques [27]. One such method is the Multi-stage Spectral-wise Transformer (MST++) [28], known for its high accuracy and low computational complexity. The MST++ architecture is based on a convolutional autoencoder

(CAE) design consisting of multiple stages of spectral-wise transformers. Each stage includes an encoder, a bottleneck, and a decoder, with spectral-wise attention blocks (SABs) and deconvolution layers. Skip connections between the encoder and decoder are employed to preserve important spatial information throughout the transformation process. The output of this module consists of 32 spectral bands, with the first 11 bands capturing information from the red channel, the next 11 bands for the green channel, and the remaining 10 bands for the blue channel.

MST++ is employed as the decomposition network in this work, which converts an RGB image into 32 spectral bands, providing a richer, more informative spectral representation of the scene. This arrangement allows for an efficient distribution of information across the channels, ensuring that the decomposition captures subtle variations and essential features in each color channel. Fig. 5 shows an example of anRGB image and some corresponding bands after conversion to a multispectral image. It is easy to see that certain bands contain more information about salient objects than others. The goal is to identify and select the most informative bands to be used as supplementary input for the segmentation module [29]. It can reduce the noise and other information that can bring false positives during the segmentation.

## 2.4 Novel Entropy-Based Band Selection Measure

**Definition 1:** To efficiently identify the most informative spectral bands, we compute the entropy-based band selection measure ($H$) for each band $k$ using the following formula:

$$H^{(k)} = \sum_{i=0}^{N} \sum_{j=0}^{M} w_{ij} H_{ij}^k ,$$

where the entropy $H_{ij}^k$ of each block is calculated.

$$H_{ij}^k = 20\left(-p_{ij}^k \log\left(p_{ij}^k\right)\right),$$

- $p_{ij}^k \approx 0.5$: indicates a balance between $AC$ and $DC$ components, meaning the block has both structure (variation) and intensity, which suggests high information content.
- $p_{ij}^k \approx 0$: indicates that the block is homogeneous with slight variation (dominated by DC), meaning low information content.
- $p_{ij}^k \approx 1$: indicates that the block is dominated by high-frequency noise or excessive variation without meaningful structure (dominated by $AC$), also leading to low information content.

$H_{ij}^k$ is the entropy calculated for the ij-th block of the k-th band, and $w_{ij}$ is the average value of the corresponding $ij$ block in the guidance map. $H_{ij}^k$ is calculated with the following steps:

1. For each block $B_{ij}$ of the image, a Fourier Transform is performed to obtain the $DC$ and $AC$ components.

$$F_{ij} = FFT\left(B_{ij}\right), \quad F_{ij}^{shift} = FFTShift(F_{ij})$$

$$DC_{ij} = |F_{ij}^{shift}(0,0)|^{\beta}, \quad AC_{ij} = \sum_{x=1,y=1}^{k} |F_{ij}^{shift}(x,y)|^{\alpha}$$

$\alpha$ and $\beta$ coefficients are selected experimentally at 0.6 and 2, respectively.

2.  A probability value $p_{ij}^k$ is computed from the ratio of the $AC$ and $DC$ components from $k$-th band.

$$p_{ij}^k = \frac{AC_{ij}^k}{AC_{ij}^k + DC_{ij}^k}.$$

After calculating $H^{(k)}$ for each $k$-th band, the top 3 bands are selected with the highest scores from each range (1-10, 11-21, 22-32). The selected bands construct a new synthetic RGB image that captures the salient object information more effectively than the original image. Some example **bands** and their corresponding **entropy scores** are illustrated in Figure 5. The final column shows the RGB image reconstructed from the selected bands. This synthetic image and the original image are merged by taking their average, as some features can be lost in synthetic RGB, which can be crucial for segmentation.

## 2.5 Segmentation Network Module

For the segmentation module, the merged image is passed through DeepLabV3 [30] network with a ResNet50 backbone. DeepLabV3 is a well-known standard in image segmentation tasks. It is part of a family of segmentation architectures that employ atrous convolution and multi-scale context aggregation to capture fine details in images. These architectures are widely used due to their efficiency and accuracy in pixel-level predictions. In this work, the network was chosen primarily to validate the concept of the proposed framework rather than to focus on optimizing segmentation performance, as it provides a robust and reliable baseline for evaluating the effectiveness of the approach.

## 2.6 Loss Functions

For training the network, we utilize two loss functions: Binary Cross Entropy (BCE) and Mean Squared Logarithmic Error (MSLE).

$$L_{BCE} = \frac{1}{N} \sum_{i=0}^{N} y_i \cdot \log(p_i) + (1 - y_i) \cdot \log(1 - p_i),$$

$$L_{MSLE} = \frac{1}{N} \sum_{i=0}^{N} (\log(1 + p_i) - \log(1 + y_i))^2.$$

BCE is commonly used for binary classification tasks, and in our case, it helps classify all pixels as either salient or non-salient regions. MSLE, similar to Mean Squared Error (MSE), introduces a logarithmic transformation to reduce the impact of large outliers, effectively treating them on the same scale as smaller values. This property makes MSLE particularly useful for creating a balanced model that is robust to noise and outliers.

## 2. Experimental Results

### 3.1 Dataset

To train and evaluate the proposed framework, we selected the most suitable benchmark dataset for optical remote sensing SOD. The first publicly available SOD dataset was ORSSD, introduced by [31]. It includes 600 training and 200 testing images, each with pixel-wise annotations for salient regions. Despite its importance to the SOD field, this dataset had limitations, particularly due to the small amount of data. To address this issue, [15] introduced an extended version called the EORSSD dataset. This dataset adds 1,200 optical remote sensing images collected from Google Earth to the existing ORSSD dataset, encompassing more complex scenes, objects, and regions. Pixel-wise saliency maps were generated using Photoshop tools, resulting in overall 2,000 images with ground-truth annotations (1,400 for training and 600 for testing). The EORSSD dataset presents several challenges: (i) multiple objects can appear in one single image, (ii) object sizes in optical remote sensing imagery (RSI) vary significantly due to the diverse satellite and airborne imaging platforms, making small object detection particularly difficult, and (iii) the dataset
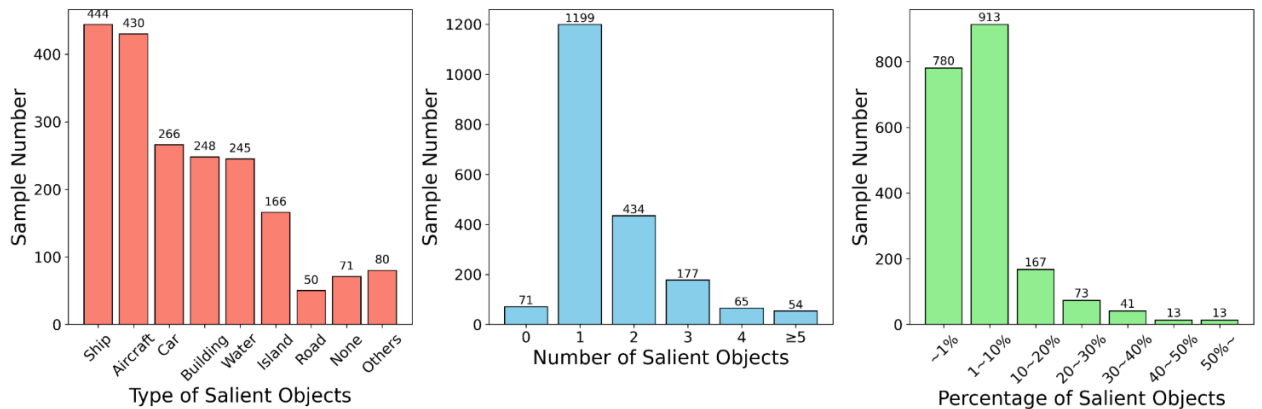


Fig. 6. Statistics about datasets object types, sizes, and counts.

includes a variety of objects such as buildings, streets, ships, aircraft, cars, water bodies, islands, and roads. In summary, the EORSSD dataset is diverse and challenging, making it a valuable resource for training and evaluating SOD models in complex remote sensing scenarios. Some statistics about the dataset are presented in Figure 6.

We evaluate MSD-Net on other remote sensing scenarios as well. To show the generalizability of the proposed method, we also evaluate it on images from the NWPU-RESISC45 [32] dataset, which was initially intended for remote sensing image scene classification. Besides that, we show the performance on **solar panels** images taken from the PV01 dataset [33], **without** providing any training example to the network.

### 3.2 Evaluation Metrics

To quantitatively evaluate the proposed method, we calculate **four** metrics, with different settings: adaptive, mean, and max $S$-measure ($S_\alpha$) [34], mean absolute error (MAE), adaptive, mean and max $E$-measure ($E_\xi$) [35] and adaptive, mean and max $F$-measure ($F_\beta$) [36]. The $S$-measure

calculates object similarity considering the structural similarity between the predicted and ground truth masks.

$$MAE = \frac{1}{NM}\sum_{i=1}^{N}\sum_{j=1}^{M}|Sal(i,j) - GT(i,j)|, \quad S_\alpha = \alpha \times S_O + (1-\alpha) \times S_r$$

$$E_\xi = \frac{1}{NM}\sum_{i=1}^{N}\sum_{j=1}^{M}\xi_s(i,j), \quad F_\beta = \frac{(1+\beta^2) \times Precision \times Recall}{\beta^2 \times Precision + Recall}$$

$\alpha = 0.5$, $S_O$ and $S_r$ are object and region similarities, respectively. *MAE* calculates the mean absolute distance of predicted and actual saliencies. The *E*-measure is an improved metric designed to calculate the degree of correspondence between global averages and individual local pixels. $\xi_s$ is the enhanced alignment matrix, capturing pixel-level matching and image-level statistics. Finally, *F*-measure calculates the weighted harmonic mean of *Precision* and *Recall*. $\beta$ is the weight coefficient and is set at 0.3 in our experiments. For each measure, we have three settings: adp (adaptive), mean, and max.
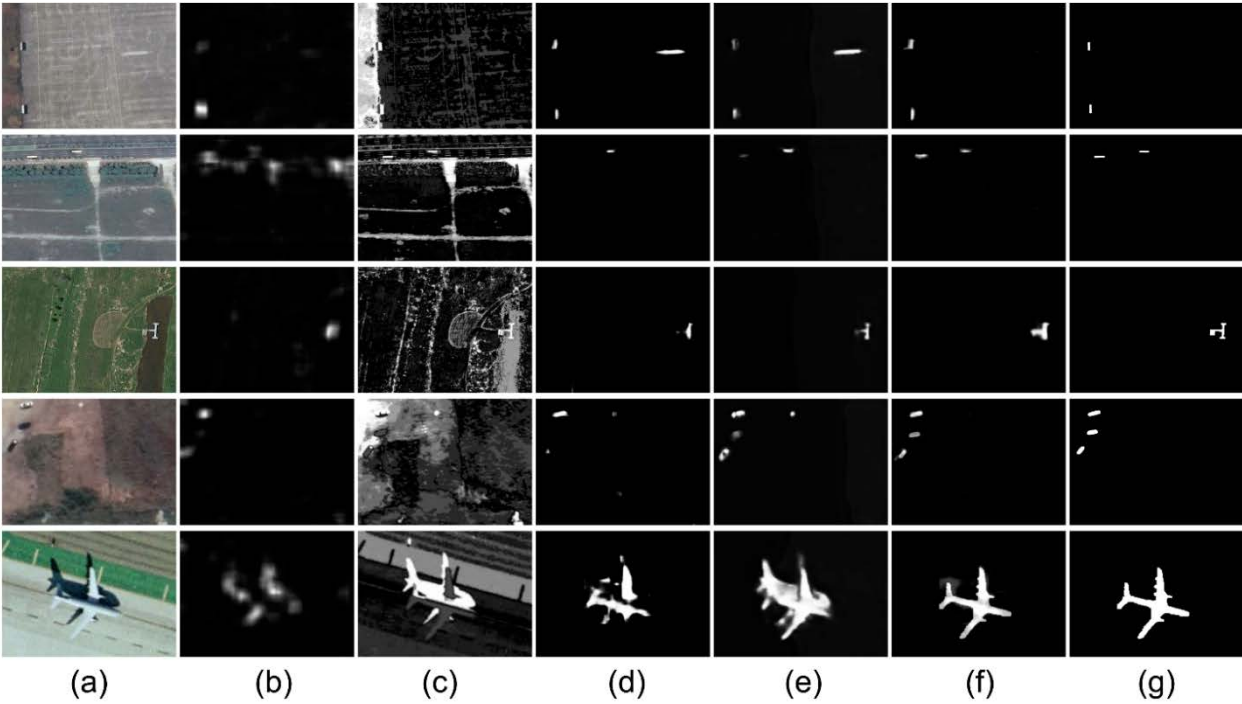


Fig. 7. Comparison of MSD-Net with others. (a) input image, (b) SRS, (c) GCR, (d) DeepLabV3, (e) GCANet, (f) MSD-Net, (g) ground truth.

Table 2. Quantitative comparison of proposed method against others on eorssd dataset.

| | S-Measure ↑ | MAE ↓ | adpEM ↑ | meanEM ↑ | maxEM ↑ | adpFM ↑ | meanFM ↑ | maxFM ↑ |
|---|---|---|---|---|---|---|---|---|
| *SRS* | 0.485 | 0.178 | 0.647 | 0.524 | 0.612, | 0.323 | 0.192, | 0.253 |
| *GCR* | 0.568 | 0.158 | 0.484 | 0.577 | 0.670 | 0.204 | 0.330 | 0.403 |
| *DeepLabV3* | 0.826 | 0.018 | 0.826 | 0.874 | 0.902 | 0.602 | 0.682 | 0.711 |
| *GSANet* | 0.801 | 0.025 | 0.834 | 0.856 | 0.871 | 0.616 | 0.67 | 0.689 |
| *MSD-Net* | **0.841** | **0.017** | **0.854** | **0.881** | **0.912** | **0.637** | **0.703** | **0.731** |

## 3.3. Experiments Setup

For a fair comparison, we train all the deep learning-based methods in our dataset split and evaluate with the same code and pipeline. For all training, the Adam optimizer was used with a learning rate $10^{-4}$. Two loss functions have equal coefficients during the training. Random horizontal and vertical flips, rotations, and shifts were used for data augmentation. Batch size and epochs were selected 16 and 200, accordingly. The patch size for the Fourier Transform was set to $K = 16$, and for the entropy measure, $K = 10$. These parameter values were chosen based on extensive computer simulations and experimental results.

## 3.4 Comparison with Other Methods

For the comparison with other methods, we choose 2 non-deep learning-based algorithms, including spectral residual SOD (SRS) [5] and Global Contrast-based SOD (GCR) [6]. While they have successfully found salient objects in some simple cases, they fail if some challenges are present in images, such as complex background scenes or low contrast. To this end, we also compare 2 deep learning based SOTA models: one for general semantic segmentation task (DeepLabV3) [30], and another trained exactly for SOD task (GCANet) [15]. As mentioned, for fair comparison, we use the code they published and train ourselves on our data and our experiment settings. Despite the promising results and improvements compared with non-deep learning methods, they still have some limitations. Visual comparison of the proposed framework with other methods is presented in Fig. 7. On the contrary, MSD-Net has successfully detected the salient objects and has better boundaries, compared to those having non clear object boundaries, false positive detected pixels, as well as missing some parts of objects. While SRS (Fig. 7-b) detected the approximate location of salient objects, it smoothed them and lost a lot of details. On the contrary, GCR (Fig. 7-c) has not lost any details and processed textures well, but it has a lot of false positive cases. Deep learning-based methods have shown better performance. [15] and [30] have false positive cases on the first and fourth images and missed one object in the second image and part of the object in the third image. The fifth image is smooth, but details are lost in both cases. On the other hand, MSD-Net successfully managed to detect better masks of salient objects. Besides qualitative comparison, we also evaluate our method quantitatively using the metrics defined above. Table 2 shows that MSD-Net shows better performance compared with others on all metrics.

We demonstrate the generalizability of the MSD-Net by running it on other images taken from the dataset introduced in [32]. Although this dataset does not provide ground truth masks, as it is not designed for saliency object detection (SOD), we observe visually good masks on various image types. While quantitative evaluation is not possible in this case, we can conduct a qualitative assessment (see Fig. 8-a). We also evaluate the performance of our method on **out-of-distribution**

solar panel images (Fig. 8-b), demonstrating strong generalization capability. In future work, we aim to further improve the accuracy and efficiency of panel detection.
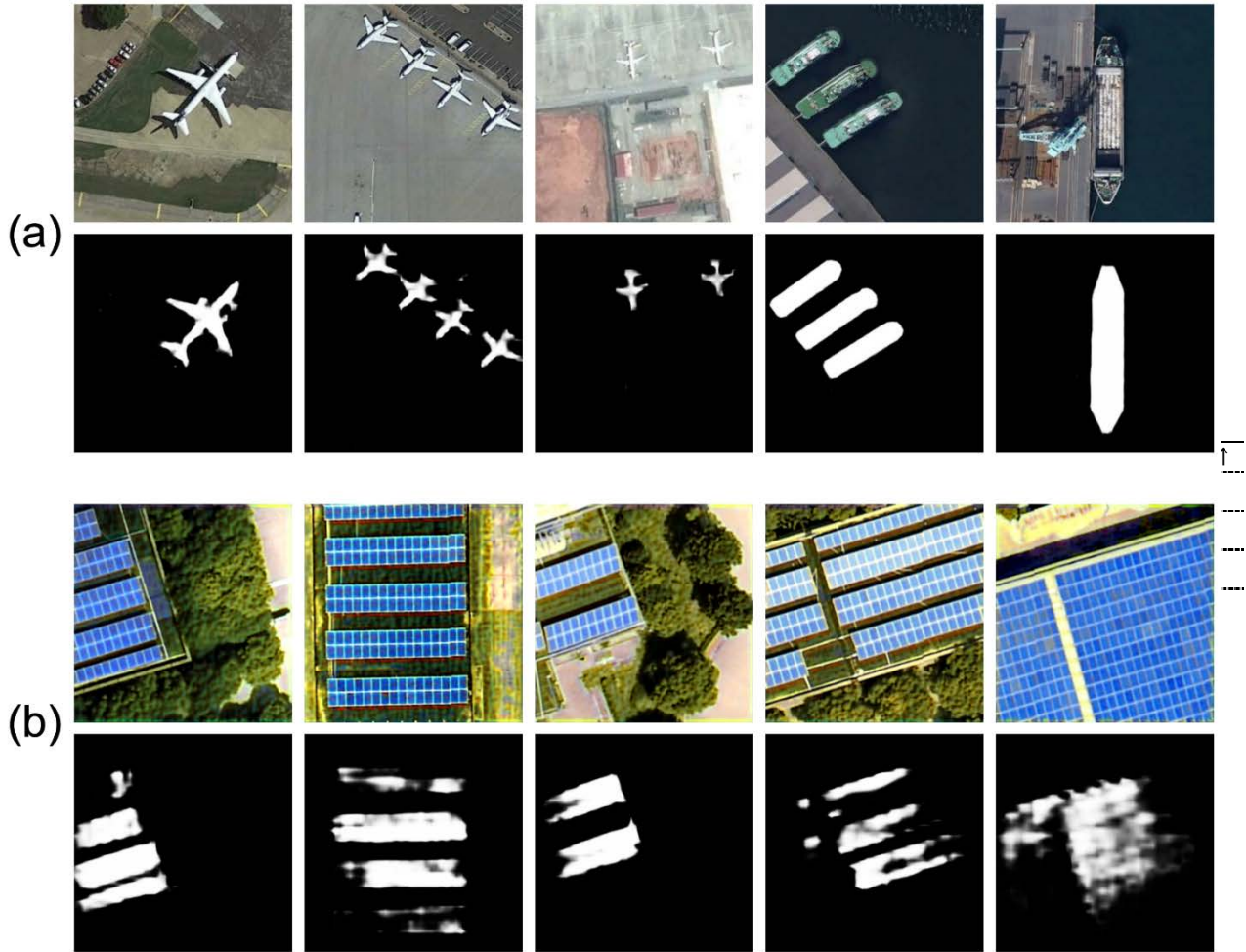


Fig. 8. Predictions of the MSD-Net on samples of **(a)** NWPU-RESISC45 dataset, **(b)** PV01 dataset.

## 3.5 Ablation Study

To investigate the effectiveness of each component, we first train the segmentation network without applying any pre-processing or synthetic RGB reconstruction steps, establishing a baseline. We then incrementally add components to the pipeline. Second, we integrate a single branch using the spectral residual saliency map, which is generated and fused with the input image to guide the segmentation network in more easily identifying salient objects. This addition improves the metrics a little. Finally, we incorporate the decomposition module, which results in

Table 3. Ablation study analysis

| | S-Measure ↑ | MAE ↓ | adpEM ↑ | meanEM ↑ | maxEM ↑ | adpFM ↑ | meanFM ↑ | maxFM ↑ |
|---|---|---|---|---|---|---|---|---|
| *Segm. only* | 0.826 | 0.018 | 0.826 | 0.874 | 0.902 | 0.602 | 0.678 | 0.711 |
| *Segm. + guide* | 0.832 | 0.018 | 0.841 | 0.881 | 0.912 | 0.622 | 0.682 | 0.720 |
| ***MSD-Net*** | **0.841** | **0.017** | **0.854** | **0.886** | **0.915** | **0.637** | **0.703** | **0.731** |

the highest performance scores when using the full pipeline. The metric values for each scenario are presented in Table 3, demonstrating the contribution and effectiveness of each block and branch in MSD-Net.

## 4. Conclusion

In conclusion, this paper presents MSD-Net, a novel framework for salient object detection (SOD) in remote sensing RGB images. MSD-Net enhances feature representation and improves detection accuracy in complex remote sensing scenarios using multispectral decomposition and frequency-based saliency detection techniques. Additionally, we introduce an entropy-based similarity measure for effective band selection and synthetic RGB reconstruction. Experimental results on the EORSSD dataset demonstrate that MSD-Net significantly outperforms state-of-the-art methods on public datasets. Furthermore, we evaluate the framework on various datasets and conduct an ablation study to analyze the contribution of each component.

## References

[1] L. Zhang and Li. Zhang, "Artificial intelligence for remote sensing data analysis: A review of challenges and opportunities", *IEEE Geoscience and Remote Sensing Magazine,* vol. 10, no. 2, pp. 270-294, 2002.

[2] X. Wang et al., "Salient object detection: a mini review", *Frontiers in Signal Processing*, vol. 4, 1356793, 2024.

[3] W. Wang et al., "Salient object detection in the deep learning era: An in-depth survey", *IEEE Transactions on Pattern Analysis and Machine Intelligence*, vol. 44, no. 6, pp. 3239-3259, 2021.

[4] A. Borji et al., "Salient object detection: A benchmark", *IEEE Transactions on Image Processing*, vol. 24, no. 12, pp. 5706-5722, 2015.

[5] X. Hou and L. Zhang, "Saliency detection: A spectral residual approach", *IEEE Conference on Computer Vision and Pattern Recognition*, 2007, DOI: 10.1109/CVPR.2007.383267

[6] Cheng Ming-Ming, et al., "Global contrast based salient region detection", *IEEE Transactions on Pattern Analysis and Machine Intelligence*, vol. 37, no.3, pp. 569-582, 2014.

[7] Li. Guanbin and Yu. Yizhou, "Visual saliency based on multiscale deep features", *Proceedings of the IEEE Conference on Computer Vision And Pattern Recognition*. 2015.

[8] J. Long, E. Shelhamer and T. Darrell, "Fully convolutional networks for semantic segmentation", *Proceedings of the IEEE Conference on Computer Vision and Pattern Recognition*, 2015, doi: 10.1109/CVPR.2015.7298965

[9] K. Simonyan and A. Zisserman, "Very deep convolutional networks for large-scale image recognition", arXiv preprint arXiv:1409.1556. 2014.

[10] K. He et al., "Deep residual learning for image recognition", P*roceedings of the IEEE Conference on Computer Vision and Pattern Recognition*, 2016, doi: 10.1109/CVPR.2016.90

[11] A. Howard, "Mobilenets: Efficient convolutional neural networks for mobile vision applications", arXiv preprint arXiv:1704.04861, 2017.

[12] G. Fang et al., "Video saliency detection using object proposals", *IEEE Transactions on*

*Cybernetics*, vol. 48, no.11, pp. 3159-3170, 2017.

[13]  A. Dosovitskiy, "An image is worth 16x16 words: Transformers for image recognition at scale", arXiv preprint arXiv:2010.11929, 2020.

[14]  N. Liu et al., "Visual saliency transformer", *Proceedings of the IEEE/CVF International Conference on Computer Vision*, 2021.

[15]   Q. Zhang et al., "Dense attention fluid network for salient object detection in optical remote sensing images", *IEEE Transactions on Image Processing*, vol. 30, pp. 1305-1317, 2020.

[16]  S. C. Nercessian, K. A. Panetta and S. S. Agaian, "Non-linear direct multi-scale image enhancement based on the luminance and contrast masking characteristics of the human visual system", I*EEE Transactions on Image Processing*, vol. 22, no. 9, pp. 3549-3561, 2013.

[17]  J. Xia, K. Panetta and S. Agaian, "Wavelet transform coefficient histogrambased image enhancement algorithms", Proc. SPIE 7708, 770812, 2010.

[18]  A. Grigoryan, J. Jenkinson and S. Agaian, "Quaternion Fourier transform based alpharooting method for color image measurement and enhancement", *Signal Processing*, vol. 109, pp. 269-289, 2015.

[19]  E. Wharton, K. Panetta and S. Agaian, "Human visual system based multihistogram equalization for non-uniform illumination and shadow correction", *Proceedings of the IEEE International Conference on Acoustics, Speech and Signal Processing*,  vol. 1, pp. I-729–I-732, 2007.

[20]  S. Nercessian, S. Agaian and K. Panetta, "An image similarity measure using enhanced human visual system characteristics", *Proceedings of the SPIE, Mobile Multimedia/Image Processing, Security, and Applications*, vol. 8063,  p. 806310, 2011.

[21]  S. Agaian, "Visual morphology", *Proc. IS&T/SPIE's Symposium on Electronic Imaging Science & Technology*, vol. 3304, pp. 153–163, 1999.

[22]  R. Kogan, S. Agaian and K. Panetta, "Visualization using rational morphology and zonal magnitude reduction", *IX Proceedings of IS&T/SPIE's Symposium on Electronic Imaging Science & Technology*, San Jose, CA, vol. 3304, pp. 153–163, 1998.

[23]  H. D. Cheng, Y.-H. Chen and Y. Sun, "A novel fuzzy entropy approach to image enhancement and thresholding", *Signal Process*, vol. 75, pp. 277–301, 1999.

[24]  S. Agaian, B. Silver and K. Panetta, "Transform coefficient histogrambased image enhancement algorithms using contrast entropy", *IEEE Trans. Image Process.*, vol. 16, pp. 741–758, 2007.

[25]  A. M. Reza, "Realization of the contrast limited adaptive histogram equalization (CLAHE) for real-time image enhancemen", *Journal of VLSI Signal Processing Systems for Signal, Image and Video Technology*, vol. 38, pp. 35-44, 2004.

[26]  T. Trongtirakul, S. Agaian and S. Wu, "Adaptive Single Low-Light Image Enhancement by Fractional Stretching in Logarithmic Domain", *IEEE Access*, vol. 11, pp. 143936-143947, 2023.

[27]  B. Arad et al., "Ntire 2022 spectral recovery challenge and data set", *Proceedings of the IEEE/CVF Conference on Computer Vision and Pattern Recognition*, 2022.

[28]  Y. Cai et al., "Mst++: Multi-stage spectral-wise transformer for efficient spectral reconstruction", *Proceedings of the IEEE/CVF Conference on Computer Vision and Pattern Recognition*, 2022.

[29]  H. Gasparyan, T. Davtyan and S. Agaian, "A novel framework for solar panel segmentation from remote sensing images: Utilizing Chebyshev transformer and hyperspectral decomposition", *IEEE Transactions on Geoscience and Remote Sensing*, vol. 62, 2024, doi: 10.1109/TGRS.2024.3386402

[30] Li.-Ch. Chen, "Rethinking atrous convolution for semantic image segmentation", arXiv preprint arXiv:1706.05587, 2017.

[31] Ch. Li et al., "Nested network with two-stream pyramid for salient object detection in optical remote sensing images", *IEEE Transactions on Geoscience and Remote* Sensing, vol. 57, no. 11, pp. 9156-9166, 2019.

[32] G. Cheng, J. Han and Xi. Lu, "Remote sensing image scene classification: Benchmark and state of the art", *Proceedings of the IEEE 105.10*, pp. 1865-1883, 2017.

[33] H. Jiang et al., "Multi-resolution dataset for photovoltaic panel segmentation from satellite and aerial imagery", *Earth System Science Data 13.11*, pp. 5389-5401, 2021.

[34] D.-P. Fan et al., "Structure-measure: A new way to evaluate foreground maps", *Proceedings of the IEEE International Conference on Computer Vision*, 2017. DOI: 10.1109/ICCV.2017.487

[35] D.-P. Fan et al., "Enhanced-alignment measure for binary foreground map evaluation", arXiv preprint arXiv:1805.10421, 2018.

[36] R. Achanta et al., "Frequency-tuned salient region detection", *IEEE Conference on Computer Vision and Pattern Recognition. IEEE*, 2009.

[37] B. Silver, S. Agaian and K. Panetta, "Contrast entropy based image enhancement and logarithmic transform coefficient histogram shifting", *Proceedings of IEEE ICASSP*, pp. 633–636, 2005.

# Բազմասպեկտրալ տրոհում և հաճախականության վրա հիմնված շրջանակ հեռահաղորդակցման Պատկերներում ակնհայտ օբյեկտների հայտնաբերման համար

Հայկ Ա. Գասպարյան

Երևանի պետական համալսարան, Երևան, Հայաստան
e-mail: hayk.gasparyan@ysu.am

## Ամփոփում

Ակնհայտ օբյեկտների հայտնաբերումը (SOD) նպատակ ունի լուսանկարներում հայտնաբերել ամենաակնառու օբյեկտները, ինչը կարևոր է այնպիսի խնդիրների համար, ինչպիսիք են՝ պատկերների սեգմենտացիան, տեսողական հետևումը, ինքնավար նավիգացիան և լուսանկարների կրճատումը: Թեև SOD-ը լայնորեն ուսումնասիրվել է բնական տեսարանների RGB պատկերներում, հեռահաղորդակցման պատկերներում ակնառու օբյեկտների հայտնաբերումը մնում է չհետազոտված՝ փոփոխական տարածական չափերի և բարդ տեսարանների պատճառով:

Այս հոդվածը ներկայացնում է SOD-ի նոր շրջանակ, որը կոչվում է Multispectral Decomposition Network (MSD-Net)՝ հեռահաղորդակցման 3-շերտ RGB պատկերներում, որը համատեղում է բազմասպեկտրային տրոհումը և հաճախականության վրա առաջնայնության հայտնաբերումը: Շրջանակը ներառում է երեք հիմնական քայլեր. (i)

Բազմասպեկտրալ տրոհում. 3-շերտավոր RGB պատկերի տրոհում 32 բազմասպեկտրային գոտիների՝ սպեկտրային տիրույթներում հատկանիշների գրավումը ուժեղացնելու համար; (ii) Սինթետիկ RGB-ի վերականգնում. Էնտրոպիայի վրա հիմնված նոր չափման կիրառում՝ նշանավոր շրջաններում առավել տեղեկատվական գոտիներ ընտրելու համար՝ վերլուծելով հաճախականության տիրույթը և կառուցելով սինթետիկ RGB պատկեր; և (iii) Saliency Fusion and Object Detection. սեգմենտավորման ցանցի ուսուցում վերականգնված պատկերների և մուտքային պատկերների միաձուլման վրա՝ բարելավված ճշգրտության համար: Հանրային տվյալների հավաքածուների համապարփակ գնահատումը ցույց է տալիս, որ առաջարկվող մեթոդն ավելի լավ է գործում, քան ժամանակակից (SOTA) մոդելները և առաջարկում է կայուն լուծում բարդ հեռահաղորդակցման պատկերներում ակնհայտ օբյեկտները հայտնաբերելու համար՝ ինտեգրելով բազմասպեկտրային և հաճախականության վրա հիմնված տեխնիկաներ:

**Բանալի բառեր՝** ակնհայտության քարտեզ, օբյեկտների հայտնաբերում, բազմասպեկտրային տրոհում, գոտու ընտրություն, հեռահաղորդակցում, Էնտրոպիա

# Мультиспектральное разложение и частотная основа для выделения заметных объектов на изображениях дистанционного зондирования

Айк А. Гаспарян

Ереванский государственный университет, Ереван, Армения
e-mail: hayk.gasparyan@ysu.am

## Аннотация

Обнаружение заметных объектов (SOD) направлено на идентификацию наиболее визуально выделяющихся объектов на изображениях, что важно для задач таких, как сегментация изображений, визуальное отслеживание, автономная навигация и кадрирование фотографий. Хотя SOD активно изучалась в изображениях естественных сцен в RGB, обнаружение заметных объектов на изображениях дистанционного зондирования остается малоизученным из-за изменчивости пространственных разрешений и сложности сцен.

В данной работе представлен новый фреймворк для SOD, называемый Сетью Мультиспектрального Разложения (MSD-Net) в 3-полосных RGB изображениях дистанционного зондирования, объединяющий мультиспектральное разложение и обнаружение заметности на основе частот. Фреймворк включает три ключевых шага: (i) Мультиспектральное разложение: разложение 3-полосного RGB изображения на 32 мультиспектральные полосы для улучшения захвата признаков через спектральные домены; (ii) Синтетическая RGB реконструкция: использование новой меры на основе энтропии для выбора наиболее информативных полос в заметных регионах путем анализа

частотного домена и построения синтетического RGB изображения; и (iii) Слияние заметности и обнаружение объектов: обучение сегментационной сети на слиянии выбранных полос и входного изображения для повышения точности. Обширные оценки на публичных наборах данных показывают, что предложенный метод превосходит существующие модели и предлагает надежное решение для обнаружения заметных объектов на сложных изображениях дистанционного зондирования, интегрируя мультиспектральные и частотно-ориентированные техники.

**Ключевые слова:** карта очевидности, обнаружение объектов, мультиспектральное разложение, выбор полосы, дистанционное зондирование, энтропия.

# Enhancing Thermal Image Classification with Novel Quality Metric-Based Augmentation Techniques

Hrach Y. Ayunts

Yerevan State University, Yerevan, Armenia
e-mail: hrach.ayunts@ysu.am

**Abstract**

Thermal image classification is critical in various applications, particularly fault detection and monitoring systems such as photovoltaic (PV) modules. However, a common challenge in these fields is the limited availability of large-scale, labeled thermal image datasets. To address this, color image augmentation is widely adopted in machine learning to artificially increase the size and diversity of training datasets, improving model generalization. Traditional augmentation techniques, such as geometric transformations, provide some benefits but may fail to fully capture the unique characteristics inherent in thermal images, which often have lower contrast and different noise patterns than visible spectrum images. So, we argued we need to develop a novel augmentation technique for thermal imaging, where data collection is costly and time-consuming.

Our research proposes a novel offline augmentation technique guided by quality metrics to enhance the performance of thermal image binary classification models. By leveraging domain-specific quality metrics, such as image clarity, thermal contrast, and noise levels, we optimize the oversampling process for thermal datasets. For example, starting with a dataset of x images, we generate y additional thermal images, resulting in a total of x + y images used to train the deep learning classification framework. Using a dataset of PV module defects, we demonstrate the effectiveness of our quality metric-based oversampling strategy across several state-of-the-art image classification networks. Our approach outperforms traditional augmentation methods regarding classification accuracy and robustness, including geometric transformations and standard image enhancement techniques. The practical implications of our research are significant, as it provides a more effective and efficient way to improve model performance for thermal imaging tasks, mainly when data availability is limited.

**Keywords:** Dataset augmentation, Image quality assessment, Thermal image classification.

**Article info:** Received 10 October 2024; sent for review 19 October 2024; accepted 26 November 2024.

**Acknowledgment:** The research is conducted within the ADVANCE Research Grant provided by the Foundation for Armenian Science and Technology funded by Sarkis and Nune Sepetjians.

I would also like to express my deepest gratitude to my supervisor, Professor Sos Agaian, for his constant guidance, support, and valuable insights throughout this work.

# 1. Introduction

Thermal image classification plays a pivotal role in various critical applications, including fault detection and monitoring of photovoltaic (PV) modules, building inspections, and medical diagnostics [1, 2, 3, 4]. The unique advantage of thermal imaging lies in its ability to capture infrared radiation, making it highly effective for detecting heat signatures and identifying invisible anomalies to standard visible-light cameras. However, the development of robust deep learning models for thermal image classification remains challenging due to the limited availability of large-scale, labeled thermal image datasets [5]. Acquiring and labeling thermal data is time-consuming and costly, which hinders the creation of models capable of generalizing well across diverse real-world conditions.

This paper aims to develop a novel quality metric-based augmentation technique for fault detection and monitoring systems such as photovoltaic (PV) modules. Our proposed method addresses the challenges of data scarcity and enhances model performance by introducing thermal-specific augmentation strategies.

Data collection is essential when public computer vision datasets are insufficient, as applications such as fault detection and monitoring systems often require more data. However, data collection for computer vision training is both expensive and labor-intensive. Image annotation, which involves creating ground-truth data for model training, requires costly human labor. Building large image datasets is incredibly challenging due to the rarity of events, privacy concerns, the need for industry experts for labeling, and the significant expense and manual effort required to record visual data. These challenges underscore the need for data augmentation in computer vision.

Data augmentation is a set of techniques that enhance the size and quality of machine learning training datasets, enabling the training of better deep learning models. The most difficult challenge is the generalizability of deep learning models, which refers to the performance difference of a model when evaluated on previously seen data (training data) versus data it has never seen before (testing data). Models with poor generalizability have overfitted the training data.

To address the limitations posed by small datasets, data augmentation techniques have become essential in computer vision [6, 7]. Traditional augmentation methods, such as geometric transformations (e.g., rotations, flips, and scaling) and brightness adjustments, artificially increase the size and diversity of training datasets. These techniques expose models to a broader range of variations, enhancing their ability to generalize across unseen data. However, traditional augmentations are unsuitable for thermal images due to their distinct characteristics [8]. Thermal images typically exhibit lower contrast, unique noise patterns, and temperature-specific information that differ from visible-spectrum images. As a result, augmentation strategies for visible-light images may distort critical thermal features like temperature gradients and hot spots, reducing the effectiveness of the models.

Recent studies have proposed various methods to improve thermal image classification for PV module fault detection by tailoring augmentation techniques to thermal data. For instance, Korkmaz et al. [5] introduced an efficient fault classification method using transfer learning and a multi-scale convolutional neural network (CNN). They applied geometric transformations and brightness adjustments to enhance their dataset, achieving notable improvements in classification accuracy. Similarly, Pamungkas et al. [8] proposed a novel method using a coupled UDenseNet architecture for efficient solar panel fault classification. Their approach combined geometric transformations with generative adversarial networks
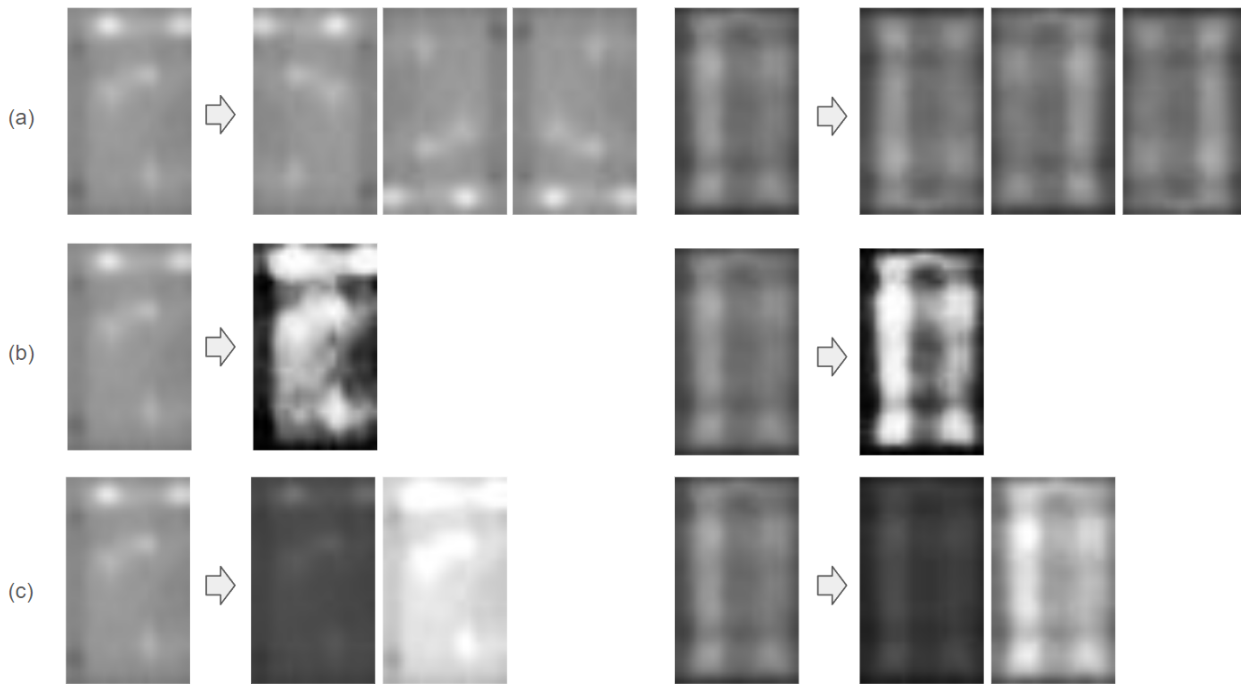
Fig.1. Examples of augmented thermal images: (a) geometric transformations (horizontal, vertical, and both flips), (b) histogram equalization, and (c) brightness adjustment.

(GANs) to generate additional synthetic thermal images, significantly boosting model performance. In another approach, Tang et al. [9] focused on automatic defect identification in PV panels using infrared (IR) images captured by unmanned aircraft. They utilized histogram equalization to enhance the contrast of the thermal images, improving the clarity of defects and anomaly detection. Some of these augmentation techniques, including geometric transformations, brightness adjustment, and histogram equalization, are depicted in Fig. 1.

In this paper, we address the limitations of traditional augmentation methods by proposing a novel offline augmentation technique guided by thermal-specific image quality metrics. These quality metrics, including clarity, thermal contrast, and noise levels, are tailored to the unique characteristics of thermal images. By optimizing the augmentation process based on these metrics, we generate additional samples that more accurately reflect real-world variations in thermal data, improving the robustness and generalization of thermal image classification models.

To validate our approach, we experiment with a PV module defect dataset [10] and apply quality metric-based oversampling to augment the training set. We evaluate our method across several state-of-the-art deep learning architectures, including CNNs like AlexNet [11] and ResNet50 [12], as well as transformer-based models such as Swin Transformer [13]. These networks, described in Table 1, are commonly employed for classification tasks and serve as a benchmark for our proposed augmentation technique. Our experimental results demonstrate that our method not only outperforms traditional augmentation techniques but also significantly improves classification accuracy and model robustness across diverse networks.

Table 1: Popular Networks for Image Classification

| Network Description | Number of Parameters |
|---|---|
| **AlexNet [11]** is a CNN architecture that won the 2012 ImageNet competition, pioneering the use of deep learning for large-scale image classification. It features five convolutional layers, followed by three fully connected layers. AlexNet's use of ReLU activation and dropout was instrumental in improving performance. *PyTorch model: alexnet* | 61 million |
| **ResNet50 [12]** introduces residual connections that enable the training of much deeper architectures by addressing the vanishing gradient problem. ResNet50, with its 50 layers, became one of the most influential models in computer vision, especially for transfer learning. *PyTorch model: resnet50* | 25.6 million |
| **SqueezeNet [14]** is a compact CNN architecture that achieves AlexNet-level accuracy with 50x fewer parameters, thanks to its "fire modules," which consist of a squeeze layer and an expand layer to reduce the number of parameters while maintaining accuracy. *PyTorch model: squeezenet1_1* | 1.2 million |
| **ShuffleNetV2 [15]** is designed for lightweight mobile and embedded vision applications. It uses group convolutions and a channel shuffle operation to reduce computational complexity while maintaining high accuracy, making it highly efficient for mobile devices. *PyTorch model: shufflenet_v2_x1_0* | 2.3 million |
| **MobileNetV3 [16]** is the third version of the MobileNet family, designed for high efficiency in mobile and embedded applications. It uses a combination of inverted residuals and squeeze-and-excitation (SE) modules to balance speed and accuracy. *PyTorch model: mobilenet_v3_small* | 2.5 million |
| **Swin Transformer [13]** is a hierarchical transformer model that applies attention within shifted windows, enabling both local and global information capture. It is scalable and effective across different vision tasks. *PyTorch model: swin_v2_t* | 28 million |

The key contributions of this work are summarized as follows:

- We introduce a novel augmentation method guided by a thermal-specific quality metric, which enhances the performance of thermal image classification models.

- We demonstrate the effectiveness of our approach using a PV module defect dataset, showing that our method improves classification accuracy and model robustness.

- We evaluate our method on various state-of-the-art deep learning architectures, including both CNN-based and transformer-based models, showcasing its general applicability.

The remainder of the paper is structured as follows. Section 2. presents our proposed quality metric-based augmentation method, followed by experimental setup and results in Section 3. Finally, Section 4. concludes the paper with a discussion of future work and practical implications.

## 2.  Proposed Method

In this study, we propose a domain-specific augmentation technique tailored for thermal images, particularly addressing the challenges presented by the unique characteristics of infrared data. Traditional image augmentation methods, such as geometric transformations and basic image enhancement, often fail to adequately improve thermal image datasets. This is primarily due to the inherently low contrast and distinct noise patterns in thermal images, which differ significantly from those in visible spectrum images. As a result, conventional approaches do not fully capture the structural and qualitative nuances required for effective thermal image classification.

To overcome these limitations, we leverage the Block-wise Image Entropy (BIE) quality metric [17], a no-reference Image Quality Assessment (IQA) technique. No-reference IQA methods are particularly important in scenarios where ground truth image quality ratings are unavailable, as they provide an objective measure of image qualtrongtirakul2022unsupervisedity without the need for reference images [18, 19]. This is crucial in thermal imaging, where acquiring high-quality, well-labeled datasets is often difficult and costly [20]. By incorporating both local and global entropy characteristics, BIE offers a more comprehensive assessment of thermal image quality than traditional methods. It evaluates the image based on entropy-driven criteria, which better aligns with the noise characteristics and structural patterns of thermal data, thus ensuring that the augmented images maintain high levels of interpretability and detail.

The BIE is defined as:

$$BIE(I) = ADP(I) \times \frac{\frac{1}{n}\sum_{k=1}^{n}(\alpha M'(I^k)^\alpha \times \ln M'(I^k))}{1 + \frac{1}{n}\sum_{k=1}^{n}E(I^k)} \times \frac{SD(I)}{1 + \frac{1}{n}\sum_{k=1}^{n}SD(I^k)}, \qquad (1)$$

where $n$ represents the number of blocks into which the image is divided, $E(I^k)$ is the entropy of each block, and $SD(I^k)$ is the standard deviation of each block. The term $ADP(I)$ denotes the Average Deviation Percentage, and $M'(I)$ is the modified modulation. These are defined as:

$$ADP(I) = 1 - \frac{|A(I) - L/2|}{L/2}, \quad M'(I) = \frac{I_{\max} - I_{\min}}{L}, \qquad (2)$$

where $A(I)$ is the average pixel value of the image, $L = 255$ represents the maximum pixel value in an 8-bit image (adjustable depending on the image format), and $I_{\max}$, $I_{\min}$ are the maximum and minimum pixel intensities, respectively. The entropy $E(I)$ is calculated using Shannon entropy [21], which is defined as:

$$E(I) = -\sum_{i=1}^{N} P(i) \log_2 P(i), \qquad (3)$$

where $E(I)$ represents the entropy of the image $I$, $N$ denotes the total number of possible intensity levels, and $P(i)$ is the probability of occurrence of intensity level $i$ within the image. Shannon entropy provides a measure of information content and randomness in the image, making it a crucial component of the BIE metric for evaluating thermal image quality.

Measure-based enhancement techniques have been widely employed in the literature to improve image quality and performance in machine learning tasks, particularly in scenarios
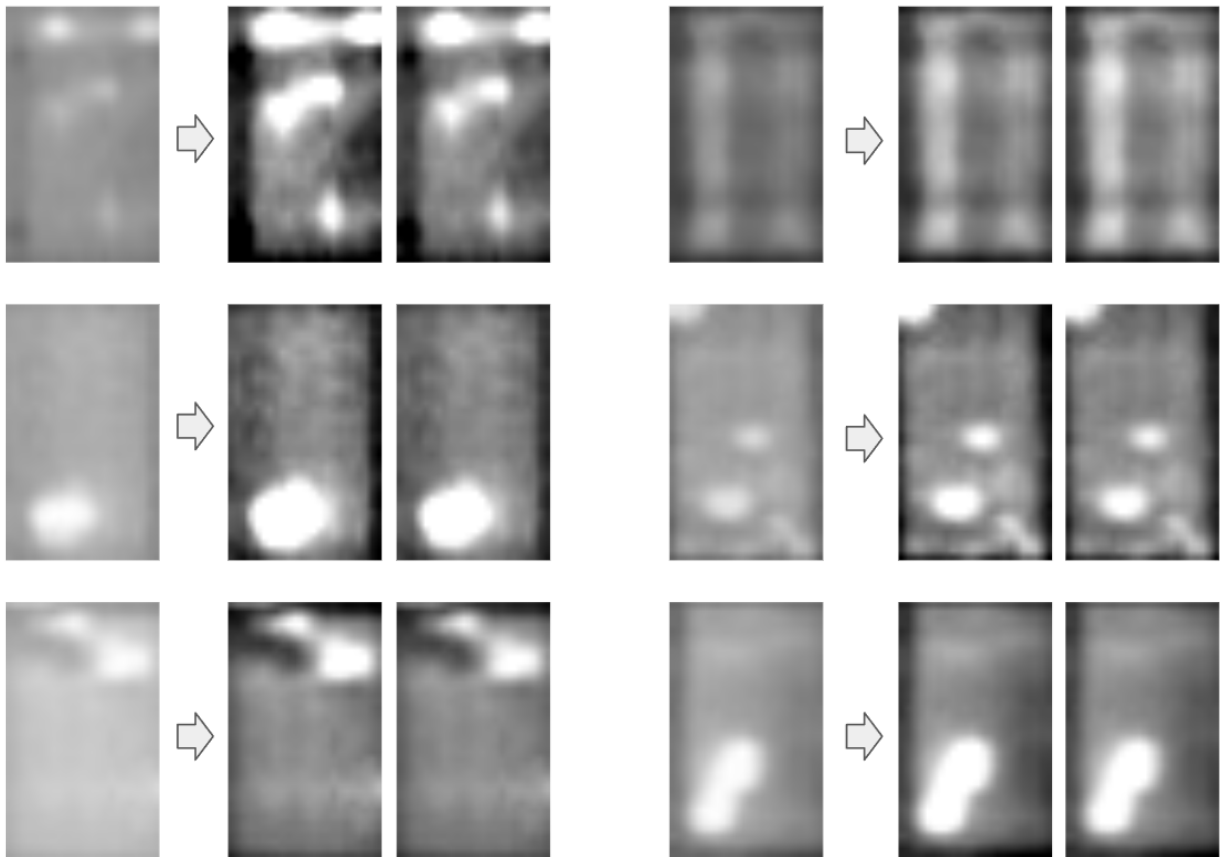
Fig. 2. Example of BIE-based contrast enhancement on thermal images of defective PV modules.

where image contrast and structural detail are crucial [22, 23, 24]. To augment the thermal images, we apply a multi-step process based on contrast enhancement using the BIE quality metric:

1. **Contrast Enhancement:** Each thermal image undergoes parametric contrast stretching to enhance the overall contrast. The stretching parameters are selected from predefined ranges.

2. **Optimization Using BIE:** The low and high stretching parameters are optimized within the ranges $[0, 150]$ and $[150, 255]$, respectively, using the BIE quality measure. The goal is to maximize the BIE value for each image.

3. **Augmentation with Best and Second-Best Images:** The images with the highest BIE value and the second-highest BIE value are selected and added to the augmented dataset, alongside the original image.

This method generates augmented versions of thermal images that have improved contrast and higher entropy, which are better suited for training deep learning models.

Fig. 2. illustrates the results of our BIE-based contrast enhancement for a defective thermal image from the Infrared Solar Modules dataset [10]. The original image, along with the images corresponding to the best and second-best BIE values, are shown.

Table 2: Description of augmentation setups and sets

| Augmentation | Description | Training set | Validation set | Test set |
|:---:|:---:|:---:|:---:|:---:|
| A0 | No augmentation | 16,000 | 2,000 | 2,000 |
| A1 | Geometric Transformations (GT) | 64,000 | 8,000 | 8,000 |
| A2 | GT + Histogram Equalization | 80,000 | 10,000 | 10,000 |
| A3 | GT + Brightness Adjustment | 96,000 | 12,000 | 12,000 |
| A4 | GT + BIE-based Oversampling | 80,000 | 10,000 | 10,000 |

The results highlight how BIE-guided contrast enhancement significantly improves image quality by enhancing local contrast and emphasizing key structural features in the thermal image.

## 3.   Results

In this section, we present the performance results of our proposed augmentation technique and the deep learning models evaluated on the PV module defect classification task. The dataset consists of 20,000 infrared images of solar modules, evenly divided between non-defective (No-Anomaly) and defective modules. The defective class includes a variety of faults, such as Hot-Spots, Soiling, Diode failures, and Cell anomalies [10]. The deep learning models used in our experiments, including CNN-based architectures and a transformer-based model, are described in Table 1. As detailed in Table 3., The augmentation setups were applied to the original dataset, which was randomly split into 80% training, 10% validation, and 10% test sets. The number of samples in each set after augmentation is also listed in Table 3..

For training the models, we used the following hyperparameters. Each model was trained for 30 epochs using the Cross-entropy loss function. We optimized the models using the stochastic gradient descent (SGD) optimizer with an initial learning rate of 0.001 and momentum set to 0.9. The batch size for all experiments was set to 32. To enhance training efficiency and mitigate overfitting, we employed a learning rate scheduler, specifically the StepLR, with a step size of 10 and a gamma of 0.5 to reduce the learning rate after every 10 epochs.

Additionally, the input images were resized to meet the requirements of each network before training and validation. For instance, images were resized to 227x227 for AlexNet and 224x224 for ResNet50.

To evaluate the performance of the models, we used four standard classification metrics: accuracy (Acc), precision (Pr), recall (Rec), and specificity (Sp). These metrics were calculated based on the following equations:

$$\text{Accuracy (Acc)} = \frac{TP + TN}{TP + TN + FP + FN} \tag{4}$$

$$\text{Precision (Pr)} = \frac{TP}{TP + FP} \tag{5}$$

$$\text{Recall (Rec)} = \frac{TP}{TP + FN} \tag{6}$$

Table 3: Quantitative results for each deep learning model trained on five different augmentation techniques. The table presents accuracy, precision, recall, and specificity for both the test and validation sets.

| | Dataset | Test | | | | Validation | | | |
|---|---|---|---|---|---|---|---|---|---|
| | Aug Method | Acc | Pr | Rec | Sp | Acc | Pr | Rec | Sp |
| AlexNet | A0 | 86.85 | 88.83 | 86.90 | 93.31 | 85.80 | 88.26 | 85.81 | 92.79 |
| | A1 | 90.88 | 91.85 | 90.91 | 95.37 | 89.28 | 90.75 | 89.28 | 94.57 |
| | A2 | 90.39 | 91.34 | 90.42 | 95.11 | 89.62 | 90.90 | 89.63 | 94.73 |
| | A3 | 88.32 | 89.61 | 88.35 | 94.02 | 87.83 | 89.52 | 87.84 | 93.81 |
| | A4 | 93.21 | 92.62 | 94.05 | 96.56 | 92.53 | 92.02 | 93.54 | 96.22 |
| ResNet50 | A0 | 89.70 | 89.92 | 89.72 | 94.61 | 89.30 | 89.89 | 89.31 | 94.45 |
| | A1 | 92.20 | 92.28 | 92.21 | 95.95 | 91.41 | 91.56 | 91.42 | 95.54 |
| | A2 | 91.99 | 92.01 | 91.99 | 95.83 | 91.28 | 91.36 | 91.28 | 95.45 |
| | A3 | 88.33 | 88.48 | 88.35 | 93.83 | 87.38 | 87.64 | 87.38 | 93.31 |
| | A4 | 93.66 | 93.06 | 94.12 | 96.75 | 93.16 | 92.57 | 93.76 | 96.51 |
| SqueezeNet | A0 | 88.10 | 88.98 | 88.13 | 93.83 | 88.30 | 89.30 | 88.31 | 93.96 |
| | A1 | 88.42 | 88.73 | 88.41 | 93.91 | 88.66 | 88.80 | 88.66 | 94.01 |
| | A2 | 88.41 | 88.47 | 88.40 | 93.86 | 88.06 | 88.12 | 88.06 | 93.66 |
| | A3 | 86.17 | 86.46 | 86.18 | 92.63 | 85.71 | 86.06 | 85.71 | 92.37 |
| | A4 | 91.34 | 90.89 | 91.09 | 95.47 | 91.71 | 91.22 | 91.63 | 95.68 |
| ShuffleNetV2 | A0 | 89.95 | 90.19 | 89.97 | 94.75 | 90.30 | 90.77 | 90.31 | 94.98 |
| | A1 | 92.35 | 92.39 | 92.36 | 96.03 | 91.75 | 91.90 | 91.75 | 95.72 |
| | A2 | 91.44 | 91.57 | 91.45 | 95.55 | 90.54 | 90.73 | 90.54 | 95.07 |
| | A3 | 90.69 | 90.83 | 90.70 | 95.14 | 89.96 | 90.20 | 89.96 | 94.75 |
| | A4 | 93.72 | 93.19 | 93.90 | 96.77 | 93.07 | 92.51 | 93.36 | 96.43 |
| MobileNetV3 | A0 | 92.65 | 92.66 | 92.65 | 96.19 | 91.20 | 91.26 | 91.20 | 95.41 |
| | A1 | 93.04 | 93.05 | 93.03 | 96.39 | 92.26 | 92.27 | 92.26 | 95.98 |
| | A2 | 92.40 | 92.41 | 92.40 | 96.05 | 92.06 | 92.09 | 92.06 | 95.87 |
| | A3 | 91.72 | 91.80 | 91.73 | 95.70 | 91.42 | 91.52 | 91.43 | 95.54 |
| | A4 | 94.59 | 94.18 | 94.64 | 97.23 | 94.08 | 93.59 | 94.27 | 96.96 |
| Swin | A0 | 88.85 | 88.91 | 88.84 | 94.10 | 88.90 | 88.90 | 88.90 | 94.12 |
| | A1 | 91.69 | 91.82 | 91.68 | 95.68 | 91.38 | 91.41 | 91.37 | 95.50 |
| | A2 | 91.60 | 91.74 | 91.59 | 95.64 | 90.96 | 90.98 | 90.96 | 95.27 |
| | A3 | 89.59 | 89.63 | 89.60 | 94.52 | 89.41 | 89.54 | 89.41 | 94.43 |
| | A4 | 93.85 | 93.38 | 93.95 | 96.84 | 93.67 | 93.13 | 93.94 | 96.75 |

$$\text{Specificity (Sp)} = \frac{TN}{TN + FP} \tag{7}$$

In these equations, $TP$ represents true positives, $TN$ represents true negatives, $FP$ represents false positives, and $FN$ represents false negatives.

The results for each deep learning model, trained using five different augmentation techniques, are summarized in Table 3. The confusion matrices for AlexNet and Swin Transformer are shown in Fig. 3.
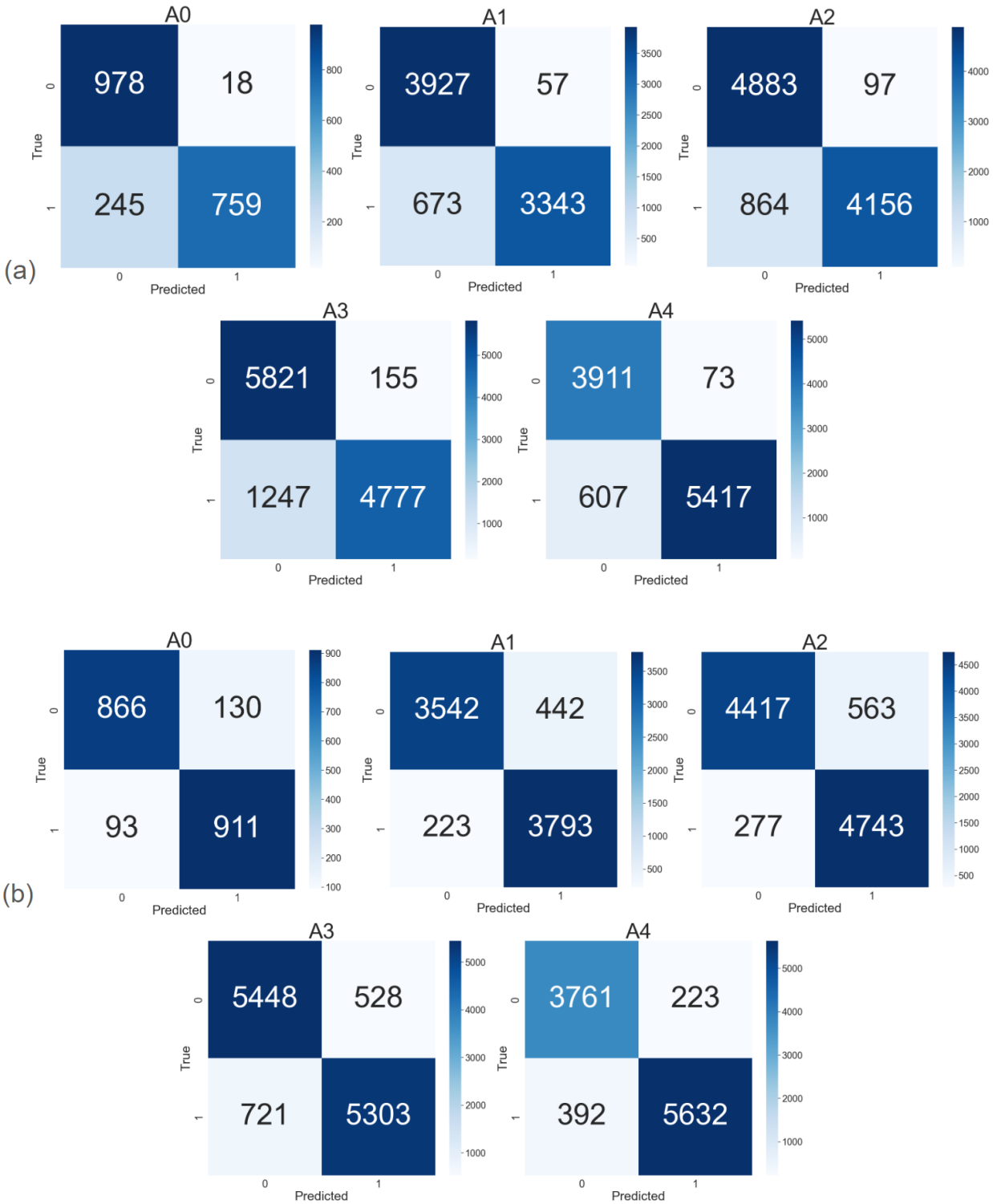
Fig. 3. Confusion matrices for binary classification using (a) AlexNet and (b) Swin Transformer, showcasing performance across different augmentation types on the test set.

As observed, the setups without augmentation and those using only brightness adjustment yielded the lowest performance metrics across all models. The setups employing geometric transformations and histogram equalization achieved moderate scores, indicating

some improvement but still lacking compared to other methods.

However, our proposed contrast enhancement augmentation, combined with geometric transformations, outperformed all other approaches. This setup achieved the best performance, particularly on MobileNetV3, with an accuracy of 94.59%, precision of 94.18%, recall of 94.64%, and a specificity of 97.23% on the test set. Swin Transformer also performed well with our augmentation technique, though its results were less impressive than those of other augmentation setups.

In conclusion, the proposed contrast enhancement method not only improves model performance but demonstrates its effectiveness in enhancing the robustness and classification accuracy of thermal image datasets, particularly when data availability is limited.

## 4. Conclusion

This paper presented a novel augmentation technique for thermal image classification, particularly for fault detection in photovoltaic modules. Given the challenges of limited thermal image datasets, traditional augmentation methods like geometric transformations and simple enhancements are often inadequate. To address this, we proposed a new augmentation method that uses thermal quality assessment-based contrast enhancement to enrich the dataset. Our approach significantly improves the diversity of the training dataset, leading to enhanced classification accuracy and robustness across several state-of-the-art models. The results demonstrate the effectiveness of the new augmentation over conventional methods, making it a valuable tool for thermal imaging applications with constrained data.

Future work will focus on improving classification accuracy by exploring thermal-specific deep-learning models and further refining our augmentation technique to optimize performance.

## References

[1] M. W. Akram, G. Li, Y. Jin, X. Chen, C. Zhu, X. Zhao, M. Aleem, and A. Ahmad, "Improved outdoor thermography and processing of infrared images for defect detection in pv modules," *Solar Energy*, vol. 190, pp. 549–560, 2019.

[2] R. H. F. Alves, G. A. de Deus Junior, E. G. Marra, and R. P. Lemos, "Automatic fault classification in photovoltaic modules using convolutional neural networks," *Renewable Energy*, vol. 179, pp. 502–516, 2021.

[3] T. Trongtirakul, S. Agaian, and A. Oulefki, "Automated tumor segmentation in thermographic breast images," *Mathematical Biosciences and Engineering*, vol. 20, no. 9, pp. 16786–16806, 2023.

[4] M. d. F. O. Baffa and L. G. Lattari, "Convolutional neural networks for static and dynamic breast infrared imaging classification," in *2018 31st SIBGRAPI Conference on Graphics, Patterns and Images (SIBGRAPI)*, pp. 174–181, IEEE, 2018.

[5] D. Korkmaz and H. Acikgoz, "An efficient fault classification method in solar photovoltaic modules using transfer learning and multi-scale convolutional neural network," *Engineering Applications of Artificial Intelligence*, vol. 113, p. 104959, 2022.

[6] Z. Yang, R. O. Sinnott, J. Bailey, and Q. Ke, "A survey of automated data augmentation algorithms for deep learning-based image classification tasks," *Knowledge and Information Systems*, vol. 65, no. 7, pp. 2805–2861, 2023.

[7] W. Li, C. Chen, M. Zhang, H. Li, and Q. Du, "Data augmentation for hyperspectral image classification with deep cnn," *IEEE Geoscience and Remote Sensing Letters*, vol. 16, no. 4, pp. 593–597, 2018.

[8] R. F. Pamungkas, I. B. K. Y. Utama, and Y. M. Jang, "A novel approach for efficient solar panel fault classification using coupled udensenet," *Sensors*, vol. 23, no. 10, p. 4918, 2023.

[9] C. Tang, H. Ren, J. Xia, F. Wang, and J. Lu, "Automatic defect identification of pv panels with ir images through unmanned aircraft," *IET Renewable Power Generation*, vol. 17, no. 12, pp. 3108–3119, 2023.

[10] M. Millendorf, E. Obropta, and N. Vadhavkar, "Infrared solar module dataset for anomaly detection," in *Proc. Int. Conf. Learn. Represent*, 2020.

[11] A. Krizhevsky, "One weird trick for parallelizing convolutional neural networks," *arXiv preprint arXiv:1404.5997*, 2014.

[12] K. He, X. Zhang, S. Ren, and J. Sun, "Deep residual learning for image recognition," in *Proceedings of the IEEE conference on computer vision and pattern recognition*, pp. 770–778, 2016.

[13] Z. Liu, H. Hu, Y. Lin, Z. Yao, Z. Xie, Y. Wei, J. Ning, Y. Cao, Z. Zhang, L. Dong, *et al.*, "Swin transformer v2: Scaling up capacity and resolution," in *Proceedings of the IEEE/CVF conference on computer vision and pattern recognition*, pp. 12009–12019, 2022.

[14] F. N. Iandola, "Squeezenet: Alexnet-level accuracy with 50x fewer parameters and¡ 0.5 mb model size," *arXiv preprint arXiv:1602.07360*, 2016.

[15] N. Ma, X. Zhang, H.-T. Zheng, and J. Sun, "Shufflenet v2: Practical guidelines for efficient cnn architecture design," in *Proceedings of the European conference on computer vision (ECCV)*, pp. 116–131, 2018.

[16] A. Howard, M. Sandler, G. Chu, L.-C. Chen, B. Chen, M. Tan, W. Wang, Y. Zhu, R. Pang, V. Vasudevan, *et al.*, "Searching for mobilenetv3," in *Proceedings of the IEEE/CVF international conference on computer vision*, pp. 1314–1324, 2019.

[17] H. Ayunts, A. Grigoryan, and S. Agaian, "Novel entropy for enhanced thermal imaging and uncertainty quantification," *Entropy*, vol. 26, no. 5, p. 374, 2024.

[18] K. Panetta, C. Gao, and S. Agaian, "No reference color image contrast and quality measures," *IEEE transactions on Consumer Electronics*, vol. 59, no. 3, pp. 643–651, 2013.

[19] H. Ayunts and S. Agaian, "No-reference quality metrics for image decolorization," *IEEE Transactions on Consumer Electronics*, vol. 69, no. 4, pp. 1177–1185, 2023.

[19] H. Ayunts and S. Agaian, "No-reference quality metrics for image decolorization," *IEEE Transactions on Consumer Electronics*, vol. 69, no. 4, pp. 1177–1185, 2023.

[20] T. Trongtirakul and S. Agaian, "Unsupervised and optimized thermal image quality enhancement and visual surveillance applications," *Signal Processing: Image Communication*, vol. 105, p. 116714, 2022.

[21] P. Bromiley, N. Thacker, and E. Bouhova-Thacker, "Shannon entropy, renyi entropy, and information," *Statistics and Inf. Series (2004-004)*, vol. 9, no. 2004, pp. 2–8, 2004.

[22] S. S. Agaian, B. Silver, and K. A. Panetta, "Transform coefficient histogram-based image enhancement algorithms using contrast entropy," *IEEE transactions on image processing*, vol. 16, no. 3, pp. 741–758, 2007.

[23] A. M. Grigoryan and S. S. Agaian, "Image processing contrast enhancement," *Wiley Encyclopedia of Electrical and Electronics Engineering*, pp. 1–22, 1999.

[24] A. M. Grigoryan, A. John, and S. S. Agaian, "Color image enhancement of medical images using alpha-rooting and zonal alpha-rooting methods on 2d qdft," in *Medical Imaging 2017: Image Perception, Observer Performance, and Technology Assessment*, vol. 10136, pp. 325–333, SPIE, 2017.

## Ջերմային պատկերների դասակարգման բարելավում որակի չափորոշիչների վրա հիմնված տվյալների ավելացման նոր մեթոդով

Հրաչ Յու. Այունց

Երևանի պետական համալսարան, Երևան, Հայաստան
e-mail: e-mail: hrach.ayunts@ysu.am

**Ամփոփում**

Ջերմային պատկերների դասակարգումը կարևոր նշանակություն ունի տարբեր ոլորտներում, մասնավորապես, անսարքությունների հայտնաբերման և մոնիտորինգի համակարգերում, ինչպիսիք են ֆոտոգալվանային (ՖՎ) մոդուլները: Այնուամենայնիվ, այս ոլորտներում ընդհանուր մարտահրավերը լայնածավալ, անոտացված ջերմային պատկերների տվյալների հավաքածուների սահմանափակ հասանելիությունն է: Այս խնդիրը լուծելու համար մեքենայական ուսուցման մեջ լայնորեն ընդունված է պատկերների ավելացումը՝ արհեստականորեն մեծացնելու տվյալների հավաքածուների չափն ու բազմազանությունը՝ բարելավելով մոդելների ընդհանրացումը: Ավանդական մեծացման մեթոդները, ինչպիսիք են երկրաչափական փոխակերպումները, տալիս են որոշ առավելություններ, սակայն կարող են չարտացոլել ջերմային պատկերներին բնորոշ յուրահատուկ հատկանիշները, որոնք հաճախ ունեն ավելի ցածր կոնտրաստ և տարբեր աղմուկի մոդելներ, քան տեսանելի սպեկտրի պատկերները: Այսպիսով, մենք պնդում ենք,

որ պետք է մշակվի ջերմային պատկերների ավելացման նոր մեթոդ, քանի որ ջերմային տվյալների հավաքագրումը ծախսատար է և ժամանակատար:

Մեր հետազոտությունն առաջարկում է տվյալների ավելացման նոր տեխնիկա, որն առաջնորդվում է որակի չափորոշիչներով՝ ջերմային պատկերների երկուական դասակարգման մոդելների արդյունավետությունը բարձրացնելու համար: Օգտագործելով տիրույթին հատուկ որակի չափորոշիչներ, ինչպիսիք են պատկերի պարզությունը, ջերմային կոնտրաստը և աղմուկի մակարդակները, մենք օպտիմիզացնում ենք ջերմային տվյալների հավաքածուների հարստացման գործընթացը: Օրինակ, $x$ քանակով պատկերների տվյալների բազայից սկսած՝ մենք ստեղծում ենք $y$ լրացուցիչ ջերմային պատկերներ, ինչի արդյունքում ընդհանուր առմամբ $x + y$ քանակով պատկերներ են օգտագործվում խորը ուսուցման դասակարգման մոդելը ուսուցանելու համար: Օգտագործելով ՖՎ մոդուլի թերությունների հավաքածուն, մենք ցուցադրում ենք մեր որակի չափման վրա հիմնված տվյալների ավելացման մեթոդի արդյունավետությունը մի քանի ժամանակակից պատկերների դասակարգման ցանցերում: Մեր մոտեցումը գերազանցում է ավանդական մեծացման մեթոդներին՝ կապված դասակարգման ճշգրտության և կայունության հետ, ներառյալ երկրաչափական փոխակերպումներն և պատկերի բարելավման ստանդարտ տեխնիկաները: Մեր հետազոտության գործնական հետևանքները նշանակալի են, քանի որ այն ապահովում է ավելի արդյունավետ միջոց ջերմային պատկերների խնդիրներում մոդելների կատարողականությունը բարելավելու համար, հիմնականում, երբ տվյալների հասանելիությունը սահմանափակ է:

**Բանալի բառեր՝** տվյալների հավաքածուի մեծացում, պատկերի որակի գնահատում, ջերմային պատկերների դասակարգում:

# Улучшение классификации тепловых изображений с использованием новых техник аугментации на основе метрик качества

Грач Ю. Аюнц

Ереванский государственный университет, Ереван, Армения
e-mail: hrach.ayunts@ysu.am

## Аннотация

Классификация тепловых изображений имеет решающее значение в различных приложениях, особенно в системах обнаружения неисправностей и мониторинга, таких как фотоэлектрические (PV) модули. Однако распространенной проблемой в этих областях является ограниченная доступность крупномасштабных аннотированных наборов данных тепловых изображений. Чтобы решить эту проблему, в машинном обучении широко применяется дополнение изображений для искусственного увеличения размера и разнообразия обучающих наборов данных, что улучшает обобщение моделей. Традиционные методы дополнений, такие как геометрические преобразования, обеспечивают некоторые преимущества, но могут не полностью улавливать уникальные характеристики, присущие тепловизионным изображениям, которые часто имеют более низкую контрастность и другие шумовые паттерны, чем

изображения видимого спектра. Поэтому мы утверждаем, что нам необходимо разработать новый метод дополнений для тепловизионных изображений, где сбор данных является дорогостоящим и отнимает много времени.

Наше исследование предлагает новый метод дополнения, руководствующийся показателями качества, для повышения производительности моделей бинарной классификации тепловых изображений. Используя специфичные для домена показатели качества, такие как четкость изображения, тепловой контраст и уровни шума, мы оптимизируем процесс дополнения для тепловых наборов данных. Например, начиная с набора данных из $x$ изображений, мы генерируем $y$ дополнительных тепловых изображений, в результате чего получается в общей сложности $x + y$ изображений, используемых для обучения фреймворка классификации глубокого обучения. Используя набор данных дефектов фотоэлектрических модулей, мы демонстрируем эффективность нашей стратегии аугментации на основе метрики качества в нескольких современных сетях классификации изображений. Наш подход превосходит традиционные методы аугментации с точки зрения точности и надежности классификации, включая геометрические преобразования и стандартные методы улучшения изображений. Практические последствия нашего исследования значительны, поскольку оно обеспечивает более эффективный и действенный способ улучшения производительности модели для задач тепловидения, в основном, когда доступность данных ограничена

**Ключевые слова:** аугментация набора данных, оценка качества изображений, классификация тепловых изображений.

# Mamba-based Thermal Image Dehazing

Sargis A. Hovhannisyan

Yerevan State University, Yerevan, Armenia
e-mail: sargis.hovhannisyan@ysu.am

## Abstract

Atmospheric phenomena such as rain, snow, urban, forest fires, and artificial disasters can degrade image quality across various applications, including transportation, driver assistance systems, surveillance, military, and remote sensing. Image dehazing techniques aim to reduce the effects of haze, dust, fog, and other atmospheric distortions, enhancing image quality for better performance in computer vision tasks. Haze not only obscures details but also reduces contrast and color fidelity, significantly impacting the accuracy of computer vision (CV) models used in object detection, image classification, and segmentation. While thermal infrared (TIR) imaging is often favored for long-range surveillance and remote sensing due to its resilience to haze, atmospheric conditions can still degrade TIR image quality, especially in extreme environments.

This paper introduces MTIE-Net, a novel Mamba-based network for enhancing thermal images degraded by atmospheric phenomena like haze and smoke. MTIE-Net leverages the Enhancement and Denoising State Space Model (EDSSM), which combines convolutional neural networks with state-space modeling for effective denoising and enhancement. We generate synthetic hazy images and employ domain-specific transformations tailored to thermal image characteristics to improve training in low-visibility conditions. Our key contributions include using the Mamba architecture with 2D Selective Scanning for thermal image enhancement, developing a specialized Enhancement and Denoising module, and creating a labeled thermal dataset simulating heavy haze. Evaluated on the M3DF dataset of long-range thermal images, MTIE-Net surpasses state-of-the-art methods in both quantitative metrics (PSNR, SSIM) and qualitative assessments of visual clarity and edge preservation. This advancement significantly improves the reliability and accuracy of critical systems used in remote sensing, surveillance, and autonomous operations by enhancing image quality in challenging environments.

**Keywords:** Thermal image, Image dehazing, Thermal image enhancement, Mamba.
**Article info:** Received 10 October 2024; sent for review 19 October 2024; accepted 26 November 2024.
**Acknowledgments:** This work was partly supported by the Advance Research Grants from the Foundation for Armenian Science and Technology, funded by Sarkis and Nune Sepetjians.
I would also like to acknowledge SOLARON LLC for providing the real-world solar panel images used in this study. Additionally, I thank Professor S. Agaian for his invaluable guidance and support throughout this project.

# 1. Introduction

Images captured in hazy or foggy weather conditions often suffer from significant degradation, making it difficult for imaging systems to identify objects and their features. The reduction in contrast and color shift further complicates imaging applications. Haze causes reduced contrast, faint surfaces, color distortion, and blurred intensity, which diminishes visibility and object perception [1]. To address this, image dehazing algorithms improve scene clarity [2,3,4,5,6]. However, this task is challenging because haze formation depends on various factors like unknown scene depth, the density and size of atmospheric particles, and the wavelength of light [7]. The effect of haze varies across different parts of the electromagnetic spectrum: shorter wavelengths in the
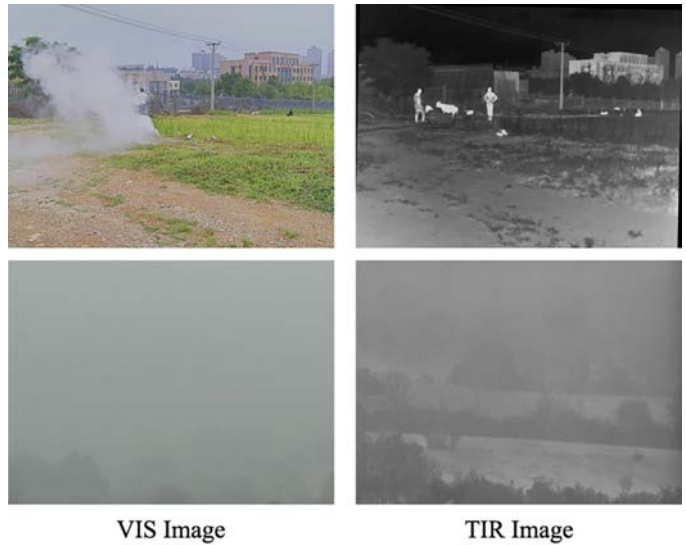


Fig. 1. Haze visibility is shown across two spectra. Heavy fog with larger particles affects both spectra compare with smoke in the first row [36, 32].

visible (VIS) are more affected, while longer wavelengths, such as those in the thermal infrared (TIR), are less affected, but factors like atmospheric absorption and scattering can degrade the quality and accuracy of thermal images, which is shown in Fig. 1. This degradation poses significant challenges for vision algorithms [8] such as pedestrian detection and segmentation [9], military target detection [10], surveillance and security [11], and remote sensing [12]. Despite its benefits, thermal imaging suffers from drawbacks like low contrast and blurred details, which limit the observation of infrared targets and hinder the development of infrared imaging applications. Thermal Image Enhancement (TIE) techniques aim to improve visibility, clarity, and overall image quality for automated processing applications [13]. These methods vary across fields and objectives, encompassing both traditional approaches and Convolution Neural Networks (CNN). Table 1 highlights the advantages and challenges of various thermal image enhancement methods, emphasizing the need for more robust techniques and exposing the need to develop more robust IIE techniques. Recent developments have introduced State Space Models (SSMs), especially the Mamba model [14], which captures global contextual information with a linearly lower complexity for input tokens. The Structured State-Space Sequence model (S4) [15] was the first to highlight the potential of SSMs, offering a novel alternative to CNNs and Transformers for handling long-range dependencies. Followed by the S5 layer [16], which introduced MIMO SSM and efficient parallel scanning. SSM-based architectures have gained significant attention in various fields [17]. For example, Mamba4KT [18] is specifically developed for knowledge tracing in intelligent education systems, utilizing the Mamba model to effectively capture long-term relationships between exercises and students' knowledge levels. The latest Mamba architecture, Mamba-2 [19], introduces an enhanced core layer within the Mamba selective SSM, achieving speeds 2 to 8 times faster while maintaining competitive performance with Transformers in language modeling.

This paper introduces the **Mamba-Based Thermal Image Enhancement Network (MTIE-Net),** a novel approach for addressing thermal image dehazing. **MTIE-Net incorporates an Enhancement and Denoising State Space Model (EDSSM),** which integrates convolutional neural networks (CNNs) with state-space modeling to denoise and enhance thermal images effectively. Additionally, the framework utilizes advanced techniques, including synthetic data generation using the Atmospheric Scattering Model (ASM) and domain-specific transformations

tailored to thermal image characteristics. These enhancements improve the model's robustness and accuracy under severe haze conditions. Our main contributions are:

1. **Introducing Mamba for thermal image enhancement** for the first time, utilizing SS2D as the computational backbone to ensure efficient and scalable dehazing.
2. **Proposing an Enhancement and Denoising (ED) module** that optimizes image enhancement and noise reduction processes, effectively addressing challenges posed by atmospheric disturbances, which is its backbone to achieve linear computational efficiency. In other words, this makes the dehazing process faster and more effective, particularly for long-range thermal imaging tasks.
3. **Creating a labeled thermal dataset** simulating heavy haze conditions will enable more realistic training and testing of dehazing models.

Table 1. Advantages and challenges of various thermal image enhancement methods.

| Method | Advantages | Challenges |
|---|---|---|
| Histogram Equalization [22] | - Enhances global contrast, is simple, and is fast to implement. | - May lead to noise amplification, it can cause an unnatural appearance and loss of detail |
| Contrast Adjustment [37] | - Flexible control over brightness and contrast. Can enhance specific regions | - May not work well with images with uneven illumination. Risk of over/under-enhancement Can cause loss of details in smooth regions. |
| Wavelet-based Methods [23] | - Effective in multi-scale analysis, good at edge and detail preservation | - It requires parameter selection/tuning and can be computationally intensive. If not properly managed, it may introduce artifacts. |
| Top-hat Transform Morphological Operation [24] | - Useful for highlighting small features. Effective in background suppression | - May not perform well with complex backgrounds, sensitive to structuring element selection and noise |
| Gradient Field Equalization [25] | - Enhances edges and local contrast. Suitable for highlighting object boundaries | - May introduce artifacts and noise. It can be sensitive to high-frequency noise. Computational intensity: making real-time processing challenging. |
| IE-CGAN [42] | - Produces visually appealing results with higher contrast and details | - It requires large datasets and computational resources, potentially overfitting and artifacts. Tends to produce unnatural sharpness in degraded images. |
| BBCNN [41] | - Maintain a natural scene appearance | - It struggles in lighter areas and with subtle contrast differences, obscuring key details. |

To validate the effectiveness of our proposed MTIE-Net, we conducted extensive evaluations using the **M3DF dataset**, which consists of long-range thermal infrared (TIR) images affected by varying degrees of atmospheric distortion. Experimental results show that MTIE-Net outperforms existing state-of-the-art methods in quantitative metrics, such as Peak Signal-to-Noise Ratio (PSNR) and Structural Similarity Index (SSIM) [20], and qualitative measures, including visual clarity and edge preservation.

The **MTIE-Net** framework advances the field of thermal image dehazing by providing a scalable and highly effective solution for improving image quality in real-world applications such as surveillance, autonomous driving, and environmental monitoring. These performance

improvements have broad practical implications: MTIE-Net can enhance the reliability and accuracy of critical systems, contributing to better overall performance and safety, whether in enhancing surveillance accuracy or improving the safety of autonomous vehicles.
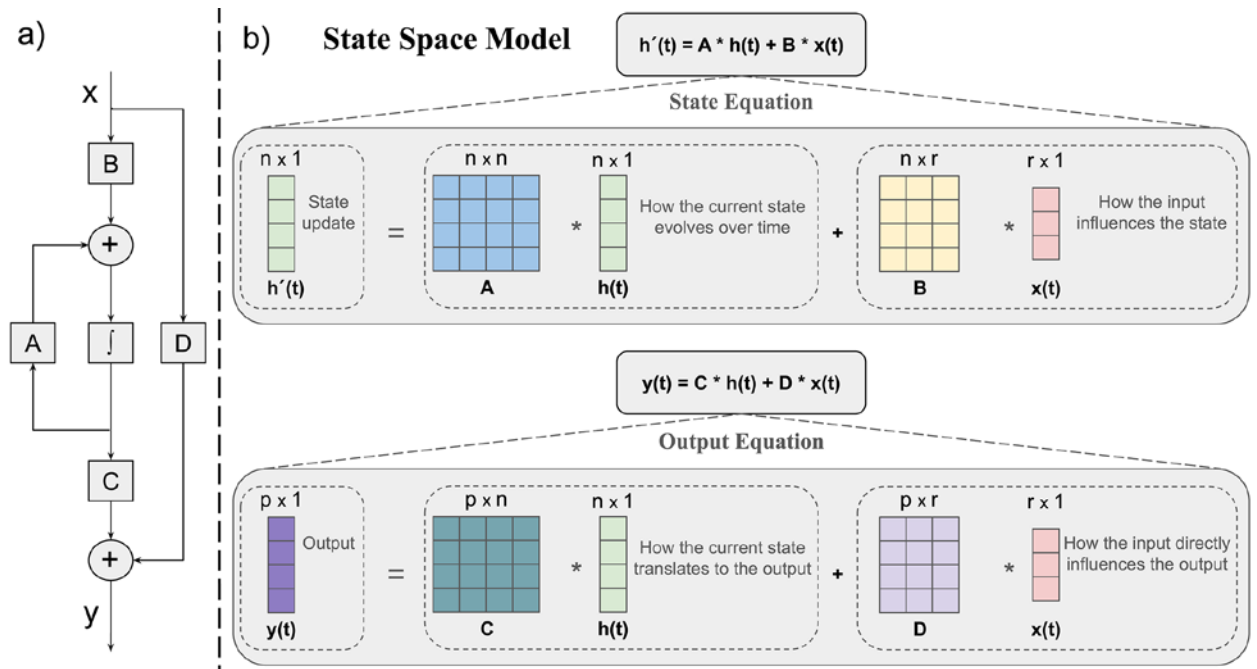


Fig. 2. Mathematical expression of the State-Space Model.

## 2. Background

## 2.1 Enhancing Thermal Imaging: Challenges and Advances

Thermal imaging cameras convert thermal energy (heat) into visible light, typically in grayscale or color scales. However, the spatial resolution of thermal images is often limited by diffraction effects in thermo-reflectance, and the signal-to-noise ratio (SNR) can affect image quality and application. Recent advancements aim to enhance thermal image quality for various applications, including geoscience, resource exploration, military surveillance, astronomy, and humanitarian missions, all of which demand high-quality, accurate thermal images. Creating high-resolution thermal images is particularly challenging for thermal cameras used on satellites or aerial platforms. These challenges include low dynamic range, lack of detail clarity, and blurred edges. Additionally, thermal images often suffer from low luminance due to factors like heat radiation intensity, object distance, and reflection angles, which can degrade the performance of vision-based systems.

Thermal image enhancement algorithms fall into two main categories: traditional and learning-based. Traditional methods [21], see Table 1, such as Histogram Equalization [22], Wavelet-Based methods [23], Top-Hat Transform [24], and Gradient Field Equalization [25], focus on improving contrast and reducing noise. While effective in some scenarios, they often struggle in complex situations, sometimes over-enhance, leading to noise amplification and brightness distortion. In contrast, learning-based methods utilize neural networks to enhance image quality, effectively addressing issues like low contrast, noise, and blurred details, making thermal images more suitable for analysis. These methods also face challenges, including high computational demands, reliance on large datasets, training instability, risk of overfitting, domain adaptation difficulties,

noise sensitivity, and limited real-time processing capabilities. Ongoing research aims to mitigate these issues, improving the robustness and practicality of learning-based approaches.

## 2.2 State Space Models (SSM)

A State Space contains the minimum number of variables describing a system. SSMs were initially developed in control theory [26] to model dynamic systems and have since been adapted into deep learning for their ability to handle sequential data effectively [17, 27]. In control theory, SSMs represent systems where the current state is influenced by prior states and external inputs, making them well-suited for capturing temporal dynamics. This framework allows for real-time tracking of system evolution over time, which is essential in dynamic processes. When SSMs were introduced into deep learning, they brought a distinct advantage: their powerful capability to model long-range dependencies in sequential data, outperforming traditional recurrent architectures like RNNs and LSTMs [28]. Unlike these traditional models, which often struggle with vanishing gradients and computational inefficiency, particularly in long sequences, SSMs are designed to maintain linear computational complexity. This makes SSMs far more efficient, allowing for the processing of long sequences without the significant computational cost typically incurred by other architectures. As a result, SSMs can handle both short-term and long-term dependencies in the data, making them highly versatile.

**State-Space Models for Linear Systems:** SSMs provide a mathematical framework for representing physical systems using inputs, outputs, state variables, and differential equations. An SSM dynamically describes a system's behavior and is constructed using two types of equations: the state equation and the output (or observation) equation.

- ☐ The **state equation** defines the temporal evolution of the system's state as a dynamical system.
- ☐ The **output equation** defines how the internal state is observed or measured through outputs.

The SSM order, or the number of differential equations required to represent a physical model, depends on the system's input and output variables. SSM-based control, a fundamental tool, is crucial in analyzing linear and non-linear systems with multiple inputs and outputs. Fig. 2(a) illustrates a block diagram of a state-space model for a linear system with a feedback control loop connected to the inputs and outputs. This model dynamically describes the system's behavior using state variables $h(t)$, inputs $x(t)$, and outputs y(t). The following equations govern the state-space model:

$$\text{State Equation: } \dot{h}(t) = A \cdot h(t) + B \cdot x(t).$$

This equation defines how the state evolves over time through the state transition matrix A, which captures the influence of the current state on the next state. Matrix B describes the impact of the input x(t) on the state changes. Here, h(t) represents the latent state at time t, and x(t) is the input at the same time step. This equation demonstrates how the system changes based on both its current state and the input it receives.

$$\text{Output Equation: } y(t) = C \cdot h(t) + D \cdot x(t).$$

The output equation converts the state into an observable output. Matrix C controls how the latent state h(t) is translated into the output y(t), while matrix D determines the direct influence of the input x(t) on the output. Matrices A, B, C, and D are all learnable parameters that can be adjusted to optimize the model's predictive accuracy. Figure 2(b) provides a visualization of both the state and output equations. It shows how the state equation governs state evolution, with matrix A capturing the influence of the current state on the future state and matrix B capturing how the input x(t) affects state transitions.
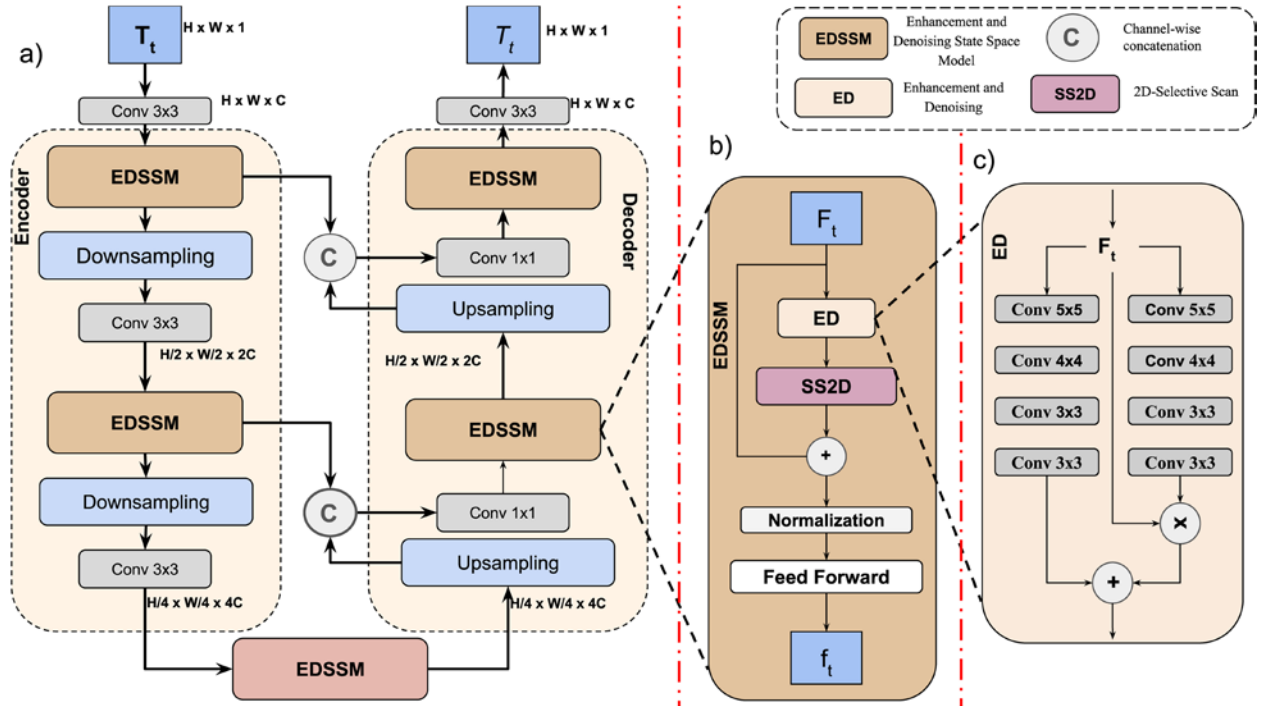


Fig. 3. Overall architecture of MTIE-Net (a), Enhancement and Denoising State Space Model (b), Enhancement and Denoising Module (c).

Solving these equations aims to uncover the statistical relationships that predict the system's future state based on the observed data (input sequences) and the previous state. This approach is fundamental in control theory and signal processing, allowing for the modeling and analysis of complex dynamic systems.

The efficiency and scalability of SSMs have drawn significant attention in areas that require analyzing sequential data, such as natural language processing, time-series forecasting, and, increasingly, computer vision tasks. In particular, SSMs have proven valuable in tasks that involve long-range dependencies, such as video analysis and image enhancement techniques like dehazing. By leveraging the strengths of SSMs, modern deep learning architectures can more effectively model both spatial and temporal relationships, improving performance in tasks where temporal and spatial consistency is critical. This ability to capture complex dependencies with high efficiency positions SSMs as a key technology in advancing deep learning capabilities in both time-dependent and spatially structured data domains.

## 2.3 Visual Mamba

The Mamba model, a dynamic state space model (SSM) with efficient selection mechanisms, is gaining traction in computer vision due to its ability to handle long-range dependencies in data while maintaining linear complexity. This significantly contrasts with traditional transformers,

which face limitations due to their quadratic complexity as image sizes increase. Mamba has demonstrated promising results in various visual tasks, including image classification, feature enhancement, and multimodal fusion [29]. Its efficiency positions it as a strong contender to replace CNNs and transformers as a foundational architecture for visual tasks.
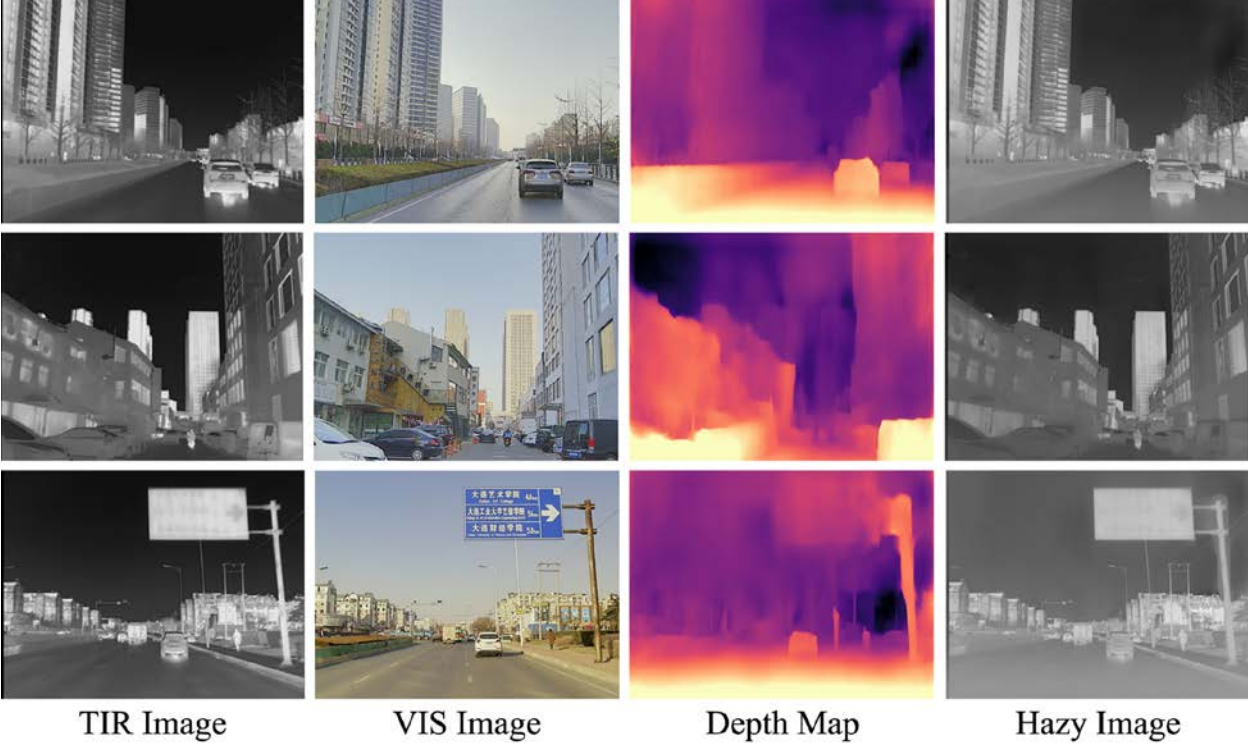


Fig. 4. This figure shows original image from M3DF, corresponding VIS image, depth map and generated hazy image.

Since 2024, Mamba has been successfully applied to diverse applications such as image enhancement, video analysis, and object detection [30]. These applications showcase their versatility and potential to significantly improve computer vision systems' accuracy and efficiency. By effectively managing long-range dependencies and maintaining computational efficiency, Mamba offers a robust solution for modern visual tasks, paving the way for advancements in the field. We adopted the integration of SSM into visual tasks, following the approach outlined in [31]. The SS2D module consists of three main operations: Scan Expanding, S6 blocks, and Scan Merging. In our model, the input images first undergo the Scan Expanding operation, systematically unfolding the image from its four corners toward the center. This process rearranges the spatial structure of the image, effectively allowing the model to capture features from different spatial regions. The height and width of the image are then flattened into a token length, turning the two-dimensional image into a one-dimensional sequence. Once the image has been flattened, each sequence is input into the S6 module, responsible for feature extraction. The S6 module operations can be expressed as:

$$h_t = Ah_{t-1} + Bx_t,$$

$$y_t = Ch_t,$$

where, $x$ is the input variable, $y$ is the output, and $A, B$ and $C$ are all learnable parameters. The outputs from the four directions of extracted features are summed and merged, and the dimensions of the merged output are readjusted to match the input size. Then, after processing the S6 blocks,

the Scan Merging operation restores the spatial structure by reorganizing the flattened sequence back into its original two-dimensional form. This combination of scan operations enables the SS2D module to capture local and global features in the image effectively, improving feature extraction for our visual tasks.



Fig. 5. This figure shows original image from M3DF, generated hazy image and generated label image.

## 3. Network Structure and Training

This section describes the proposed network and its training strategy for thermal image enhancement.

### 3.1 Structure

Fig. 3(a) illustrates our MTIE-Net framework, which consists of an encoder-decoder structure, capturing both local and long-range contextual features. Both processes are symmetric and divided into two levels. Each downsampling level consists of an EDSSM (see Fig. 3(b)), and a convolutional layer with kernel size of $3 \times 3$ (stride=2). Similarly, upsampling involves two levels, each including a upsampling operation, a $1 \times 1$ convolution applied to the merged features from the corresponding downsampling layer, and an EDSSM. Finally, a $3 \times 3$ convolution is applied to the image to reduce dimensionality and restore it to grayscale with a single channel. EDSSM block includes an Enhancement and Denoising (ED) module (see Fig. 3(c)) consisting of two branch processing: the first branch outputs a single-channel feature map, which is element-wise multiplied with the input image, enhancing contrast and preserving important edge information. The second branch processes the input, and its output is added to the multiplied result from the first branch, effectively removing noise and artifacts from the image.
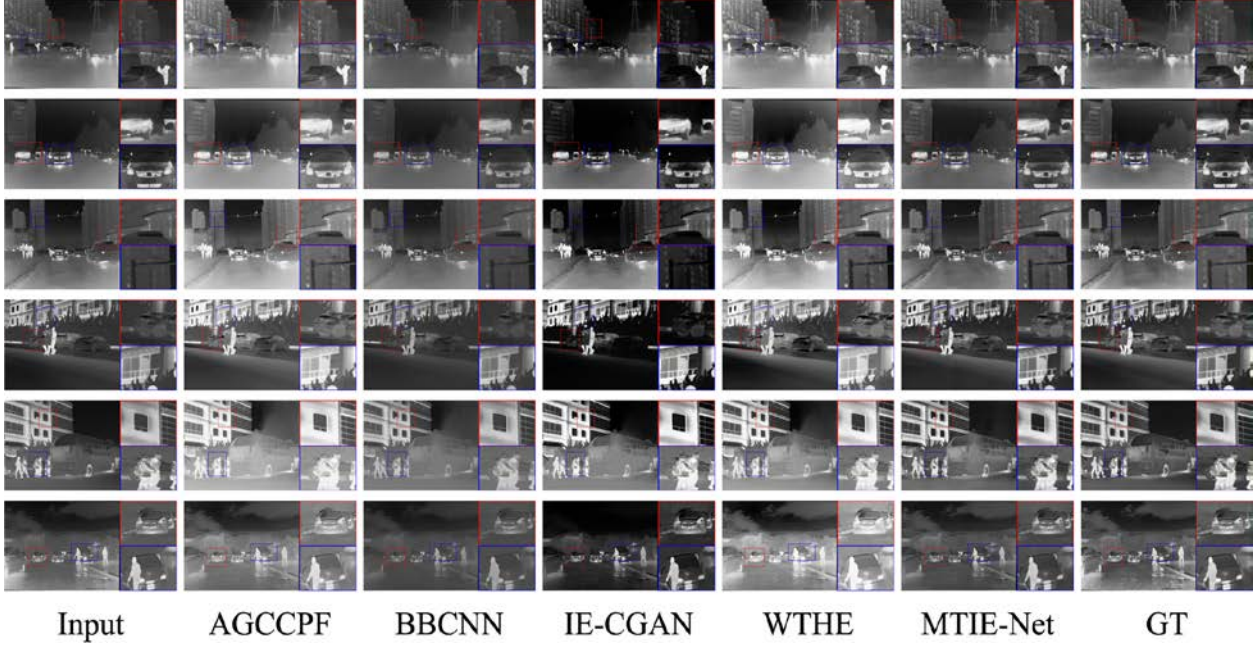
|  Input | AGCCPF | BBCNN | IE-CGAN | WTHE | MTIE-Net | GT |

Fig. 6. Qualitative comparison of MTIE-Net.

## 3.2 Training and Dataset

We selected the M3DF [32] dataset for training due to its unique provision of pixel-aligned TIR and VIS image pairs. The dataset was captured using a synchronized system consisting of one binocular optical camera and one binocular infrared sensor, ensuring accurate alignment between the TIR and VIS images. The scenes feature diverse environments, including campus areas and roads, with a total of 4,200 image pairs as well as an additional 300 pairs from independent scenes, which we used as the test set. We employed the atmospheric scattering model (ASM) to create synthetic hazy images widely used in dehazing methods [33]. ASM models a hazy image $I(x)$ as

$$I(x) = J(x) \cdot t(x) + A \cdot \big(1 - t(x)\big),$$

where $J(x)$ is the haze-free image, A the atmospheric light and

$$t(x) = e^{-\beta \, d(x)}$$

is the transmission matrix [34] with $\beta$ being the atmospheric scattering coefficient and $d(x)$ the depth map. For this approach, both the image and its corresponding depth map are required. We utilized corresponding VIS images to generate depth maps for the TIR images, as many depth estimation algorithms work well for visible images. We used the DIFFNet [35] method for generating depth maps, results shown in Fig. 4. The scattering coefficient $\beta$ was selected uniformly from the range [0.6, 1.8], while A from [0.2, 0.6], following [36]. Finally, we added Gaussian noise to make the synthetic TIR images more realistic. For the ground truth label images, we applied the Contrast Limited Adaptive Histogram Equalization [37] technique to enhance the input images, using a clip limit 1.2.

Since thermal images inherently contain noise, we incorporated the Non-local Means Denoising algorithm [38] to reduce noise levels while preserving important features. To retain essential details that might be lost during denoising, we merged the denoised image with the enhanced image using a coefficient of 0.4. We further combined this result with the original input

image using a coefficient of 0.2 (as shown in Fig. 5). This multi-step merging process ensures that the final output maintains the critical features of the original input while effectively denoising and enhancing the image. The network was trained for 300 epochs using the Adam optimizer (Adaptive Moment Estimation) with an initial learning rate of $1\times10{-}4$. Input images were cropped to $256\times256$ pixels to ensure consistent processing and to optimize the training efficiency.

## 3.3 Loss Function

The network training process minimizes the loss between the predicted images and the corresponding high-quality ground truth images. We use the Mean Squared Error (MSE) metric, which calculates the average of the squared differences between predicted and actual values. MSE assigns greater weight to larger errors, making it sensitive to outliers and effective for minimizing the overall error in the model. The loss function is defined as follows:

$$L_{MSE} = MSE(I_{pred}, I_{gt}),$$

where

$$MSE(I_{pred}, I_{gt}) = \sum_{i=1}^{M} \sum_{j=1}^{N} \left( I_{pred_{ij}} - I_{gt_{ij}} \right)^2, \tag{1}$$

where $I_{pred}$ is the predicted image, $I_{gt}$ is the ground truth image $M, N$ are the width and height of the image, respectively. The MSE ensures consistency between the network's predictions and the reference images, guiding the model to improve its accuracy.
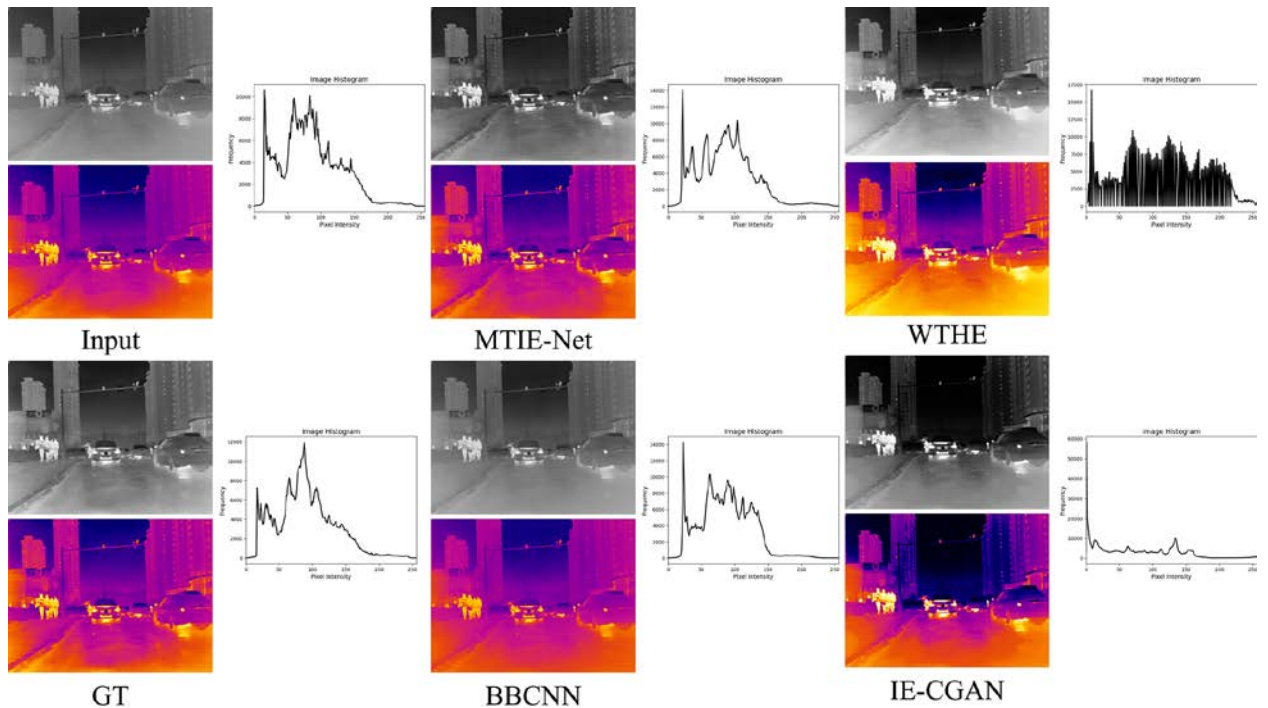


Fig. 7. This figure shows our ability to recover both high-level and low-level features compared with BBCNN, IE-CGAN and WTHE.
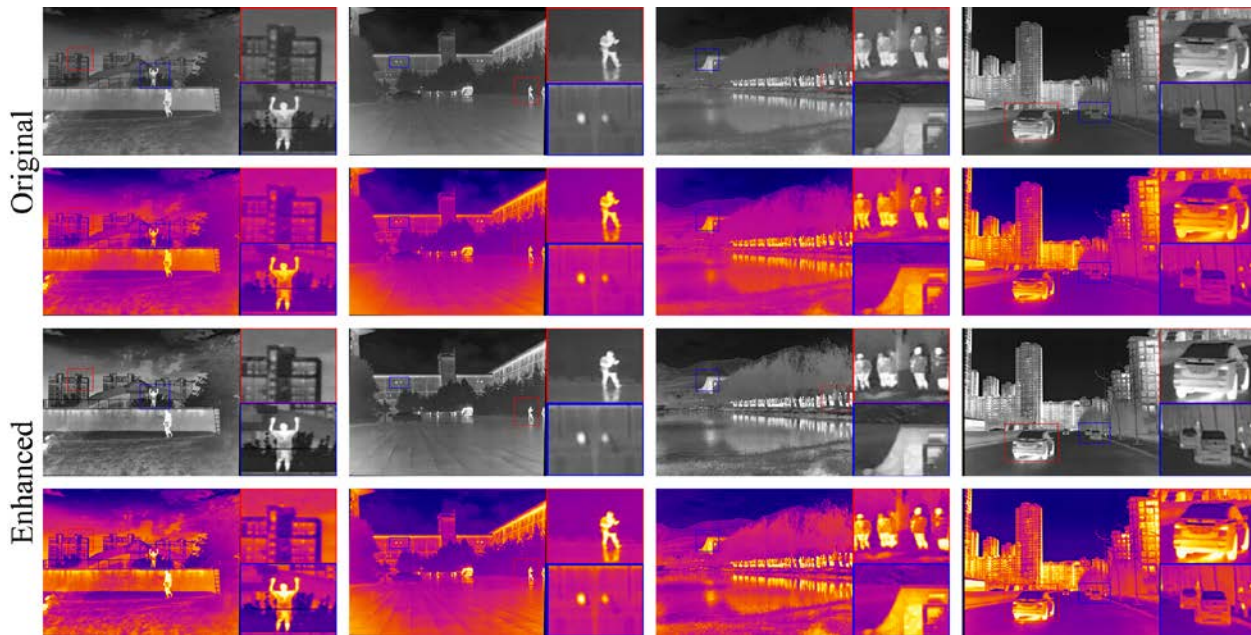
Fig. 8. Performance of MTIE-Net on M3DF dataset.

## 4. Experimental Results

This section presents the experimental results of our proposed approach in comparison with several existing methods, including AGCCPF [39], WTHE [40], BBCNN [41], and IE-CGAN [42]. Through this comparative analysis, we aim to highlight the strengths and weaknesses of each method and evaluate the effectiveness of MTIE-Net against these techniques. MTIE-Net provides a more robust foundation for object detection, tracking, and classification applications by maintaining optimal visibility across various image degradation scenarios.

## 4.1 Qualitative Comparison

Figure 6 compares MTIE-Net qualitatively against other thermal image enhancement techniques. As seen in the figure, IE-CGAN successfully reduces haze but makes the image too dark, leading to the loss of crucial details. For example, in the third row, it fails to recover the traffic light and loss of car information, which is critical for applications like pedestrian or vehicle detection. AGCCPF and WTHE tend to over-enhance road textures, losing essential details, particularly in lighter (hazy) areas. However, WTHE performs better in handling contrast in extremely dark regions. BBCNN often produces unnatural sharpness and introduces halo artifacts, negatively affecting overall image quality. In contrast, MTIE-Net provides a balanced enhancement of hazy regions while preserving essential details, maintaining natural contrast and depth information as shown in Fig. 7. It restores image details without introducing halo artifacts, making it more applicable for real-world applications. Although to understand the generalizability of our approach, we ran the algorithm on the original M3DF dataset, showing its performance on real-world thermal images (see Fig. 8). MTIE-Net effectively enhances thermal images captured in natural conditions, where haze, noise, and low contrast are naturally present. Unlike the previous experiments with simulated hazy images, this evaluation demonstrates the model's robustness and adaptability to complex, real-world degradations.

MTIE-Net successfully restores essential details and preserves natural contrast without introducing halo artifacts. Also, using basic colorization methods on thermal images makes the

results easier to interpret, giving a clearer and more intuitive view of the scene. This improvement is crucial for tasks like autonomous driving and surveillance, where clarity and detail are vital.

## 4.2 Quantitative Comparison

To evaluate the effectiveness of MTIE-Net architecture, we utilize five image quality metrics:

(i) Peak Signal-to-Noise Ratio (PSNR), which measures the ratio between the maximum possible signal power and the power of noise that affects image quality, commonly used for assessing the reconstruction quality in lossy image compression codecs. Given a reference image $I$ and a test image $J$, both of size $M{\times}N$, the PSNR between $I$ and $J$ is defined by:

$$PSNR(I,J) = 10\log\left(\frac{255^2}{MSE(I,J)}\right),$$

where MSE is defined in (1).

(ii) Structural Similarity Index Measure (SSIM) [20], which evaluates image degradation based on perceived structural information. SSIM considers factors such as luminance and contrast masking to assess the similarity between two images. SSIM is defined as:

$$SSIM(I,J) = l(I,J) \cdot c(I,J) \cdot s(I,J),$$

where $l(I,J)$ is the luminance comparison function that measures the closeness of the two images mean luminance, $c(I,J)$ is the contrast comparison function that measures the closeness of the contrast between the two images (where contrast is measured by the standard deviation), and $s(I,J)$ is the structure comparison function that measures the correlation coefficient between the two images [20, 43].

(iii) Measure of Enhancement (EME) [44], which assesses the entropy of block-wise image contrasts rather than individual pixel values. This metric is crucial for evaluating the quality of enhanced images, as it highlights contrast differences within blocks. The EME metric is defined as:

$$EME(I) = \frac{1}{n}\sum_{i=1}^{n} 20\,ln\left(\frac{I_{max}^k}{I_{min}^k + c}\right)$$

where $I$ image is partitioned into n blocks, $I_{max}^k$, $I_{min}^k$ are the maximum and minimum values of the k block, and c is a small constant to avoid division by zero.

(iv) Block-Based Information Measure (BDIM) [45], which evaluates the amount of information present in image blocks by considering both local contrast and structural details. This measure provides insight into the effectiveness of enhancement by focusing on small image regions, ensuring that fine details are preserved and enhanced across blocks.

(v) Global Contrast Measure of Enhancement (MDIMTE) [46], which combines features accounting for the human visual system, information theory, and distribution-based measures. This metric provides a holistic view of enhancement quality, considering global contrast improvements

that align with how humans perceive image quality and how efficiently information is distributed throughout the image.

High scores across these metrics indicate superior image enhancement and a more natural visual appearance. Table 2 presents the comparative analysis results, showcasing MTIE-Net performance against existing methods. Our method outperforms both traditional and CNN-based approaches, achieving the highest average scores in SSIM, PSNR. These results underscore the superior capability of MTIE-Net in enhancing thermal images while preserving essential details and maintaining a realistic look.

Table 2. Quantitative Comparison of MTIE-Net with Other State-of-the-Art Methods

| Measure | AGCCPF [39] | BBCNN [41] | IE-CGAN [42] | WTHE [40] | MTI-Net |
|---|---|---|---|---|---|
| PSNR ↑ | 15.204 | 22.638 | 19.535 | 15.406 | **24.303** |
| SSIM ↑ | 0.852 | 0.909 | 0.718 | 0.872 | **0.948** |
| EME ↑ | 1.600 | 1.688 | 1.496 | 2.618 | **3.001** |
| BDIM ↑ | 0.922 | 0.928 | 0.912 | 0.921 | **0.939** |
| MDIMTE ↑ | 52.987 | 54.931 | 48.111 | 51.131 | **57.584** |

## 5. Ablation Study

We conducted a series of ablation experiments to assess the contribution of the SS2D and ED blocks to the thermal image enhancement task. Specifically, we trained MTIE-Net with and without these modules to understand their impact on performance. In one variant, only the ED block was retained while the SS2D block was removed, and in another variant, only the SS2D block was retained while the ED block was removed. As shown in Table 3, the highest PSNR, SSIM, EME, BDIM and MDIMTE values were achieved when both the ED and SS2D blocks were integrated, indicating that their combination significantly improves the model's ability to enhance overall image

Table 3. Ablation Study on M3DF Dataset

| Methods | MTIE-Net w/o SS2D | MTIE-Net w/o ED | MTIE-Net |
|---|---|---|---|
| PSNR ↑ | 22.915 | 23.143 | **24.303** |
| SSIM ↑ | 0.911 | 0.932 | **0.948** |
| EME ↑ | 2.837 | 2.877 | **3.001** |
| BDIM ↑ | 0.934 | 0.934 | **0.939** |
| MDIMTE ↑ | 56.821 | 57.193 | **57.584** |

quality. This demonstrates that integrating ED and SS2D is critical for achieving superior performance in thermal image enhancement.

In addition to the experiments conducted on the M3DF dataset, we further evaluated the data independence of MTIE-Net using real-world solar panel images provided by SOLARON LLC. These images offer a diverse set of real-world conditions, enabling us to test the model's ability to generalize beyond training data.
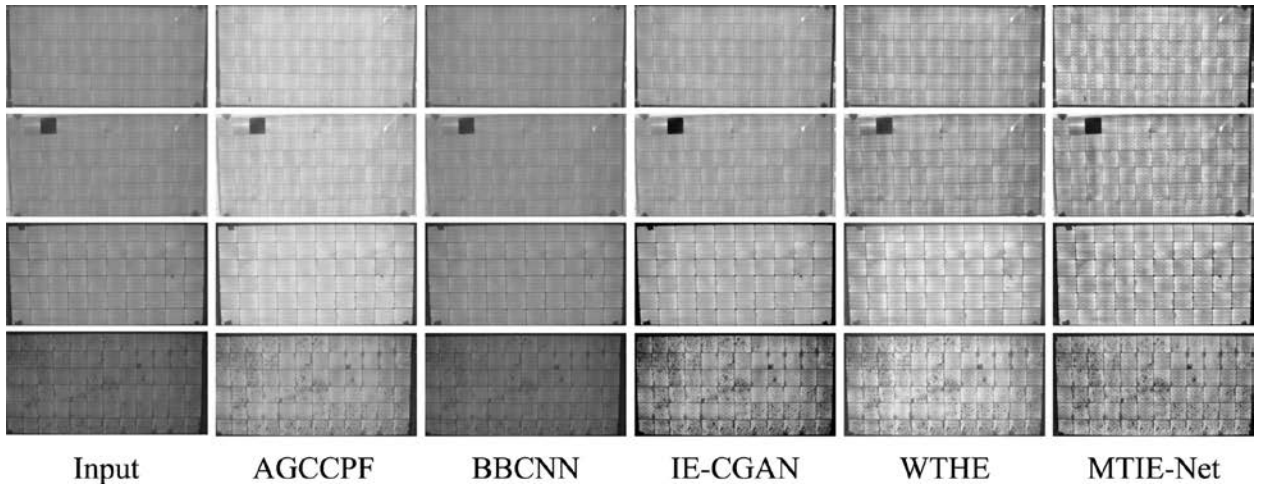
Fig. 9. Qualitative comparison of MTIE-Net on Solar Panel Images.

Fig. 9 presents a qualitative comparison of MTIE-Net against other enhancement techniques on the solar panel dataset. MTIE-Net consistently outperforms the other methods, making clearer and more detailed images while maintaining critical features, such as panel textures and fault regions. This demonstrates the robustness of MTIE-Net in handling different real-world datasets beyond the original thermal images used for training. To provide a more detailed visualization,
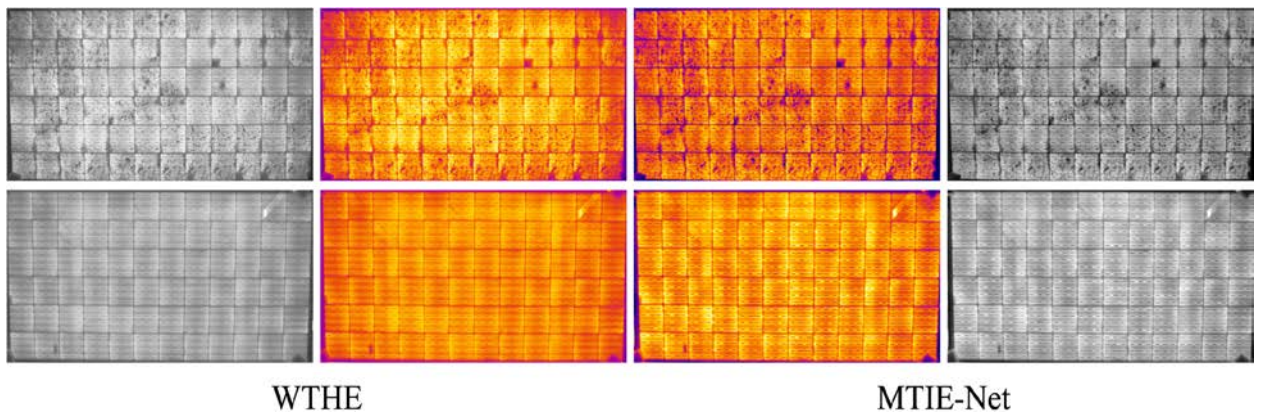


Fig. 10. Detailed Visualization of MTIE-Net (our) and WTHE on Solar Panel Images (the best one).

Fig. 10 shows two selected solar panel images enhanced by the best-performing model from the previous comparisons, with the simple colorization technique applied. These images highlight specific visual improvements, such as better contrast and detail preservation. The results underline the data-independent nature of MTIE-Net, confirming its ability to generalize effectively to new datasets.

## 6. Conclusion

In conclusion, this paper introduces the novel MTIE-Net architecture for thermal image dehazing, building upon the Mamba model to achieve superior performance. We enhanced feature extraction capabilities by integrating an advanced ED module with the SS2D model, significantly improving image quality and clarity. We also incorporated labeled thermal infrared (TIR) data for degradation enhancement, utilizing depth information from aligned visible-infrared (VIS-TIR) image pairs.

Our extensive quantitative and qualitative evaluations demonstrate that MTIE-Net outperforms state-of-the-art methods such as IE-CGAN, BBCNN, AGCCPF, and WTHE on the M3DF dataset. The results validate MTIE-Net's robustness and reliability across various imaging scenarios, showing consistently superior performance in both objective measures and visual assessments compared to other approaches. MTIE-Net shows significant potential for advancing thermal image-based applications. Future work will focus on developing a unified network capable of processing multi-scale and multi-spectral images, thereby broadening the versatility and applicability of our approach.

Additionally, we plan to integrate domain adaptation techniques to address the challenges of different imaging conditions and environments, ensuring more generalized performance. We will also explore real-time processing capabilities to make the network suitable for applications that require immediate analysis, such as autonomous navigation, surveillance, and disaster response. This ongoing development aims to enhance thermal imaging performance further, offering valuable improvements for diverse applications, including environmental monitoring, security, and beyond.

# References

[1] B. Li et al., "Benchmarking single image dehazing and beyond", *IEEE Transactions on Image Processing*, vol. 28, no. 1, pp. 492–505, 2019.

[2] S. Hovhannisyan et al., "AED-Net: A Single Image Dehazing", in *IEEE Access*, vol. 10, pp. 12465-12474, 2022.

[3] S. Hovhannisyan, H. Gasparyan and S. Agaian, "EOD-Net: enhancing object detection in challenging weather conditions using an innovative end-to-end dehazing network", *Twelfth International Conference on Image Processing Theory, Tools and Applications (IPTA)*, Paris, France, pp. 1-6, 2023.

[4] D. Berman, T. Treibitz and S. Avidan, "Single image dehazing using haze-lines", *IEEE Transactions on Pattern Analysis and Machine Intelligence,* vol. 42, no. 3, pp. 720–734, 2020.

[5] Z. Chen, Z. He and Z. -M. Lu, "DEA-Net: single image dehazing based on detail-enhanced convolution and content-guided attention", *IEEE Transactions on Image Processing*, vol. 33, pp. 1002-1015, 2024.

[6] A. Oulefki, T. Trongtirakul, S. Agaian et al., "multi-view vr imaging for enhanced analysis of dust accumulation on solar panels", *Solar Energy*, vol. 279, pp. 112708, 2024.

[7] A. Parihar, Y. Gupta, Y. Singodia, V. Singh and K. Singh, "A comparative study of image dehazing algorithms", *5th International Conference on Communication and Electronics Systems (ICCES)*, IEEE, pp 766–771, 2020.

[8] A. Wilson et al., "Recent advances in thermal imaging and its applications using machine learning: A review", *IEEE Sens. J.,* vol. 23, pp. 3395–3407, 2023

[9] J. Baek, S. Hong, J. Kim and E. Kim, "Efficient Pedestrian detection at nighttime using a thermal camera" *Sensors*, vol. 17, no. 8, p. 1850, 2017.

[10] A. Goldberg, T. Fischer and Z. Derzko, "Application of dual-band infrared focal plane arrays to tactical and strategic military problems" *in Proc. SPIE*, vol. 4820, pp. 500–514, 2003.

[11] W. Wong, H. Lim, C. Loo and W. Lim, "Home alone faint detection surveillance system using thermal camera" *in Proc. 2nd Int. Conf. Comput. Res. Develop*., pp. 747–751, 2010.

[12] J. Berni, et al., "Remote sensing of vegetation from UAV platforms using lightweight multispectral and thermal imaging sensors", *Int. Arch. Photogramm. Remote Sens. Spat. Inform. Sci.* 38:6, 2008.

[13] T. Trongtirakul and S. Agaian "New retinex model-based infrared image enhancement", *Proc. SPIE 12526, Multimodal Image Exploitation and Learning*, 1252606, 2023.

[14] A. Gu and T. Dao, "Mamba: linear-time sequence modeling with selective state spaces", *arXiv* preprint arXiv:2312.00752, 2023.

[15] E. Nguyen et al., "Modeling images and videos as multidimensional signals with state spaces", *Advances in neural information processing systems*, vol. 35, pp. 2846–2861, 2022.

[16] J. Smith, A. Warrington and S. Linderman, "Simplified state space layers for sequence modeling, " *arXiv* preprint arXiv:2208.04933, 2023.

[17] B. Patro and V. Agneeswaran, "Mamba-360: Survey of state space models as transformer alternative for long sequence modelling: Methods, applications, and challenges", *arXiv* preprint arXiv:2404.16112, 2024.

[18] Y. Cao and W. Zhang, "Mamba4KT: An Efficient and Effective Mamba-based Knowledge Tracing Model", *arXiv* preprint arXiv:2405.16542, 2024.

[19] T. Dao and A. Gu, "Transformers are ssms: Generalized models and efficient algorithms through structured state space duality", *arXiv* preprin arXiv:2405.21060, 2024.

[20] Z. Wang, A. Bovik, H. Sheikh and E. Simoncelli, "Image quality assessment: From error visibility to structural similarity", *IEEE Trans. Image Process.*, vol. 13, no. 4, pp. 600–612, Apr. 2004.

[21] L. Lu, et. al., Comparative study of histogram equalization algorithms for image enhancement. Mob. Multimed. Image Process. Secur. Appl. 2010, 7708, 337–347

[22] J. Wang, et al., "Range-restricted pixel difference global histogram equalization for infrared image contrast enhancement", *Opt Rev 28*, 145–158, 2021.

[23] T. Mudavath and V. Niranjan, "Thermal image enhancement for adverse weather scenarios: a wavelet transform and histogram clipping approach", *SIViP 18*, pp. 6547–6558, 2024.

[24] R. Soundrapandiyan, et al. "A comprehensive survey on image enhancement techniques with special emphasis on infrared images", *Multimed Tools Appl 81*, 9045–9077, 2022.

[25] A. Grigoryan and S. Agaian, "Asymmetric and symmetric gradient operators with application in face recognition in Renaissance portrait art", *Proc. of SPIE, Defense + Commercial Sensing, Mobile Multimedia/Image Processing, Security, and Applications*, vol. 10993, p. 12, Baltimore, Maryland, April 2019.

[26] R. Kalman, "A new approach to linear filtering and prediction problems", 1960.

[27] M. Ahamed and Q. Cheng, "TSCMamba: Mamba meets multi-view learning for time series classification", *arXiv* preprint arXiv:2406.04419, 2024.

[28] S. Hochreiter and J. Schmidhuber, "Long Short-Term memory", *Neural computation*, vol. 9, no. 8, pp. 1735–1780, 1997.

[29] C. Yuan, D. Zhao and S. Agaian, "MUCM-Net: a mamba powered ucm-net for skin lesion segmentation", *arXiv* preprint arXiv:2405.15925.

[30] H. Zhang et. al., "A survey on visual mamba", *arXiv* preprint, arXiv:2404.15956v2, 2024.

[31] L. Zhu et al., "Vision mamba: Efficient visual representation learning with bidirectional state space model", *arXiv* preprint arXiv:2401.09417, 2024.

[32] J. Liu et al., "Target-aware dual adversarial learning and a multi-scenario multi-modality benchmark to fuse infrared and visible for object detection", *IEEE/CVF International Conference on Computer Vision and Pattern Recognition (CVPR)*, 2022.

[33] T. Trongtirakul and S. Agaian, "New Retinex model-based infrared image enhancement", *Proc. SPIE 12526, Multimodal Image Exploitation and Learning,* 1252606, 2023.

[34] T. Trongtirakul, and S. Agaian, "Transmission map optimization for single image dehazing*", Proc. SPIE 12100, Multimodal Image Expl. and Learning*, 121000C, May, 2022.

[35]  H. Zhou, D. Greenwood and S. Taylor, "Self-supervised monocular depth estimation with internal feature fusion", *British Machine Vision Conference (BMVC)*, 2021.

[36]  F. Erlenbusch et al., "Thermal infrared single image dehazing and blind image quality assessment", *IEEE/CVF Conference on Computer Vision and Pattern Recognition Workshops (CVPRW)*, Vancouver, BC, Canada, 2023, pp. 459-469, 2023.

[37]  A. Reza, "Realization of the contrast limited adaptive histogram equalization (CLAHE) for real-time image enhancement", *J. VLSI Sig. Proc. Syst. Signal Image Vid. Tech..*, vol. 38, no. 1, pp. 35-44, 2004.

[38]  A. Buades, B. Coll and J. Morel, "Non-local means denoising," *Image Processing On Line*, 1, pp. 208–212, 2011.

[39]  B. Gupta and M. Tiwari, "Minimum mean brightness error contrast enhancement of color images using adaptive gamma correction with color preserving framework", *Optik* 127, no. 4, pp. 1671-1676, 2016.

[40]  Q. Wang and and R. Ward, "Fast image/video contrast enhancement based on weighted thresholded histogram equalization", *IEEE Trans. On Consumer Electronics* 53, no. 2, 757-764, 2007.

[41]  K. Lee  et al., "Brightness-based convolutional neural network for thermal image enhancement", *IEEE Access*, vol. 5, pp. 26867-26879, 2017.

[42]  K. Xiaodong et al., "Single infrared image enhancement using a deep convolutional neural network", *Neurocomputing*, vol. 332, pp. 119-128, 2019.

[43]  A. Horé and D. Ziou, "Image quality metrics: PSNR vs. SSIM", *20th International Conference on Pattern Recognition,* pp. 2366-2369, Turkey, 2010.

[44]  S. Agaian et al., "A new measure of image enhancement", *IASTED Int. Conf. on Signal Proc. & Comm.*, Sept. 2000.

[45]  W. Yang et al., "Blind image quality assessment with a multi-task CNN for enhanced measurement", *Sig. Pr.: Im. Com.,* 105, 116672, 2022.

[46]  S. Agaian, M. Roopaei and D. Akopian, "Thermal-image quality measurements", *IEEE International Conference on Acoustics, Speech and Signal Processing (ICASSP)*, 2014.

# Մամբայի վրա հիմնված ջերմային պատկերի մառախուղի հեռացում

Սարգիս Ա. Հովհաննիսյան

Երևանի պետական համալսարան, Երևան, Հայաստան
e-mail: sargis.hovhannisyan@ysu.am

## Ամփոփում

Մթնոլորտային երևույթները, ինչպիսիք են անձրևը, ձյունը, քաղաքային, անտառային հրդեհները և արհեստական աղետները, կարող են վատթարացնել պատկերի որակը տարբեր կիրառություններում, ներառյալ տրանսպորտը, վարորդների աջակցության

համակարգերը, հսկողությունը, ռազմական և հեռահաղորդակցական համակարգերը: Պատկերի մշակխողի հեռացման տեխնիկաները նպատակ ունեն նվազեցնել մշակխողի, փոշու և այլ մթնոլորտային աղավաղումների հետևանքները` բարելավելով պատկերի որակը` համակարգչային տեսողության առաջադրանքների ավելի լավ կատարման համար: Մշակխողը ոչ միայն թաքցնում է մանրամասները, այլև նվազեցնում է կոնտրաստը և գույնի հավաստիությունը` զգալիորեն ազդելով համակարգչային տեսողության (CV) մոդելների ճշգրտության վրա, որոնք օգտագործվում են օբյեկտների հայտնաբերման, պատկերների դասակարգման և սեգմենտավորման մեջ: Թեև ջերմային (TIR) պատկերները հաճախ նախընտրելի են երկար հեռավորության հսկողության և հեռահաղորդակցության համար` շնորհիվ դրանց դիմադրողականության մշակխողին, սակայն մթնոլորտային պայմանները կարող են վատթարացնել նրանց որակը, հատկապես եղանակային ծայրահեղ միջավայրերում: Այս հոդվածը ներկայացնում է MTIE-Net` նոր մամբայի վրա հիմնված ցանց` մթնոլորտային երևույթների շնորհիվ դեգրադացված ջերմային պատկերների բարելավման համար, ինչպիսիք են մշակխողը և ծուխը: MTIE-Net-ը օգտագործում է Enhancement and Denoising State Space Model (EDSSM), որը համատեղում է կոնվոլյուցիոն նեյրոնային ցանցերը State Space մոդելավորման հետ` արդյունավետ աղմուկի հեռացման և նկարի բարելավման համար: Մենք ստեղծում ենք սինթետիկ մշակխողապատ պատկերներ և կիրառում ողորտին հատուկ փոխակերպումներ, որոնք հարմարեցված են ջերմային պատկերի հատկություններին` ցածր տեսանելիության պայմաններում ուսուցումը բարելավելու համար: Մեր հիմնական ներդրումներն են մամբա ճարտարապետության կիրառումը 2D ընտրողական սկանավորմամբ` ջերմային պատկերների բարելավման համար, աղմուկի հեռացման և պատկերի բարելավման մոդուլի մշակումը և ջերմային պատկերների համար սինթետիկ մշակխողապատ տվյալների հավաքածուի ստեղծումը: M3DF երկար հեռավորության ջերմային պատկերների տվյալների հավաքածուի վրա գնահատվելով` MTIE-Net-ը գերազանցում է ժամանակակից մեթոդները ինչպես քանակական չափումների (PSNR, SSIM), այնպես էլ տեսողական պարզության և եզրերի պահպանման որակական գնահատականներում: Այս առաջընթացը զգալիորեն բարելավում է հեռահաղորդակցման, հսկողության և ավտոմատ համակարգերի հուսալիությունն ու ճշգրտությունը` մթնոլորտային վատ միջավայրերում պատկերի որակի բարելավման շնորհիվ:

**Բանալի բառեր`** ջերմային պատկեր, պատկերի բարելավում, ջերմային պատկերների բարելավում, Մամբա:

# Удаление тумана с тепловизионных изображений на основе Мамба

Саргис А. Оганнисян

Ереванский государственный университет, Ереван, Армения
e-mail: sargis.hovhannisyan@ysu.am

## Аннотация

Атмосферные явления, такие как дождь, снег, городские и лесные пожары, а также искусственные катастрофы, могут ухудшать качество изображения в различных областях, включая транспорт, системы помощи водителям, видеонаблюдение, военные и телекоммуникационные системы. Технологии удаления тумана с изображений направлены на снижение последствий тумана, пыли и других атмосферных искажений, улучшая качество изображения для более эффективного выполнения задач компьютерного зрения. Туман не только скрывает детали, но и снижает контраст и цветовую точность, что существенно влияет на точность моделей компьютерного зрения (CV), используемых для обнаружения объектов, классификации изображений и сегментации. Хотя тепловизионные изображения (TIR) часто предпочитаются для дальнего контроля и телекоммуникаций благодаря их стойкости к туману, атмосферные условия все же могут ухудшить их качество, особенно в экстремальных погодных условиях.

В этой статье представлен MTIE-Net — новая сеть на основе Mamba для улучшения тепловизионных изображений, искаженных атмосферными явлениями, такими как туман и дым. MTIE-Net использует Enhancement and Denoising State Space Model (EDSSM), которая сочетает в себе сверточные нейронные сети и моделирование состояний для эффективного удаления шума и улучшения изображения. Мы создаем синтетические изображения с туманом и применяем специфические для домена преобразования, адаптированные к характеристикам тепловизионных изображений, для улучшения обучения в условиях низкой видимости. Наши ключевые достижения включают использование архитектуры Mamba с 2D избирательным сканированием для улучшения тепловизионных изображений, разработку модуля для удаления шума и улучшения изображения, а также создание набора данных с синтетическим туманом для тепловизионных изображений. Оцененный на наборе данных M3DF для дальних тепловизионных изображений, MTIE-Net превосходит современные методы как по количественным показателям (PSNR, SSIM), так и по качественным оценкам визуальной четкости и сохранения краев. Это достижение значительно улучшает надежность и точность телекоммуникационных, систем наблюдения и автоматических систем за счет улучшения качества изображения в сложных атмосферных условиях

**Ключевые слова:** тепловизионное изображение, улучшение изображения, улучшение тепловизионного изображения, Мамба.

## Կանոններ հեղինակների համար

ՀՀ ԳԱԱ ԻԱՊԻ "Կոմպյուտերային գիտության մաթեմատիկական խնդիրներ" պարբերականը տպագրվում է 1963 թվականից: Պարբերականում հրատարակվում են նշված ոլորտին առնչվող գիտական հոդվածներ, որոնք պարունակում են նոր` չհրատարակված արդյունքներ:

Հոդվածները ներկայացվում են անգլերեն` ձևավորված համապատասխան "ոճով" (style): Հոդվածի ձևավորման պահանջներին ավելի մանրամասն կարելի է ծանոթանալ պարբերականի կայքէջում` http://mpcs.sci.am/:


## Rules for authors

The periodical "Mathematical Problems of Computer Science" of IIAP NAS RA has been published since 1963. Scientific articles related to the noted fields with novel and previously unpublished results are published in the periodical.

Papers should be submitted in English and prepared in the appropriate style. For more information, please visit the periodical's website at http://mpcs.sci.am/.


## Правила для авторов

Журнал «Математические проблемы компьютерных наук» ИПИА НАН РА издается с 1963 года. В журнале публикуются научные статьи в указанной области, содержащие новые и ранее не опубликованные результаты.

Статьи представляются на английском языке и оформляются в соответствующем стиле. Дополнительную информацию можно получить на веб-сайте журнала: http://mpcs.sci.am/.

The electronic version of the periodical "Mathematical Problems of Computer Science" and rules for authors are available at

http://mpcs.sci.am/